

THE GEOLOGY AND GEOCHEMISTRY OF THIRTEEN CINDER CONES AT
CRATER LAKE NATIONAL PARK, OREGON

by

ELIZABETH M. PRUEHER

A THESIS

Presented to the Department of Geology
and the Graduate School of the University of Oregon
in partial fulfillment of the requirements
for the degree of
Master of Science

March 1985

APPROVED:



Dr. A. R. McBirney

An Abstract of the Thesis of

Elizabeth M. Prueher for the degree of Master of Science
in the Department of Geology to be taken March 1985

Title: THE GEOLOGY AND GEOCHEMISTRY OF THIRTEEN CINDER CONES
AT CRATER LAKE NATIONAL PARK, OREGON

Approved: _____


Dr. A. R. McBirney

Major and trace-element variations exhibit an increase in excluded elements and a decrease in included elements as differentiation increases, indicative of crystal fractionation of olivine, clinopyroxene, orthopyroxene, and plagioclase.

LREE patterns for the rocks are irregular. First, basalt is enriched in LREE relative to other members of the suite. Second, there is a repeated pattern of three pairs of basalt and andesite; with each successive basalt enriched in LREE relative to the preceding andesite. From consideration of the REE data it is apparent that the cinder cones were derived from more than one partial melt.

Compositional variations in the magmas of the cinder cones support the conclusion that they were generated by more than one partial melting event. Partial melting of a

mantle source region with the composition of peridotite could have produced primitive basaltic magmas. Subsequent mixing and fractional crystallization produced the more differentiated basaltic to andesitic magmas.

VITA

NAME OF AUTHOR: Elizabeth M. Prueher

PLACE OF BIRTH: Champaign, Illinois

DATE OF BIRTH : April 9, 1957

UNDEGRADUATE AND GRADUATE SCHOOLS ATTENDED:

University of Wisconsin-Eau Claire
University of Oregon

DEGREES AWARDED:

Bachelor of Science, 1980, University of Wisconsin-Eau
Claire
Master of Science, 1985, University of Oregon

AREAS OF SPECIAL INTEREST:

Volcanology
Planetary Geology
Igneous Petrology
Geochemistry

PROFESSIONAL EXPERIENCE:

Laboratory Assistant, Instrumental Neutron Activation
Analysis Laboratory, University of Oregon, Eugene,
1982-84.

Assistant Curator, Condon Museum of Geology,
University of Oregon Museum of Natural History,
Eugene, Oregon, 1983-85.

Tutor in Geology and Geography, Educational
Opportunities Program, University of Oregon, Eugene,
1982-83.

AWARDS AND HONORS:

Student Research Fund Grant, University of Oregon,
1981
GSA Penrose Research Grant, 1982

PUBLICATIONS:

- Alff, A., and Prueher, L., 1977, Dike or Xenolith?: in
Guidebook for the 9th University of Wisconsin
Student Field Conference, p. 23-28, University of
Wisconsin, Eau Claire, Wisconsin.
- Prueher, L., 1984, Geology and Geochemistry of
Selected Cinder Cones At Crater Lake, Oregon; in
Proceedings of the Oregon Academy of Sciences,
vol. 20, p. 53.
- Prueher, L., 1985, Evolution of the Mount Mazama
Cinder Cones, Crater Lake National Park, Oregon: in
Proceedings of the Oregon Academy of Sciences,
vol. 21, (in press).
- Prueher, L. M., and McBirney, A. R., 1985a, Geology
and Geochemistry of Cinder Cones at Crater Lake
National Park, Oregon [abs.]: Geological Society of
America Abstracts with Programs, vol. 17, no. 6,
(in press).
- Prueher, L. M., and McBirney, A. R., 1985b, Geo-
chemistry of Thirteen Cinder Cones at Crater Lake
National Park, Oregon: Journal of Volcanology and
Geothermal Research, (in prep).

ACKNOWLEDGEMENTS

Dr. McBirney suggested the project and provided computer time, funds for the AA analyses, and encouragement throughout the course of the project. Reviews by Drs. McBirney, Goles, and Ulerick greatly improved the quality of the manuscript. Dr. Charles Bacon provided some rock powders for analysis and useful information during discussions in the field. Discussions with Dr. Gordon Goles helped in the interpretation of the INAA data.

This project was supported in part by a grant from the Student Research Fund, Geology Department, University of Oregon, and a Penrose Research Grant from the Geological Society of America.

I would like to thank the following people at Crater Lake National Park for their assistance and permission to work within the Park: Mr. Jim Rouse, Park Superintendent; Mr. Roger Rudolph, Chief Ranger; and Mr. Mark Forbes, Resource Management Specialist. I would also like to thank the 1982 and 1983 summer seasonals at Crater Lake for their assistance, hospitality, and invitations to enjoyable extra-curricular activities, including the valiant 1982 Search and Rescue Team. Discussions with Rod Cranson were helpful. The contributions of the following people are greatly appreciated: Colette, Denise, Dave, Kevin, Young Tom, and Teddy.

Thank you to the following people who assisted me in the field, some of whom are non-geologists but came anyway: Renate, Harold, Maureen, and Lumei. Colette, Dave, and Tom gave up their days off to assist me in the field.

Special thanks to the Physical Therapy department at the U of O Health Center, especially Nancy and Jane, and the staff at the Easter Seals Pool of Eugene, for help in my rehabilitation.

Thanks to all the people who made my stay in Eugene more enjoyable including, Pfeffer (a great paperweight), Aime (who helped with the drafting), Ellen, Kate the three Toms, Mark, Bea, all the Colbaths, Nikolaus, Holly, Helen, the D and D players, Judith, and Carol (thanks for everything). Last, but not least, thank you to my family; none of this would have been possible without the support of my parents.

TABLE OF CONTENTS

Chapter	Page
ONE. INTRODUCTION.....	1
Objectives.....	2
Location.....	3
Regional Geology.....	4
Western Cascade Range.....	4
High Cascade Range.....	5
Klamath Mountain Province.....	11
Basin and Range Province.....	12
Previous Work.....	16
TWO. THE GEOLOGY OF CRATER LAKE NATIONAL PARK.....	17
Summary of the Geologic History of Mount Mazama.....	17
Post-Caldera Volcanism.....	24
Other Volcanoes Within the Park Boundaries.....	26
THREE. CINDER CONES.....	28
Introduction.....	28
General Characteristics of Cinder Cones... Comparisons of Cinder Cone Eruptions.....	31
Morphology.....	33
Degradation of Cinder Cones.....	39
Emplacement of Cinder Cone Fields.....	41
Crater Lake Cinder Cones.....	42
Mount Mazama Cinder Cones.....	49
Timber Crater Cinder Cones.....	58
Union Peak Cinder Cones.....	59
Ages of Cinder Cones.....	60
Morphological Characteristics of the Mount Mazama Cinder Cones.....	66

FOUR.	PETROGRAPHIC AND GEOCHEMICAL FEATURES.....	68
	Petrography.....	68
	Mount Mazama Cinder Cones.....	68
	Cinder Cones of Timber Crater and Union Peak.....	80
	Chemical Variation.....	82
	Cinder Cones of Mount Mazama.....	82
	Cinder Cones of Timber Crater and Union Peak.....	90
	Discussion.....	97
	Mass-balance Calculations.....	104
	Rare-earth Elements (REE).....	109
	Fractional Crystallization and Partial Melting.....	113
	Spatial Distribution of Vents.....	116
	AFM Diagram.....	124
	Comparisons with Other Cascade Volcanoes.....	126
	Summary.....	129
FIVE.	CONCLUSIONS.....	132
APPENDICES		
A.	DESCRIPTIONS OF REPRESENTATIVE THIN SECTIONS.....	137
B.	CHEMICAL ANALYSES.....	143
REFERENCES.....		154

LIST OF TABLES

Table		Page
1.	Characteristics of Four Cinder Cone Eruptions.....	32
2.	Morphological Characteristics of Cinder Cone Fields.....	38
3.	The Relationship between % SiO ₂ and Rock Names Used to Describe ² Samples.....	48
4.	Measured Ages of the Mount Mazama Cinder Cones.....	61
5.	Morphological Characteristics of Mount Mazama Cinder Cones.....	62
6.	$\sum r^2$ for Mass-Balance Calculations where $\sum r^2 < 0.10$	106
7.	Examples of Two Mass-Balance Calculations.....	107

LIST OF FIGURES

Figure		Page
1.	Index Map of the Cascade Range.....	6
2.	Segment Boundaries of the Cascade Range.....	9
3.	Index Map Showing Major Structures of Southern Oregon.....	10
4.	Geologic Map of Crater Lake National Park.....	19
5.	The Collapse of the Crater Lake Caldera.....	21
6.	Location of Cinder Cones and Dacitic Domes in the Crater Lake Area.....	23
7.	Floor of Crater Lake.....	25
8.	Diagram Illustrating Measurements of Cinder Cone Parameters.....	36
9.	Cone Height Versus Basal Cone Diameter.....	37
10.	Diagram Illustrating Morphological Characteristics.....	40
11.	Geologic Map of Crater Lake National Park.....	43
12.	Sample Location on Red Cone.....	45
13.	Hand Sample of Scoria from Bald Crater.....	47
14.	Hand Sample of Lava Flow from Red Cone.....	47
15.	Desert Cone Bombs.....	51
16.	Red Cone Bomb.....	51
17.	Wizard Island.....	55
18.	Lava Flows Extending from the Western End of Wizard Island.....	55
19.	Williams Crater.....	57

20.	Bomb from Williams Crater.....	57
21.	H _{co} Versus W _{co} for Eight Mount Mazama Cinder Cones.....	66
22.	Relationship Between Rock Name and Abundance of Phenocryst Phases.....	69
23.	Photomicrograph of a Euhedral Olivine Phenocryst.....	72
24.	Photomicrographs of Pyroxene Phenocrysts.....	74
25.	Photomicrograph of a Plagioclase Macro- phenocryst.....	77
26.	Sketch of Types of Inclusions in Plagioclase Macrophenocrysts.....	77
27.	Plot of Na ₂ O + K ₂ O Versus SiO ₂	83
28.	Harker Diagrams for the Mount Mazama Cinder Cones.....	84
29.	Trace Elements Versus Differentiation (DI) for the Mount Mazama Cinder Cones.....	88
30.	Harker Diagrams for the Timber Crater and Union Peak Cinder Cones.....	91
31.	Trace Elements Versus Differentiation Index (DI) for the Timber Crater and Union Peak Cinder Cones.....	94
32.	Comparison of Variation Diagrams for the Cinder Cones of Mount Mazama, Timber Crater, and Union Peak.....	99
33.	REE Abundance Versus Ionic Radius for the Crater Lake Cinder Cones.....	110
34.	Calculated REE Patterns.....	112
35.	Fractional Crystallization Versus Partial Melting.....	115
36.	Rb Versus Ni for the Crater Lake Cinder Cones..	115
37.	H/M Versus H Diagrams.....	117

38.	Excluded Elements Versus SiO_2 and MgO	119
39.	Spatial Distribution of Vents Versus Age.....	122
40.	Vent Distribution Versus SiO_2	123
41.	Vent Distribution Versus Rb	123
42.	AFM Diagram for the Crater Lake Cinder Cones.....	125
43.	Comparison Diagram for the Crater Lake Cinder Cones, Mount Mazama, Mount Bailey, and Mount McLoughlin.....	128
44.	Schematic Representation of the Evolution of the Crater Lake Cinder Cones.....	136

CHAPTER ONE

INTRODUCTION

Most studies of andesitic volcanic chains, such as the Cascade Range of southern British Columbia, Washington, Oregon, and northern California, have been restricted to the andesitic cones and the more silicic products of the volcanoes. The cinder cones associated with the andesitic volcanoes have for the most part, been ignored.

Most cinder cones are monogenetic, i. e. they erupt only once, and tend to be active for a few months or at most a few years. They are composed of pyroclastic material and commonly erupt lava flows. The maximum basal diameter of cinder cones is 2 to 2.5 km (Wood, 1980a). Cones larger than this are rare, perhaps because larger cinder cones may evolve into composite volcanoes (Crowe, Halleck, and Nolf, 1978).

In some cases a cinder cone is the initial stage in the evolution of a composite cone. With continued eruptions, the basal diameter, mechanical strength, height, and volume of the cinder cone increase. Injection of dikes and sills increases the mechanical strength of the cone (Crowe, Halleck, and Nolf, 1978), and facilitates the transition from cinder cone to composite cone.

Aspects of the early history of composite cones may be

revealed by study of cinder cones. Because their rocks represent some of the most primitive magmas found in a region of andesitic volcanism, they are important elements in understanding the evolution of larger magmatic systems.

Objectives

Crater Lake National Park is an ideal location to study a classic Cascade andesitic volcano and its associated cinder cones. The area is young geologically and the volcanic products are relatively fresh. The area has remained almost undisturbed by man since Crater Lake National Park was established in 1902 to preserve the spectacular scenery surrounding the lake in the caldera of ancestral Mount Mazama. The presence of the caldera provides an unusual opportunity to study the past history and internal structure of Mount Mazama. The intermediate and silicic products of the volcano have been studied comprehensively (Williams, 1942; Ritchey, 1979; Bacon, 1983).

Twenty cinder cones are located within the boundaries of Crater Lake National Park. The thirteen cones that are the subject of this study can be divided into two groups on the basis of age:

1. Four cinder cones associated with the older, pre-Mount Mazama volcanoes, Union Peak and

Timber Crater, which are basaltic shield volcanoes within the boundaries of Crater Lake National Park.

2. Nine cinder cones associated with Mount Mazama.
 - A. Eight pre-caldera cinder cones
 - B. One post-caldera cinder cone

The phrase Crater Lake cinder cones will be used to refer to the thirteen cinder cones in this study. The term Mount Mazama cinder cones will be used to refer to the nine cinder cones associated with Mount Mazama.

The objectives of this study are, first, to describe the morphological, mineralogical, and geochemical characteristics of cinder cones associated with an andesitic volcano of the High Cascade Range, and, second, to determine the ages and genetic relationships, if any, between their magmas and that of Mount Mazama.

Location

Crater Lake National Park is located in Klamath County, Oregon, and is part of the Southern Oregon High Cascade Range (Figure 1). The Park can be reached from Highways 97 and 138 from the north (north entrance), and Highway 62 from the south (south entrance). Access is limited to the south entrance during the winter.

Regional Geology

The Cascade Range extends from Mount Garibaldi in British Columbia, to Mount Lassen in California, and can be divided into two parts, the Western Cascade Range and the High Cascade Range. Crater Lake National Park is located on the axis of the High Cascade Range (Figure 1). The Klamath Mountain Province is located southwest of Crater Lake National Park. Rocks similar to those found in the Klamath Mountains are believed to underlie the Crater Lake area. The Klamath Mountain structure is believed to continue into the Crater Lake area (Barnes and Ritchey, 1978) and to have had some affect on the tectonics of the Crater Lake area. The Basin and Range province of southern Oregon is east and southeast of Crater Lake National Park (Figure 1). Basin and Range style of faulting and extension may extend into the Crater Lake area (Blank, 1968). The following is a brief discussion of the regional setting for the area.

Western Cascade Range

Calc-alkaline volcanism in the Western Cascades began in the Oligocene (McBirney, 1978). The vents for this early activity were located west of the present axis of the Cascades. A change in eruptive products with time can be

observed in the Western Cascade sequence. Andesite and rhyolite were predominant before the mid-Miocene, andesite became dominant in the mid-late-Miocene, and basalt was more important during the Pliocene and Pleistocene (White and McBirney, 1978), when coalescing shield volcanoes formed the platform upon which the High Cascades are built.

High Cascade Range

Rocks of the Western Cascade Range are unconformably overlain by rocks of the High Cascade Range. The High Cascades are the result of Quaternary volcanic activity concentrated along a north-south trend.

Early Pleistocene activity consisted mainly of basaltic cones, flows, and overlapping shield cones. The lavas were olivine basalts and olivine-bearing basaltic andesites. Basaltic eruptions continued after the andesitic cones began to build.

Construction of the andesitic cones of the High Cascades began about one million years ago; the cones formed in a relatively short time. One known constraint on the ages is provided by observations of magnetic polarities. Few reversely polarized lavas have been found in the High Cascades. The most recent magnetic reversal occurred approximately 700,000 years ago. Therefore, the majority of the material exposed in the High Cascades has

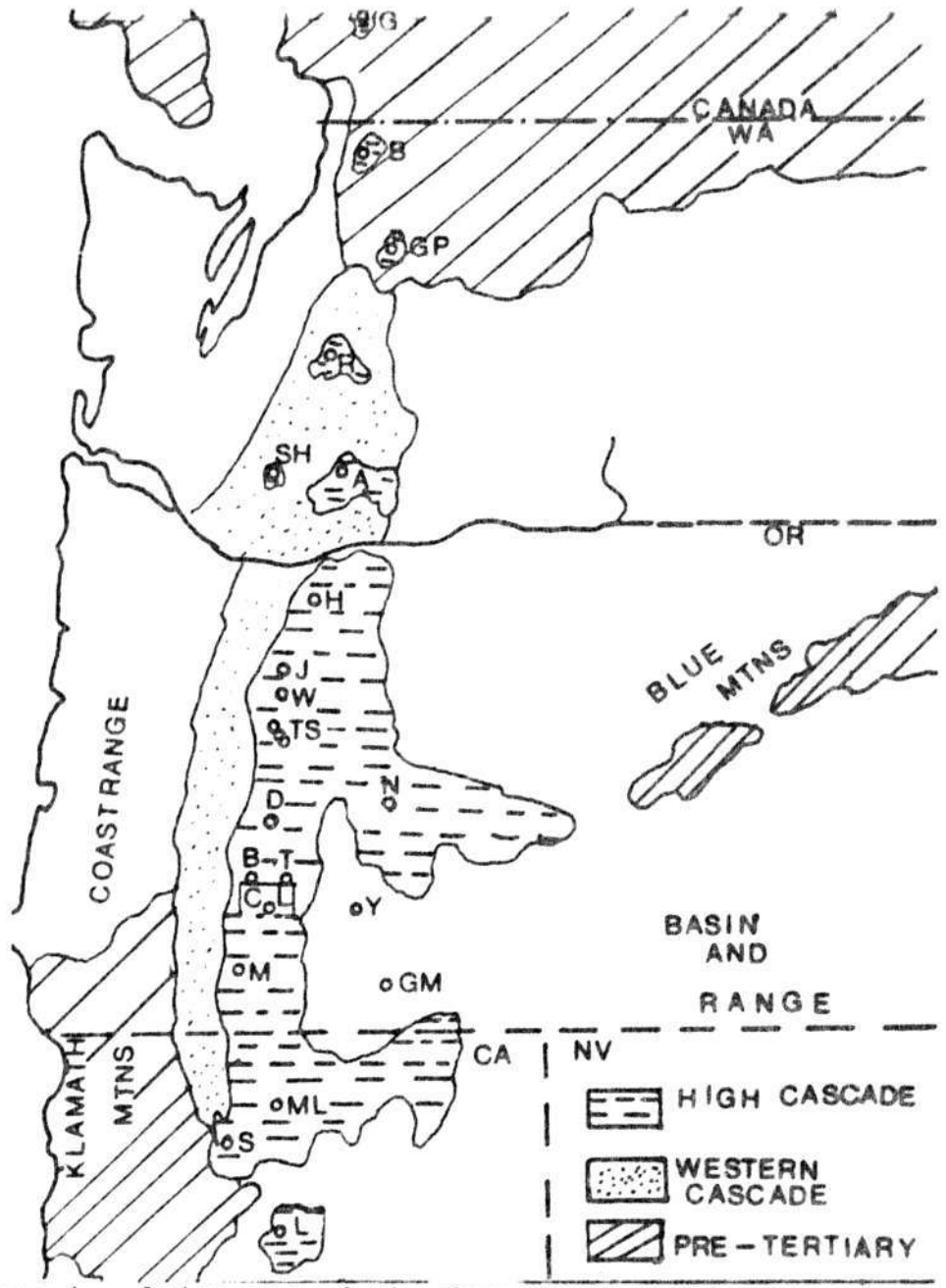


Figure 1. Index map of the Cascade Range showing physiographic provinces and volcanic centers. Abbreviations: G-Mt. Garibaldi, GP-Glacier Peak, B-Mt. Baker, R-Mt. Rainier, SH-Mt. St. Helens, A-Mt. Adams, H-Mt. Hood, J-Mt. Jefferson, TS-The Three Sisters, W-Mt. Washington, D-Diamond Peak, B-Mt. Bailey, T-Mt. Thielsen, CL- Crater Lake, M-Mt. McLoughlin, S-Mt. Shasta, L-Lassen Peak, N-Newberry Caldera, Y-Yamsay Mountain, GM-Gearhart Mountain, ML-Medicine Lake.

been erupted within the preceding 700,000 years.

Basalt is volumetrically predominant in the central part of the Cascades, whereas andesite is relatively more abundant to the north and south. This may be because the central Cascade volcanoes (The Three Sisters, Mount Jefferson) are underlain by thin, oceanic crust of Tertiary age. The volcanoes of the northern and southern parts of the chain are underlain by thick, crystalline, continental crust of pre-Tertiary age.

The High Cascade volcanoes can be divided into three groups based on composition: (1) volcanoes composed largely of andesite with small amounts of dacite erupted in the final stages of activity, e. g., Mount Rainier, Mount Hood and Mount Jefferson; (2) volcanoes composed largely of basaltic andesite, e. g., North Sister and Mount Thielsen; and (3) volcanoes largely composed of andesite and dacite, with eruption of divergent magmas during later stages of activity, e. g., South Sister, Mount Mazama, and Mount Shasta.

A second classification scheme describes the High Cascade volcanoes as coherent or divergent volcanoes on the basis of the composition of eruptive products (McBirney, 1968). Coherent volcanoes erupt largely andesite or basaltic andesite with a small range in composition. The lack of rhyolite is characteristic. Mount Rainier, Mount Hood, Mount Jefferson, and Mount Thielsen are examples of

coherent volcanoes.

Divergent volcanoes initially erupt andesite and dacite, but later eruptions produce basalt and rhyolite. In the Cascades, divergent volcanoes are found in the northern part of the Range, and south of North Sister, and include Mount St. Helens, South Sister, Mount Mazama, and Mount Shasta.

A correlation can be made between the type of volcano, coherent or divergent, and its position along the axis of the Cascade Range. Hughes, Stoiber, and Carr (1980), divided the Cascade chain into six segments based on the distribution and alignment of the volcanoes (Figure 2). The Cascade Range consists of six segments that make up the volcanic front, and three divergent centers, Simcoe Volcanic Field, Newberry Volcano, and Medicine Lake Highlands, that lie behind the volcanic front.

Coherent volcanoes are located within segments along the volcanic front. Divergent volcanoes are located along or near segment boundaries, or behind the volcanic front (Figure 2). Volcanoes near segment boundaries exhibit a wide range of composition and evidence of explosive eruptions, e. g., Glacier Peak, Mount St. Helens, and Mount Mazama.

The composite volcanoes of the Cascade chain, as well as cinder cones and boundary faults of the Cascade Graben, follow a north-south trend (Figure 3). Mid-Miocene

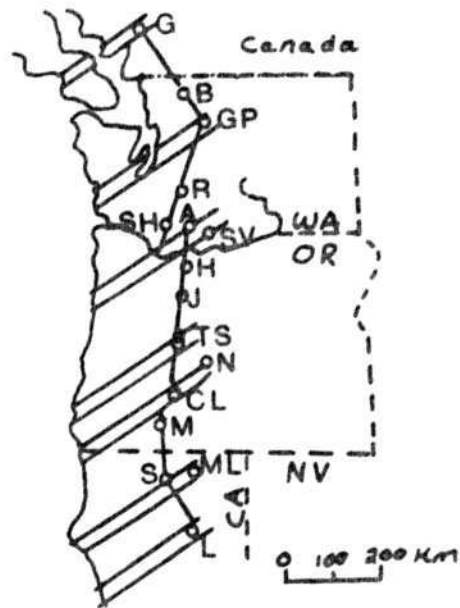


Figure 2. Segment boundaries of the Cascade Range. Abbreviations as in Figure 1 and, c-coherent volcanoes, d-divergent volcanoes. Circles-volcanoes, heavy lines-volcanic front, stippled area-segment boundary zones. After Machey, Stauber and Carr, 1980.

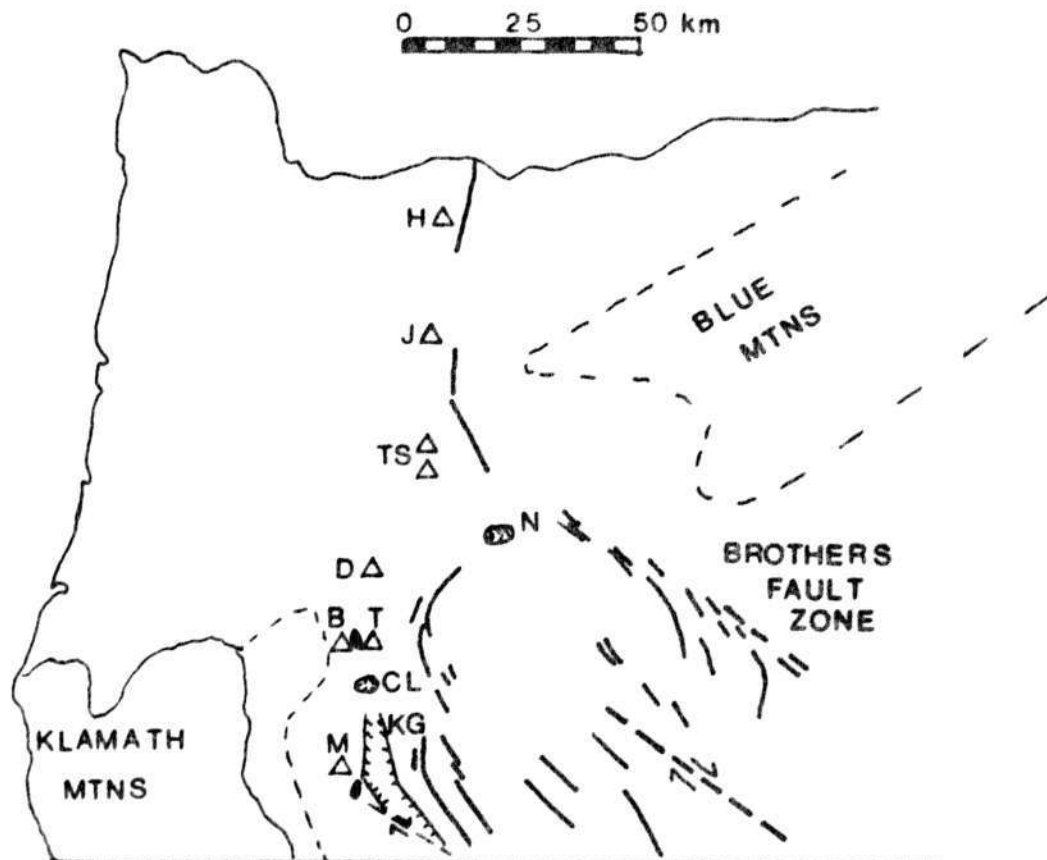


Figure 3. Index map showing major structures of southern Oregon. Abbreviations as in Figure 1 and KG- Klamath Graben. Heavy lines-normal faults, dashed lines-strike-slip faults, hachured lines, boundary faults of the Klamath Graben. Dashed pattern-inferred extension of the Klamath Mountain block (from Barnes and Ritchey, 1978). After Ritchey, 1979.

block-faulting caused uplift and westward tilting of the Western Cascades, with synchronous subsidence of the basement beneath the High Cascades (McBirney, 1978). This subsidence resulted in formation of the Cascade Graben, most of which is now filled by products of High Cascade volcanism.

Klamath Mountain Province

The Klamath Mountain Province, located southwest of Crater Lake (Figure 3), consists of folded, faulted, and deformed metaigneous, metasedimentary, ultramafic, and plutonic rocks. Fold axes and fault traces trend northeast to north-northeast. Crystalline rocks of the same age as the Klamath Mountain Province are found in the Blue Mountain Province of Eastern Oregon (Figure 3), suggesting that these rocks are continuous beneath the Cascades. If this is the case, then the volcanic rocks should reflect the structure of the underlying rocks. The trend of faults of the Cascade Range south of latitude $43^{\circ}30'$ is north-northeast to northwest, and this area is under an extensional regime (Barnes, 1978). The north-northeast trending faults parallel the trend of the Klamath Mountain Province. Barnes and Ritchey (1978) outlined a block they believe to be underlain by rocks of the Klamath Mountain Province (Figure 3).

Gravity data support this interpretation. A steep gradient parallels the boundary of the block, and the Bouger gravity values decrease eastward, indicating either thinner crust east of the outlined area, or a thick crust composed of low density material, such as sediments or volcanic material (Barnes, 1978).

Basin and Range Province

The Basin and Range Province extends into southern Oregon, and terminates against the eastern margin of the Cascades. Topographically, the Basin and Range is characterized by block-faulted mountains and the adjacent valleys. Normal faulting as a result of crustal extension produced horsts and grabens. Basaltic and bimodal volcanism is characteristic of the region. The Basin and Range of south-central Oregon is characterized by calc-alkaline volcanoes and younger and more mafic volcanism than the Nevada-Utah Basin and Range (Armstrong, 1978). Several of these volcanoes have been studied (Figure 3), including Medicine Lake Highland (Mertzmann, 1977), Newberry Volcano (MacLeod, Sherrod, Chitwood, and McKee, 1981), Yamsay Mountain (Hering, 1981), and Gearhart Mountain (Brikowski, 1983).

Medicine Lake and Newberry Volcano are basaltic shield volcanoes with calderas, located along the boundary between

the Cascades and the Oregon Basin and Range. Both volcanoes lie behind (to the east of) the Cascade volcanic front, along segment boundaries. Thus, by the scheme of Hughes, Stoiber, and Carr (1980), these volcanoes are divergent. Recent volcanism at both centers was predominantly basaltic cinder cones and rhyolitic flows. Rhyolite is present, both as pumice and obsidian flows, and hypersthene andesite is rare or totally absent. These characteristics distinguish Newberry and Medicine Lake from the Cascade volcanoes.

Faulting and shearing characteristic of the Basin and Range province extend into the Crater Lake area. In southern Oregon, the normal faults of the Basin and Range trend northwest. The northwest trending faults in southern Oregon are en echelon faults that define more extensive fault zones. Three major fault zones, the Brothers Fault Zone, the Eugene-Denio Fault Zone, and the Mount McLoughlin lineament (Lawrence, 1976; Figure 3), separate blocks broken by normal faults. South of Crater Lake, the northwest trend of the normal faults swings to the north to form the boundary faults of the Klamath Graben. If extended northward, the faults appear to converge beneath Crater Lake (Figure 2).

Barnes (1978) suggested that the Diamond Lake Basin occupies a graben that if projected to the south, would pass beneath Crater Lake. A graben extending south from

Diamond Lake is suggested by a chain of vents and cinder cones that extends from near the rim of the Crater Lake caldera northward to Diamond Lake. Two cinder cones included in this study, Red Cone and Desert Cone, are located along this trend (Figure 3). The Diamond Lake and Klamath Graben appear to be related to a north-south trending extensional feature that passes beneath Crater Lake and may be a part of the Cascade Graben.

Blank (1968) conducted gravity and magnetic studies of the Crater Lake region, and observed that the dominant lineaments trend northwest, while a lesser lineament trends northeast. The north-south lineament characteristic of the High Cascades is not apparent in the gravity or magnetic surveys. The northwest lineament may reflect either an extension of the Basin and Range into this region, or shearing related to the Brothers Fault Zone. The northeast lineament may reflect either tension associated with shearing, or an extension of Klamath Mountain structure into this region.

A major northwest-trending structure comes into the Crater Lake region from the southwest and is truncated by a northeast-trending structure near the northwest wall of the caldera. This structure is visible on the gravity and magnetic surveys. Blank (1968) proposes that the location of this structural intersection may have contributed to formation of the Crater Lake caldera. If these structures

represent some sort of intersecting fracture system, a greater volume of magma could have moved into the area and facilitated collapse of the caldera.

MacLeod, Walker, and McKee (1976) observed a decrease in the age of rhyolitic volcanism from southeast to northwest along the eastern edge of the High Cascades; the youngest volcanism is located just west of Newberry Volcano. On the basis of the symmetry of ages and the decrease in ages toward the northwest, MacLeod et. al., propose that extension is occurring along a northwest-propagating rift. Both Newberry Volcano and Crater Lake are situated near the edges of this zone of extension (Ritchey, 1979). The similarity in setting may be one reason for the similarities in composition and eruptive history between Crater Lake and Newberry Volcano.

In summary, Crater Lake National Park is located in the High Cascade Range of Oregon. The Klamath Mountain Province, located southwest of Crater Lake, is composed of crystalline rocks similar to rocks believed to underlie the Cascade Range. The Oregon Basin and Range abuts against the eastern margin of the Cascade Range. Basin and Range type faulting and shearing extend into the Crater Lake area and may have influenced the structural regime of Crater Lake National Park, and the movement of magma into Mount Mazama.

Previous Work

Diller and Patton (1902) published the first geologic study of Crater Lake National Park. Their study included a brief petrographic discussion of the following cinder cones: Bald Crater, Crater Peak, Desert Cone, Red Cone, Timber Crater, and Wizard Island.

Howel Williams (1942) published a comprehensive study of Crater Lake National Park and Mount Mazama. He included major-element analyses and petrographic descriptions of Crater Peak, Forgotten Crater, Red Cone, Timber Crater, and Wizard Island.

The divergent magmas associated with the climactic eruption of Mount Mazama were studied by Ritchey (1979). He included major and trace element studies of Red Cone and Wizard Island, and proposed that Red Cone lavas were similar in composition to the parental magmas proposed for the divergent magmas.

Bacon (1983) studied the eruptive history of Mount Mazama. Included in his study is a brief discussion of the Williams Crater Complex and Red Cone.

CHAPTER TWO

THE GEOLOGY OF CRATER LAKE NATIONAL PARK

Summary of the Geologic History of Mount Mazama

Crater Lake was discovered by white men June 12, 1853. A party of three gold miners, including John Wesley Hillman, came upon the lake while looking for the Lost Cabin gold mine. William Steel, founder of the Mazama Mountaineering Club, first visited Crater Lake in 1885. Known as the Father of Crater Lake, Steel proposed that the extinct volcano be named Mount Mazama, after the club, and was largely responsible for the establishment of Crater Lake as the nation's fifth national park in 1902.

Mount Mazama was a composite cone of the High Cascades, composed largely of hypersthene-augite andesite, which reached a height of approximately 3,500 meters. Mount Mazama was not a single symmetrical cone like many of the other Cascade volcanoes such as Mount St. Helens or Mount Hood, but was a cluster of as many as twelve overlapping cones with different vents active at different times (Bacon, 1983). No reversely magnetized lavas have been found from Mount Mazama; therefore, the volcano is younger than approximately 700,000 years, the time of the most recent magnetic reversal.

The oldest rocks in the caldera walls are exposed at the base of Dutton Cliff (Figure 4). These rocks are the remnants of a pre-Mount Mazama volcano, Phantom Cone, with an age of approximately 400,000 years, (Bacon, 1983). Phantom Cone was buried by the products of Mount Mazama, and subsequently exposed by the collapse of the caldera. Phantom Ship, located within the caldera, is composed largely of andesitic dikes radial to Phantom Cone. The remainder of Phantom Ship consists of tuff (Williams, 1942).

Hillman Peak on the western rim of the caldera (Figure 4), is the remnant of Hillman Cone. Hillman Cone was the westernmost cone of the group making up Mount Mazama, and has an age of approximately 67,000 years (Bacon, 1983). The collapse of the caldera bisected Hillman Cone. The Williams Crater Complex (discussed in Chapter 3) lies on the edge of Hillman Flow, a thick andesitic lava, that moved westward from Hillman Peak.

Llao Rock is a thick flow of rhyodacite located on the western edge of the caldera (Figure 4). Llao Rock is underlain by air-fall pumice erupted about 7015 years ago from the same vent (Bacon, 1983).

The Cleetwood Flow is a rhyodacitic lava on the northern rim of the caldera (Figure 4). Its age is between 6845 and 7800 years (Bacon, 1983). The Cleetwood Flow is

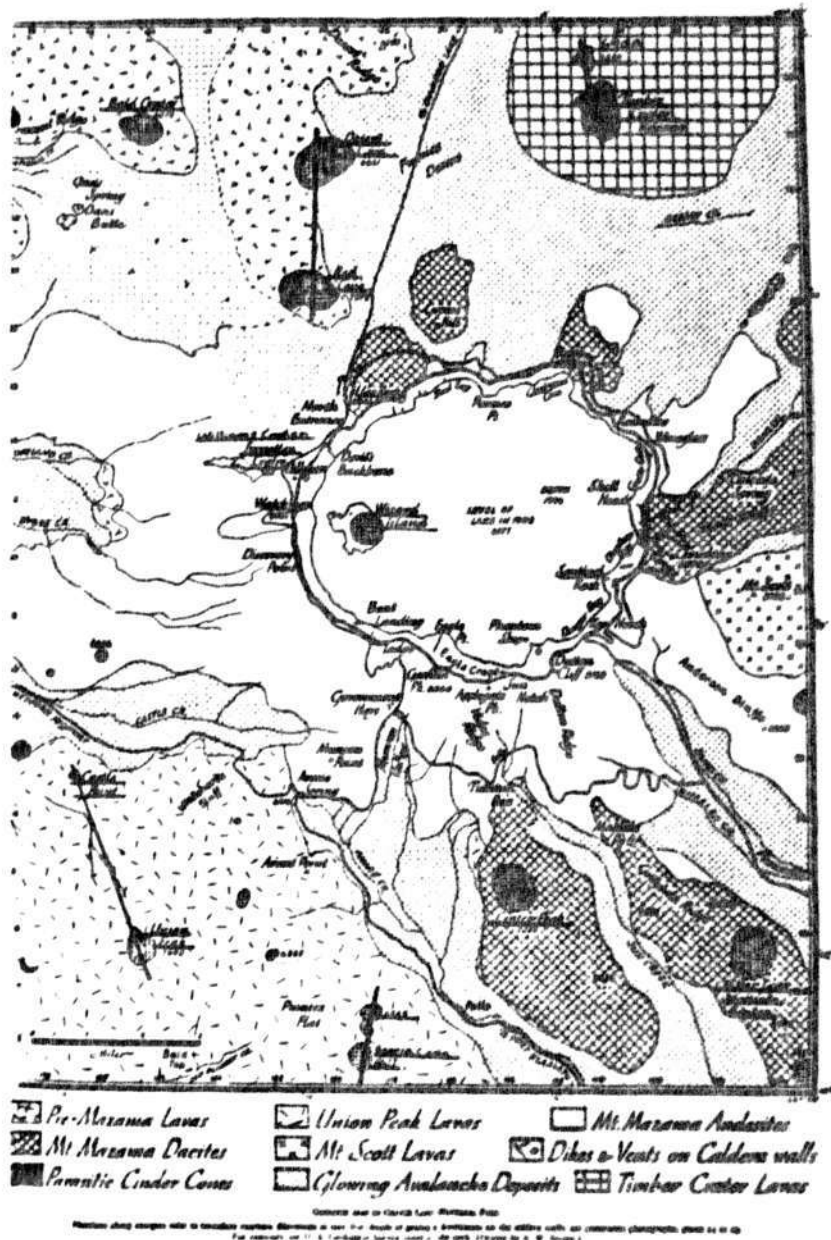


Figure 4. Geologic map of Crater Lake National Park. Cinder cones included in this study indicated by underlining of name. Includes name changes since 1942. From Williams, 1942.

only a few months older than the pumice fall from the caldera-forming eruption of Mount Mazama. This is shown by the following observations (Bacon, 1983): (1) the air-fall pumice from the climactic eruption is oxidized and welded on top of the Cleetwood Flow near the caldera, and (2) the Cleetwood Flow had not cooled completely at the time of the caldera collapse. The flow was still plastic at the time of the caldera collapse, and was able to flow down the caldera walls. In the Cleetwood Cove area, the lava flowed down the caldera walls to lake level.

The climactic eruption began soon after the eruption of Cleetwood Flow. The eruption was triggered by the extrusion of four to twelve km³ of magma, the preclimactic rhyodacite flows of Liao rock, Grouse Hill, Redcloud Cliff, and Cleetwood Flow, over a period of time possibly as short as 100-200 years (Bacon, 1983).

Removal of this amount of magma is thought to have reduced the pressure within the magma chamber, and triggered vesiculation of the magma at depth. As gases exsolved, the magma was driven up and out of the magma chamber, causing the magma to leave the chamber explosively. The magma chamber was emptied very rapidly leaving the roof of the chamber unsupported and causing it to collapse to form the caldera (Figure 5).

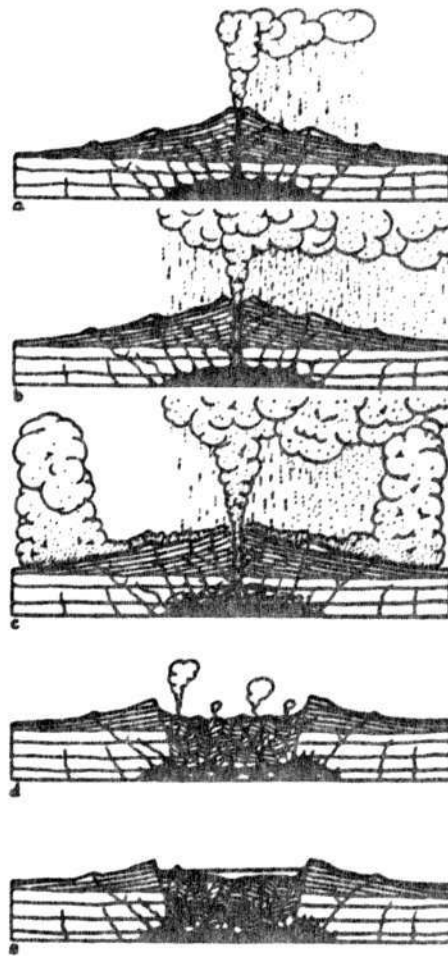


FIG. 5. The evolution of Crater Lake:

a. Beginning of culminating eruptions. Magma high in conduit; mild eruption of pumices.

b. Activity increases in violence. Showers of pumice more voluminous and ejects larger. Magma level lowers to top of feeding chamber.

c. Activity approaches the climax. Combination of vertically directed explosions with glowing avalanches (*avalanches ardentes*). Chamber being emptied rapidly; roof commencing

to fracture and founder. Magma also being drained from the chamber through fissures at depth.

d. Collapse of the cone as a jumble of enormous blocks, some of which are shown sinking through the magma. *Fumaroles* on the caldera floor.

e. Crater Lake today. Post-collapse eruptions have formed the cone of Wizard Island and probably have covered parts of the lake bottom with lava. Magma in the chamber largely crystallized.

Figure 5. The collapse of the Crater Lake caldera. From Williams, 1942. Recent work by Bacon (1983) has changed this interpretation. Mount Mazama was not a single cone, but a series of overlapping cones. The climactic eruption began with a single-vent phase, followed by the eruption of ash-flows from a ring of vents. Caldera collapse, in a manner similar to that shown here, followed the ring-vent phase.

The climactic eruption began with an explosive eruption that hurled ash high into the atmosphere. Air-fall pumice was blown in two main directions, east and northeast, by the prevailing winds. The pumice fall was followed by pumice flows in the form of glowing avalanches. These flows scoured the upper flanks of the volcano and were deposited in valleys downslope. In places, the deposits reached thicknesses of several hundred meters. For example, the Pinnacles deposit is about 65 meters thick (Figure 4).

Cinder cones and dacitic domes are located in and around Crater Lake National Park (Figure 6). Contemporaneous eruption of divergent magmas (basalt and dacite in this case) is common in the later stages of activity of many andesitic volcanoes throughout the world, and has been observed in other Cascade volcanoes (Williams, 1942). Williams (1942) believed: (1) the dacitic domes and basaltic cinder cones in the Crater Lake area are of approximately the same age, and (2) the eruptions that produced the cones and domes were among the last activity to occur before the climactic eruptions of Mount Mazama began.

The dacitic domes were of the Peléan type (Williams, 1942). The largest concentration of domes is found east of Mount Scott. Most form clusters; a few are aligned along

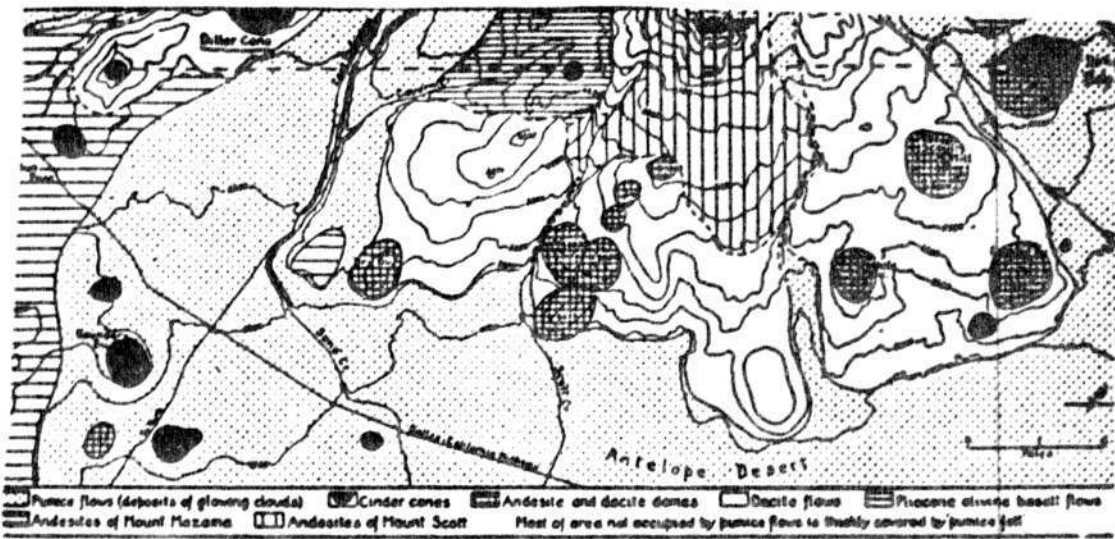


Figure 6. Location of cinder cones and dacitic domes in the Crater Lake area. From Williams, 1942.

trends radial to Mount Mazama. Weathering appears to have had little effect on the domes. The rocks appear to be relatively fresh and the associated lava flows have steep fronts (Williams, 1942).

The cinder cones included in this study are located within the boundaries of Crater Lake National Park. Other cinder cones occur outside the Park, with the large concentration to the east and south. Williams (1942) believed these cones to be of the same age and erupted from the same magma reservoir as those cones located within the Park.

Post-Caldera Volcanism

Post-caldera volcanism within the caldera produced lava flows on the floor of the caldera and two cones have been constructed. Merriam Cone is located near the northern end of the lake (Figure 7), below lake level. The cone is 402 meters high and lacks a summit crater (Williams, 1961). The large angle of repose of the ejecta (31° - 33°) indicates that Merriam Cone was erupted under subaerial conditions (Williams, 1961). It is likely, therefore, that Merriam Cone formed soon after the formation of the caldera. Wizard Island is a cinder cone composed of basaltic andesite to andesite, and is located

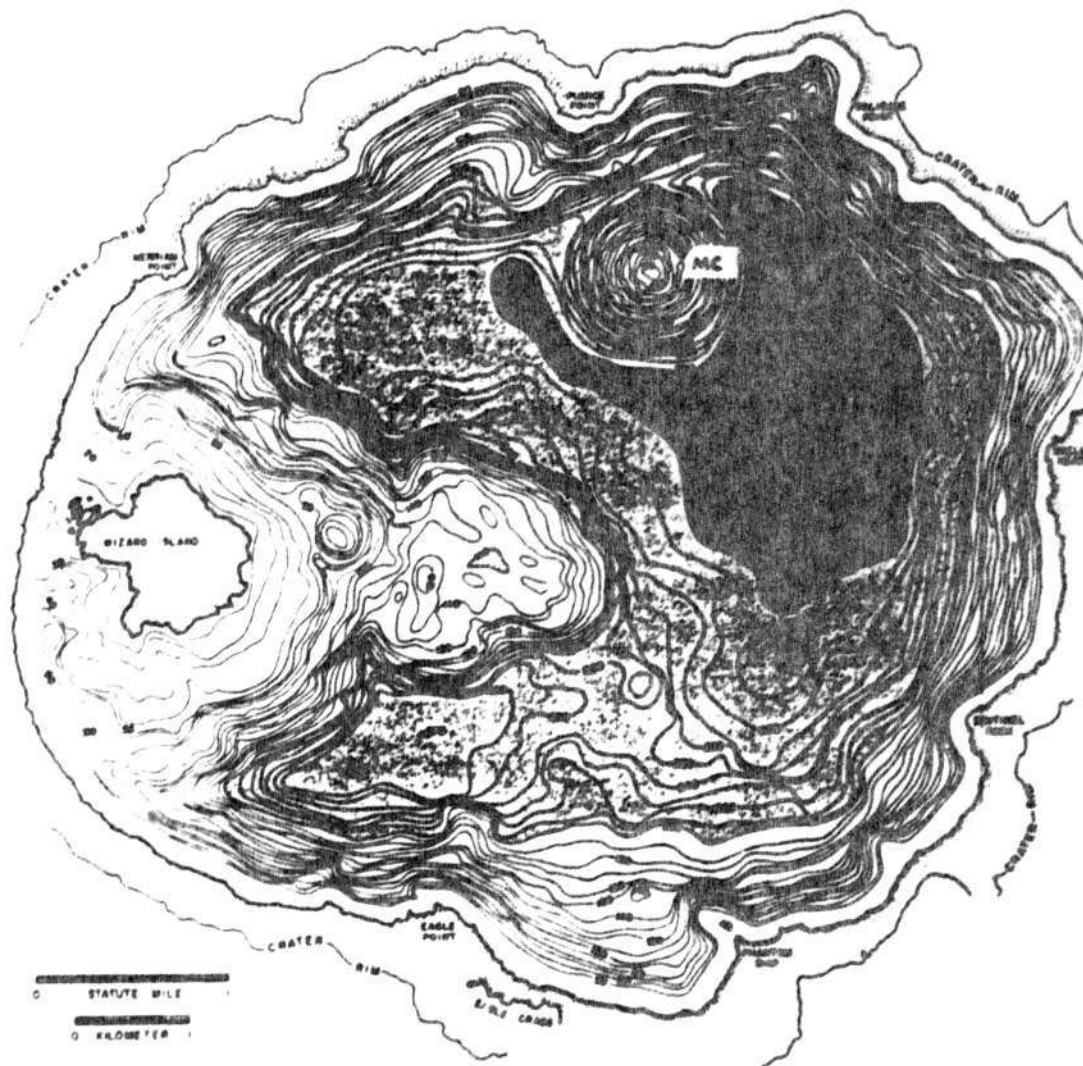


Figure 7. Floor of Crater Lake, showing the location of Wizard Island and Merriam Cone (MC). Contour interval 10 fathoms. From Byrne, 1965.

near the southwestern caldera wall (Figure 4,7). Wizard Island will be discussed in Chapter 3.

Other Volcanoes Within The Park Boundaries

Union Peak is a shield volcano with a summit cinder cone located southwest of Crater Lake (refer to Figure 4). It is composed of olivine basalt and olivine-bearing basaltic andesite and is topped by a craggy peak formed by intrusion of a plug of norite (Williams, 1942). The intrusion of the plug disturbed the bedding of the summit cinder cone and carried pieces of the cone upward; pieces of scoria can be seen in the walls of the plug. Union Peak has been heavily dissected by glaciation. From the degree of dissection, it seems likely that activity had ceased before the onset of Pleistocene glaciation. Williams (1942) noted that eruptions at Union Peak had largely come to an end by the time activity began at Mount Mazama. In appearance Union Peak is very similar to Mount Thielsen, a shield volcano north of Crater Lake National Park (refer to Figure 1). Union Peak and Mount Thielsen are also similar in terms of their evolution and structure (Williams, 1942). The summit cinder cone of Union Peak will be discussed in Chapter 3.

Timber Crater, a shield volcano in the northeastern

corner of the Park (Figure 4), is composed of olivine basalt and basaltic andesite. Mazama pumice is found at the summit of Timber Crater. Evidently, activity at Timber Crater had ended by the time of the climactic eruptions of Mount Mazama. Timber Crater must have been covered by glacial ice at one time, because glacial striae and polish can be seen on some of its lava flows. Its summit cinder cone will be discussed in Chapter 3.

CHAPTER 3

CINDER CONES

Introduction

Cinder cones are the most common subaerial volcanic features, yet are among the least studied. Notable studies of cinder cone eruptions include those of Parícutin, Mexico (Foshag and Gonzalez, 1956; Wilcox, 1948), Lunar Volcanic Field, Nevada (Scott and Trask, 1971), Pincate, Mexico (Gutmann, 1979), and Colima, Mexico (Luhr and Carmichael, 1981). Porter (1972), in a study of cinder cones on Mauna Kea, Hawaii, introduced a quantitative method for morphological studies. Pike (1978), Settle (1979), Wood (1979, 1980a), and Pike and Clow (1981), used Porter's (1972) morphological measurements in statistical studies of cinder cones. Wood (1980b) and Scott and Trask (1971) studied the morphology of cinder cone degradation.

The discovery of cone-shaped edifices of possible volcanic origin on Venus, Mars, the Earth's moon, and Io has led to an increased interest in morphological studies of terrestrial volcanic features, which, in turn, has led to a better understanding of those in other parts of the solar system.

General Characteristics of Cinder Cones

Cinder cones are products of Strombolian eruptions, and most are formed by a single eruption lasting from a few days to a few years. Wood (1980a) noted that fifty percent of observed eruptions last less than thirty days, and ninety-five percent are over in less than one year. The cones are small and have a summit crater. Lava flows commonly erupt from the summit or near the base of the cone. Lava flows may become interbedded with the scoria.

Cinder cones are composed mainly of well-stratified pyroclastic ejecta with a size range from bombs and blocks to ash. The majority of the ejecta is lapilli. Variations in the size of the ejecta indicate changes in the strength of the eruption, or changes in the direction or strength of wind (Williams and McBirney, 1979, p. 185). The erupted fragments fall close to the vent as a result of following short or high-angle trajectories (Wood, 1980a), then tumble downslope and come to rest at the angle of repose, usually between 30° to 33° . Ejecta also are deposited beyond the slopes of the cone to form a blanket around the cone.

In this way, a cinder cone forms by the accumulation of ejecta around a vent. The shape of the cone is governed by many factors including vent location, prevailing wind direction, presence of groundwater, and the volume.

viscosity, and gas content of the magma. If the eruption occurs along a fissure, an elongated cone will result. An asymmetrical cone will be built if the prevailing winds blow in one direction during the eruption, with the resulting cone skewed in the direction the wind was blowing.

If the rising magma encounters groundwater, features characteristic of phreatomagmatic eruptions, such as tuff cones, ash cones, or maars, are constructed. These cones are composed of fine, ash-size particles and glassy ejecta. Tuff rings and cones are similar in origin. A tuff ring is a crater surrounded by a low ring of ejecta. The crater floor is above the topographic level of the surrounding terrain. A maar is similar to a tuff ring, but the crater floor lies below the topographic level of the surrounding terrain.

The eruption of spatter occurs as a result of a volatile decrease in the magma during a volcanic eruption. Spatter is sticky fragments of lava that fall near the vent because they are not blown high into the air. If enough heat is retained in the fragments this spatter may be welded when deposited. If welding occurs, the cinder cone is topped by a ring of spatter or "agglutinate".

Comparisons of Cinder Cone Eruptions

Wood (1980a) compared the following eruptions:(1) Parícutin, Mexico, 1943-1952; (2) Gorschov's cone, Tolbachik volcano, Kamchatka, U.S.S.R., 1975; (3) Mt. De Fiore Superior, Mt. Etna volcano, Italy, 1974; and (4) Cratere Ducrot, located in the caldera of Piton de la Fournaise, Reunion, 1972 (Table 1). In all cases, an increase in seismic activity, followed by a decrease, preceded the eruptions. Activity began along fissures with the eruption of gaseous clouds. Within a few hours after the eruption began, the intensity of the eruption increased, explosions began (0.5 to 1 explosion/sec), and large amounts of pyroclastic material were ejected. The cinder cones reached full height within a few days. Lava flows were erupted one to two days after the eruption began. The intensity of the eruption decreased as the cone approached its final height. The volume of ejecta decreased, and the volume of lava flows increased, with a decrease in eruption intensity. In general, the total volume of lava flows is greater than the total volume of the cinder cone. For larger cinder cone eruptions, the total volume of pyroclastic material (the cinder cone plus ejecta deposited beyond the slopes of the cone) is greater than the total volume of lava flows.

Table 1. Characteristics of four cinder cone eruptions
(from Wood, 1980a).

property	Paricutin ¹ , Mexico	Gomshov's Cone ² , U.S.S.R.	De Fiore Superior ³ , Italy	Ducrot ⁴ , Reunion
Cone basal diameter (km)	1.07	1.65	0.8	0.13
Cone height (km)	0.20	0.33	0.06	0.04
Crater diameter (km)	0.27?	0.33?	0.07?	0.01
Cone volume (10 ⁶ m ³)	157	165	2.7	0.2
Lava volume (10 ⁶ m ³)	700		0.5	4.0
Total volume (10 ⁶ m ³)	2100		3.6	4.2
Eruption energy (erg)	3.9×10 ¹⁴			1.5×10 ¹⁴
Eruption duration (days)	3299	35	18	18
Max. gas velocity (m/s)	170	260		
Gas/solid ratio	0.011	0.90		
Max. bomb height (km)	1.2	2.5	0.7	0.1
Max. height eruption cloud (km)	6	8-12	2.6	
Duration warning tremors (days)	16	8	10	
Time to first lava flow (days)	1	23	1	0
Lava type	basalt to basaltic andesite	alkali basalt	alkali basalt	olivine basalt

The volumes of Parícutin and Gorschov's cone are very similar even though the eruption of Parícutin lasted much longer (Table 1). Wood (1980a) attributes the phenomenon to a difference in the viscosity of the magmas. He proposes that the Parícutin magmas were more viscous, and that the system was less energetic. Lower heights of bombs and the eruptive column, lower gas velocities, and a smaller gas/solid ratio for the Parícutin eruption support Wood's deduction (Table 1).

Morphology

Cinder cones evolve in four stages, of which the first, third and fourth, may not occur at every cone.

1. Basal lava flows precede the Strombolian eruptions that build the cone.
2. Pyroclastic material accumulates around the vent forming the cinder cone.
3. Lava lakes form at the summit of the cone; dikes and sills are injected.
4. The cone is breached by summit and/or flank lava flows.

The maximum observed basal diameter of a cinder cone is 2.0-2.5 km. Two factors control this parameter:

1) evolution of the cinder cone into a composite cone (Crowe, Halleck, and Nolf, 1978), and 2) crustal thickness (Wood, 1980a).

The injection of sills and dikes in the later stages of cone growth increases the strength of a cinder cone. The increasing strength allows the cone to grow by summit eruptions. If activity continues and the basal cone diameter becomes greater than 2.5 km, the cinder cone evolves into a composite cone, by definition. This will be true only for cinder cones with the characteristics of a larger cone. In other words, the cone must have a large volume and rate of growth and effusion, and the eruption must be such that it continues beyond the few days or weeks characteristic of a monogenetic eruption.

Cinder cones occur in two volcanic provinces (Settle, 1979): (1) cone fields on the flanks of volcanoes where the clusters of cones tend to be aligned along radial trends, and (2) cone fields on relatively flat platforms where the cones are associated with widespread lava flows. There may be no systematic arrangement of the cones; they tend to be scattered throughout the field.

Morphological characteristics of cinder cones can be used to distinguish the two provinces. Porter (1972), in a study of cinder cones on the flanks of Mauna Kea, introduced a system of measuring these characteristics.

The important parameters are (Figure 8):

W_{cr} = crater width
 D_{cr} = crater depth
 H_{cr} = cone height
 W_{co} = basal cone diameter
 α_{co} = maximum slope angle

The following values of $H_{co} = xW_{co}$ have been reported:

$H_{co} = 0.18W_{co}$, Porter (1972), 30 Mauna Kea cinder cones,
 $H_{co} = 0.18W_{co}$, Wood (1980a), 83 cinder cones from various parts of the world,
 $H_{co} = 0.19W_{co}$, Bloomfield (1975), young Pleistocene cinder cones, central Mexico, and,
 $H_{co} = 0.21W_{co}$, Bloomfield (1975), Holocene cinder cones, central Mexico.

Settle (1979) plotted H_{co} versus W_{co} (note that Settle uses D_{co} instead of W_{co}) for two cinder cone fields on the flanks of Mauna Kea and Mount Etna, and two cinder cone fields on platforms, the San Francisco Field and Nunivak Island (Figure 9). The line $H_{co} = 0.20 W_{co}$ is plotted for reference. Comparison of H_{co}/W_{co} values suggests that this line may represent the initial shape of cinder cones in both types of cone fields, before any degradation occurs (Settle, 1979).

H_{co}/W_{co} values decrease as degradation increases. One result of degradation is a decrease in cone height and an increase in basal cone diameter, which results in a decrease in H_{co}/W_{co} values. Settle (1979) notes that the

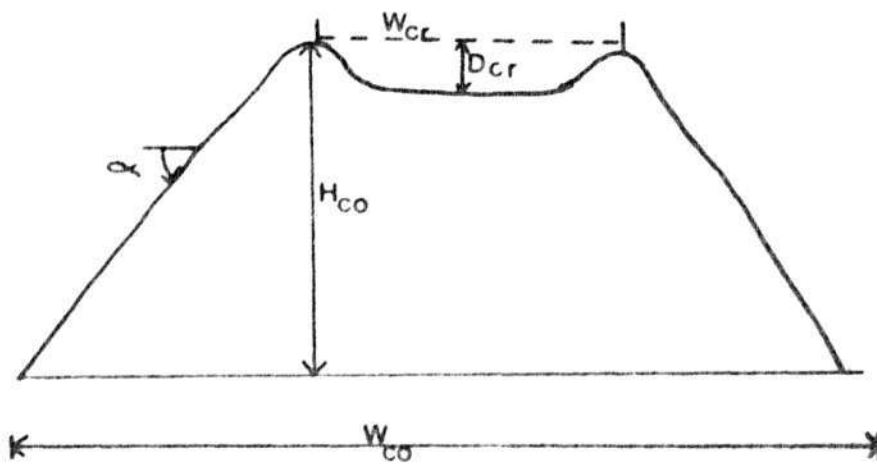


Figure 8. Diagram illustrating measurements of cinder cone parameters. Abbreviations: W_{cr} = crater width, D_{cr} = crater depth, H_{co} = cone height, W_{co} = basal cone diameter, and α = maximum slope angle.

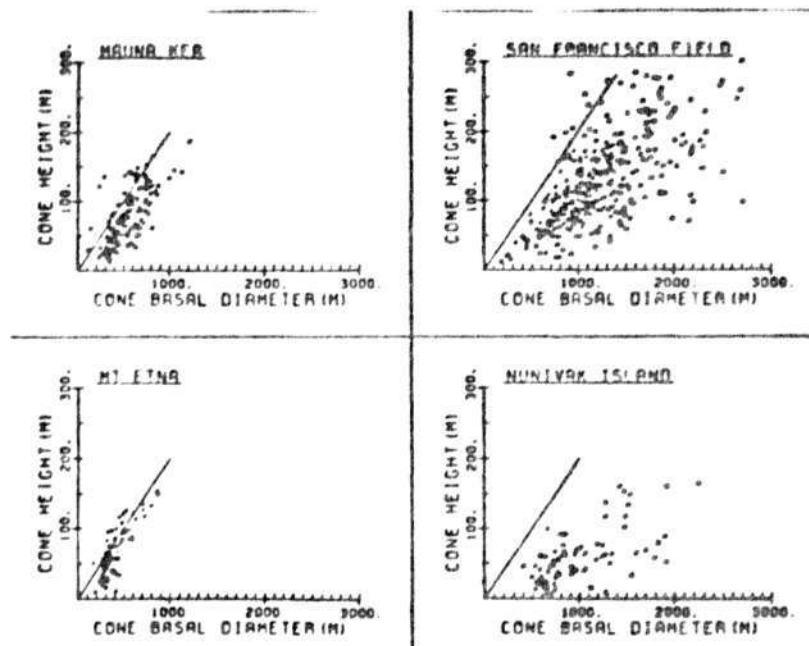


Figure 9. Cone height versus basal cone diameter for two cone fields on volcanoes, Mauna Kea and Mt. Etna, and two platform cone fields, San Francisco field and Nunivak Island. The straight line represents $H_{co} = 0.20 W_{co}$. (From Settle, 1979).

majority of the Mauna Kea cinder cones plot below the $H_{co}/W_{co}=0.20$ line, suggesting that the above type of degradation is occurring.

In summary, morphological characteristics of cinder cones can be used to distinguish the two types of fields (Table 2). The ratio of cone height to basal cone diameter is smaller for cone fields on volcanoes, whereas basal cone diameter and cone separation distance are smaller for cone fields on volcanoes.

Table 2
Morphological Characteristics of Cinder Cone Fields
(Settle, 1979)

	Cinder cone fields on volcanoes	Cinder cone fields on platforms
Basal cone diameter	300-400	900-1000
Cone height	60-80	60-80
Cone separation distance	600-800	1000-1200

Values are in meters and given as modal averages.

Degradation of Cinder Cones

Morphological studies of cinder cones can be used to examine the effects of weathering and erosion. Four factors influence the modification of cone shape: 1) Climate which controls the weathering environment, 2) the movement of materials downslope, 3) cone size which affects the rate of erosion because smaller cones erode at a faster rate, and 4) the burial of the cone flanks by subsequent lava flows. Erosional processes result in an increase in W_{CO} values, and a decrease in H_{CO} , α , and H_{CO}/W_{CO} values. W_{CR}/W_{CO} values are relatively unaffected by weathering, chemical composition, or particle size (Wood, 1980b).

Scott and Trask (1971) studied the degradation of cinder cones at Lunar Crater Volcanic Field, Nevada. They introduced measurements used in degradation studies (Figure 10), r =basal cone radius, calculated as 1/2 basal cone diameter, and s =length of the maximum slope. Other values are the same as those described on page 35. Values for r/H_{CO} increase and H_{CO}/W_{CO} decrease as age increases for the cinder cones at Lunar Crater Volcanic Field (Scott and Trask, 1971). The smaller H_{CO}/W_{CO} may be due to the elevation of the surrounding terrain as a result of the emplacement of lava flows (Scott and Trask, 1971), or the

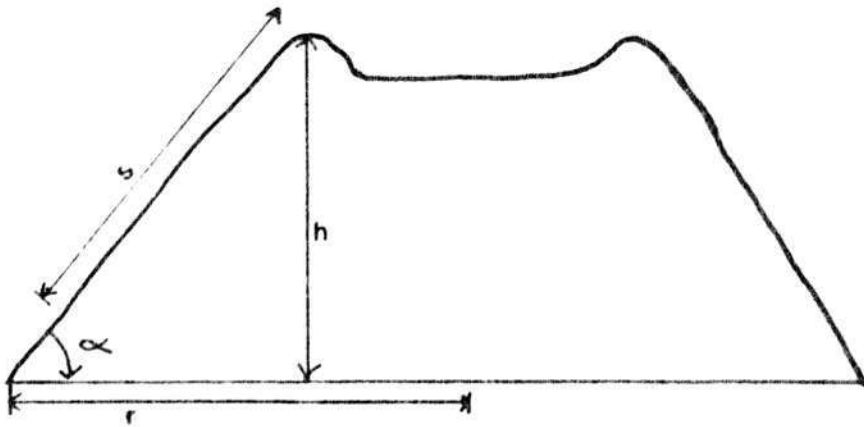


Figure 10. Diagram illustrating morphological characteristics used in degradation studies (after Scott and Trask, 1971).

result of degradation, as mentioned earlier.

The relative ages determined through the use of morphological characteristics can be affected by a variety of factors (Scott and Trask, 1971). Any change that results in the cinder cone not having a normal shape and structure will affect the pattern of erosion. This, in turn, affects the ages determined. The most important factors to consider are the internal structure of the cone, irregular cone shape, and the original shape of the cone.

Emplacement of Cinder Cone Fields

The alignment and distribution of cinder cones can provide information about regional structures. The distribution of cinder cones is largely controlled by near-surface fractures (Settle, 1979). Magma intruded into a platform cone field encounters a series of fractures in the crust. The magma is channelled into fracture intersections, producing a scattered distribution of cinder cones (Settle, 1979). Magma moving into a volcano encounters the fracture system of that volcano and will be channelled along these fractures. At the surface, the cinder cones will tend to be distributed along fractures radial to the volcano. Studies by Porter (1972), Settle (1979), and Wood (1980a), show that the distances between cinder cones are, in most cases, larger for

Crater Lake Cinder Cones

The Mount Mazama cinder cones are located on or near the flanks of Mount Mazama, or, in the case of Wizard Island, within the caldera (Figure 11). Many of these cones are aligned along trends radial to Mount Mazama, perhaps the surface expression of basement fracture systems. Three groups of cinder cones and the Williams Crater Complex are aligned along trends that suggest a structural control (Figure 11).

The alignment of cinder cones associated with Timber Crater and Union Peak (Figure 11) also suggests control by underlying structures. Castle Point and the summit cinder cone of Union Peak are aligned northwest-southeast. Hill 6902 and both vents of the summit cinder cone of Timber Crater are aligned north-south.

Most of the Mount Mazama cinder cones are concentrated south and west of Crater Lake. The cones are monogenetic and are composed mainly of pyroclastic ejecta, although small lava flows are visible on some of the cones. The ejecta are predominantly scoriaceous, with a size range of fragments from bombs and blocks to lapilli and ash. The lapilli and ash form a loose matrix in which the bombs and blocks are deposited (Figure 12). Red is the most common color of ejecta; black and brown ejecta are subordinate.

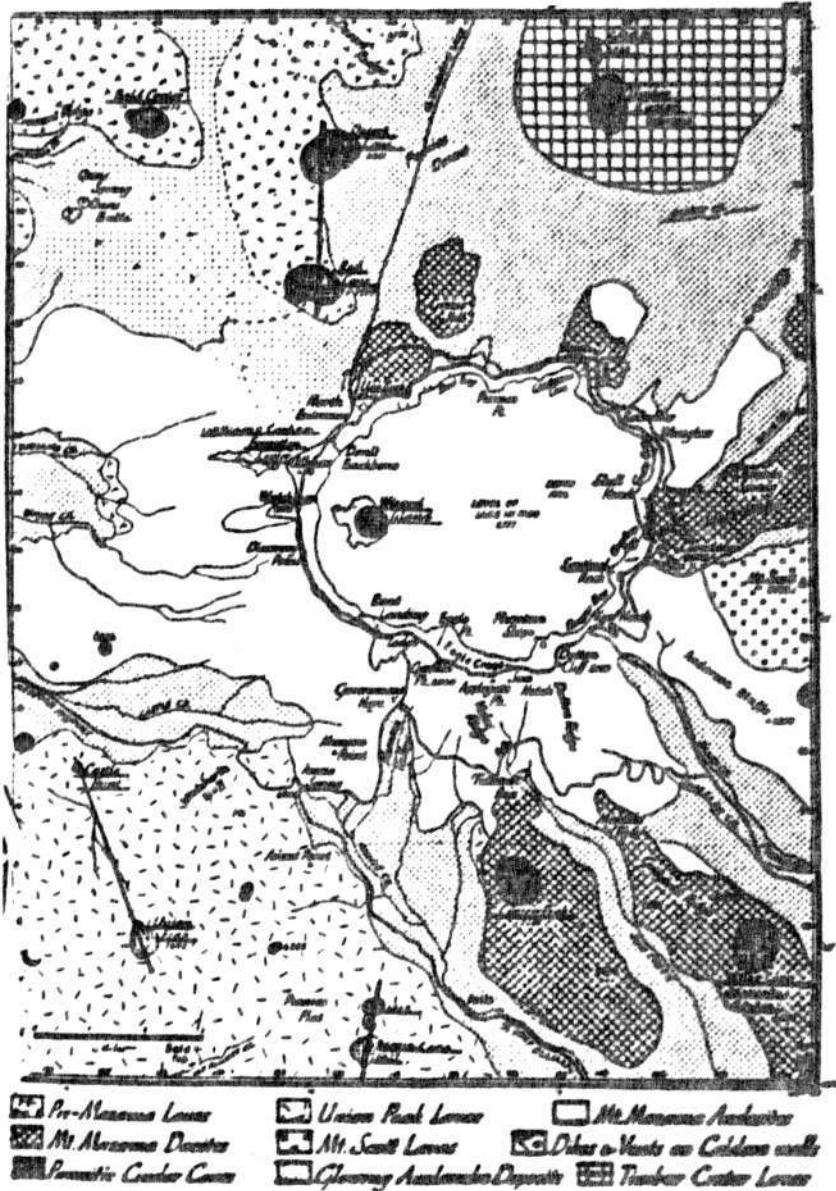


Figure 11. Geologic map of Crater Lake National Park. Cinder cones in this study indicated by underlining of name. Trends of cinder cones indicated by heavy lines. Includes name changes since 1942. After Williams, 1942.

Most, if not all, of the cinder cones probably erupted lava flows, but for various reasons the flows are no longer visible. Three probable burial mechanisms are: subsequent volcanic activity, soil formation, and slides. First, the flows may have erupted low on the flanks of the cones, or near the base. These flows would have been buried by younger activity from the cone or from Mount Mazama. Some of the ash flow deposits from the climactic eruption of Mount Mazama are known to be hundreds of meters thick. Many of the cinder cones were partly buried by these flows. Second, most of Crater Lake National Park is heavily wooded. It is likely that many lava flows have been covered by soil and vegetation. Third, scoria slides have occurred on many of the cinder cones. The material deposited by the slides has totally or partly buried some lava flows.

Most samples collected from each cinder cone are lithologically similar. A brief description of each rock type, scoria and lava flow, will be included here. The scoriaceous samples are porphyritic with a glassy

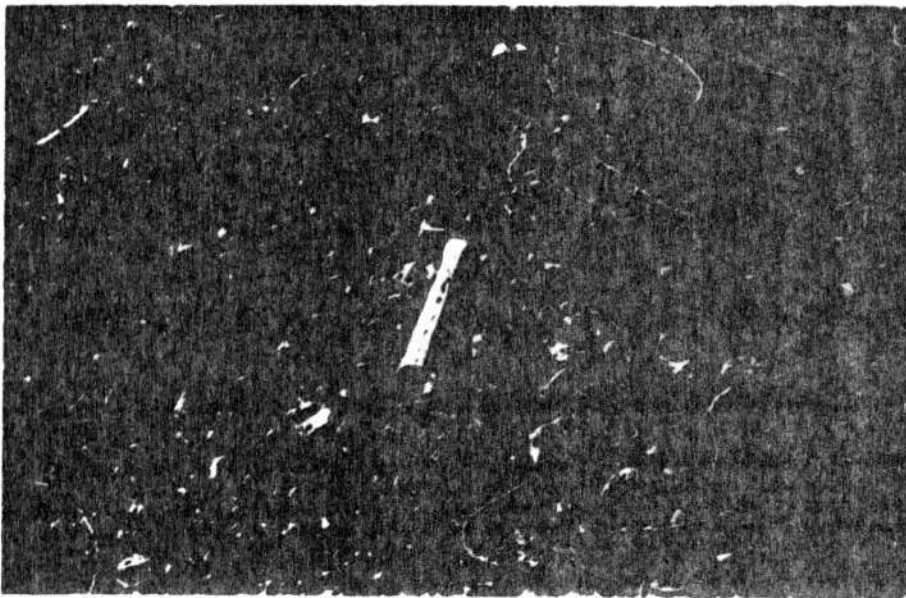


Figure 12. Sample location on Red Cone. Note the size range of the ejecta. The majority of the ejecta are bombs and lapilli.

groundmass. The vesicles range from less than 0.1 mm to 3 cm, and compose forty to ninety percent of the rock (Figure 13). The vesicles are smaller near the outside of the sample and increase in size toward the center. In some samples the vesicles are flattened and aligned. In both rock types plagioclase is the most commonly observed phenocryst, followed by olivine and pyroxene. The amount of visible phenocrysts decreases as the amount of vesicles increases.

In hand sample, many of the lava flows resemble a typical basalt (Figure 14). Most are gray in color; others are black or red. The rocks are porphyritic and some contain ten to twenty percent vesicles.

The cinder cones included in this study are similar in appearance. Those of Mount Mazama will be described first before turning to the Timber Crater and Union Peak cones. See Figure 11 for location and Table 5 for the physical characteristics of the cinder cones. Table 3 shows the relationship between rock name and percent SiO_2 .

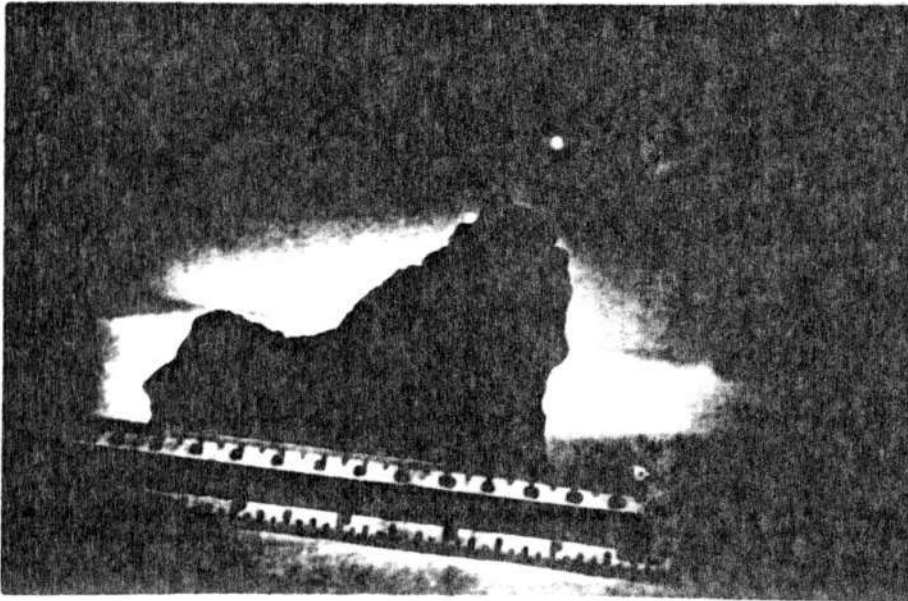


Figure 13. Hand sample of scoria from Bald Crater.

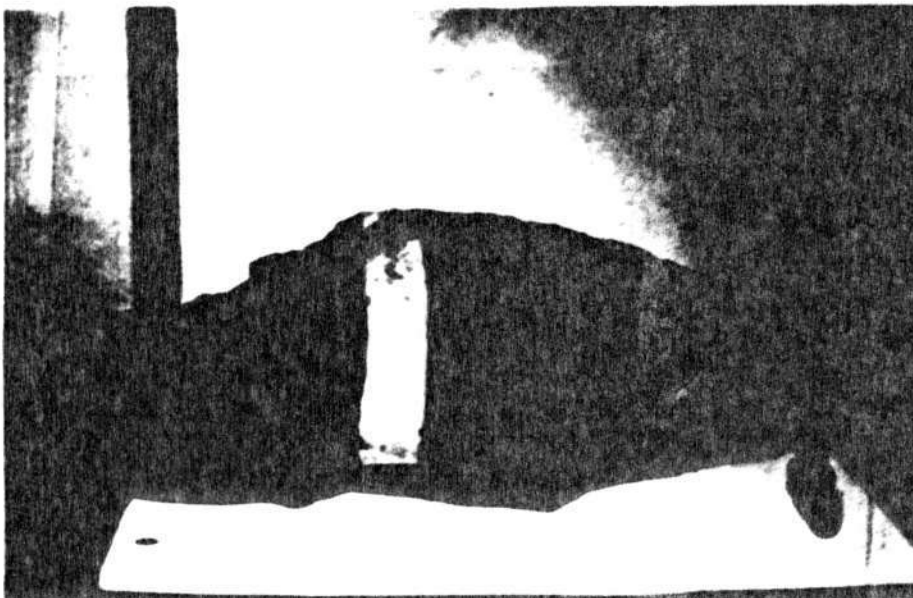


Figure 14. Hand sample of lava flow from Red Cone.

Table 3. The relationship between % SiO₂ and rock names used to describe samples.

Rock name	Weight percent SiO ₂
Basalt	< 53.5
Andesitic basalt	53.5 - 56
Basaltic andesite	56 - 58
Andesite	58 - 63
Dacite	63 - 68
Rhyodacite	68 - 72
Rhyolite	> 72

Mount Mazama Cinder Cones

Bald Crater (BC) (Letters in parentheses are used to identify cones in Figures, Tables, and Appendices.)

Bald Crater is a heavily vegetated cinder cone located in the northwest part of Crater Lake National Park. The cone was partly buried by ash flows from the caldera-forming eruption of Mount Mazama. Lava flows have been exposed near the summit by scoria slides. The summit of the cone is nearly flat with no trace of a vent, and the flanks are composed of scoria with a few lava flows. All samples analysed from this cone contain about 54% SiO_2 .

Desert Cone (DC)

Desert Cone is located in the Pumice Desert, and has been partly buried by ash flows from Mount Mazama. The cone is heavily vegetated, but slides have exposed scoria and lava flows. The ejecta consist of bombs and lesser amounts of lapilli. A shallow depression at the summit may mark the vent. Figure 15 shows two bombs from Desert Cone. Samples from Desert Cone contain about 53% SiO_2 .

Red Cone (RC)

Red Cone is located south of Desert Cone, also in the Pumice Desert. Red Cone is among the least vegetated cones in the Park, and is easily identified as a cinder cone. The cone itself is nearly symmetrical and has a shallow summit crater breached on the north. Glacial striae and polish on its flows show that ice was once present on the cone. It is also likely that the lower flanks of Red Cone were scoured by ash flows from the climactic eruption of Mount Mazama. The cone is composed of ejecta and lava flows. Agglutinate is abundant near the summit. The ejecta are predominantly red scoria bombs, blocks, and lapilli, although ash is present in small amounts. Bombs have a variety of shapes and sizes (Figure 16). Samples from Red Cone contain 53 to 54% SiO_2 .

Hill 6545 (65) and Scoria Cone (SC)

Hill 6545 and Scoria Cone are located south of Crater Lake, and stand on lavas of Union Peak. These cones are regarded as Mount Mazama cinder cones, because they lie on a fissure radial to Mount Mazama (Williams, 1942), and are similar in petrographic characteristics and chemical

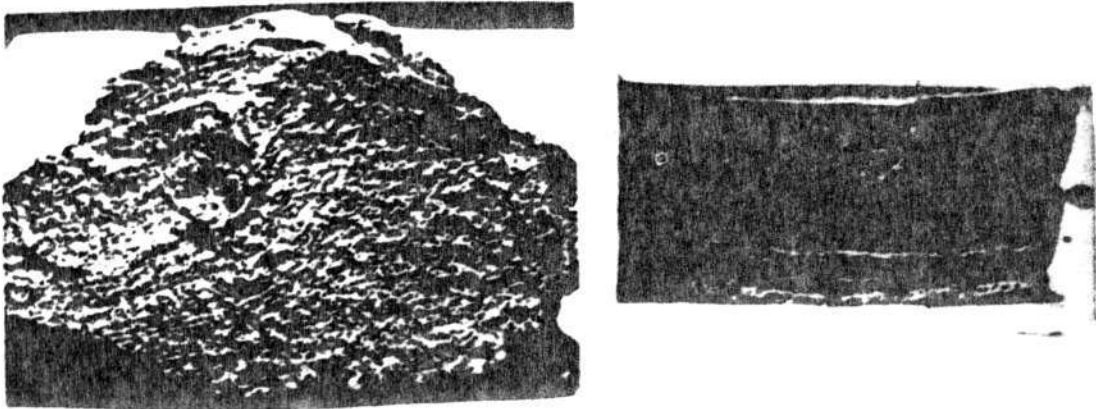


Figure 15. Desert Cone bombs.
a. spindle bomb b. ribbon bomb

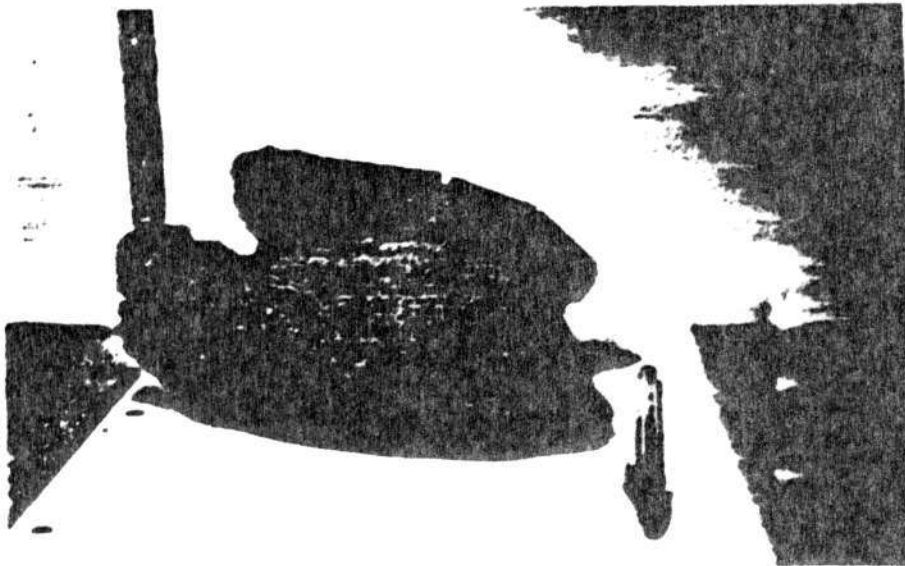


Figure 16. Red Cone bomb. Note breadcrust texture on
outer edges and streamlined shape.

composition to the other Mount Mazama cinder cones.

Hill 6545 is small and covered by vegetation. The cone consists largely of small fragments of red ejecta. An analyzed sample contains 53% SiO_2 .

Scoria Cone is also vegetated but not as heavily. It consists of red scoria bombs and lapilli with minor ash. Agglutinate is abundant near the summit. A double crater is present at the summit. The larger crater is the older crater and explosive in origin (Mertzman, 1980). This is the vent from which Scoria Cone was built. The inner crater was formed by collapse, analogous to Hawaiian pit craters (Williams, 1942). Samples from Scoria Cone contain 54 to 55% SiO_2 .

Crater Peak (CP)

Crater Peak stands on the southern flank of Mount Mazama. It is a symmetrical, vegetated cone with a shallow, summit depression. The cone consists of red, black, and brown bombs and lapilli. Red agglutinate is found at the summit, and lava flows were erupted from near the base of the cone. Crater Peak samples contain 56 to 59% SiO_2 .

Maklaks Crater (MC)

Maklaks Crater is a symmetrical cone on Grayback Ridge in the southeastern corner of Crater Lake National Park. The cone is heavily vegetated and, although not much rock is exposed, scoria is exposed near the summit and isolated outcrops of andesitic basalt can be found on the flanks of the cone. The exposed material is red scoriaceous bombs with some agglutinate and a few lava flows. The summit is flat. The rocks contain 52 to 53% SiO₂.

Wizard Island (WI)

Wizard Island, located in the Crater Lake caldera, is a symmetrical cone with a well-preserved summit crater (Figure 17). Lava flows surround the cone and extend westward from the base (Figure 18). The cone consists of blocks and lapilli, with lesser amounts of bombs and little ash. Red and black agglutinate is abundant at the crater rim and in the crater. The majority of the ejecta is black scoria but smaller amounts of red and brown ejecta are found. Most of the ejecta is angular to subangular, indicating that the fragments were nearly solid at the time of eruption. Many of the samples contain volcanic

inclusions, some of which were ripped from the conduit as the magma rose to the crater. The summit crater is approximately thirty meters deep. On the crater floor, the location of the vent is marked by black, scoriaceous lava filled with inclusions.

After the cone was built lava flows erupted from vents near the base. An aa flow spread to the west of Wizard Island with conspicuous concentric ridges (Figure 18). A second, younger flow that spread to the northwest is more scoriaceous and brown on weathered surfaces. Samples from Wizard Island contain 58 to 60% SiO_2 .

Williams Crater Complex (WC)

The Williams Crater Complex is located near the west rim of the Crater Lake caldera (Figure 19). Williams Crater differs from the other cinder cones in this study in that it consists of a basalt flow and a fissure vent system, flows or domes of mixed, andesitic to dacitic lavas (Bacon, 1983), and a cinder cone. The cinder cone, fissure vent, and the vents for the mixed lava flows, are oriented $\text{N}70^\circ\text{W}$. The basaltic flow lies near the base of the cinder cone, and may be older than the cone. The mixed lavas overlie the basalt flow and the cinder cone and are presumably younger.

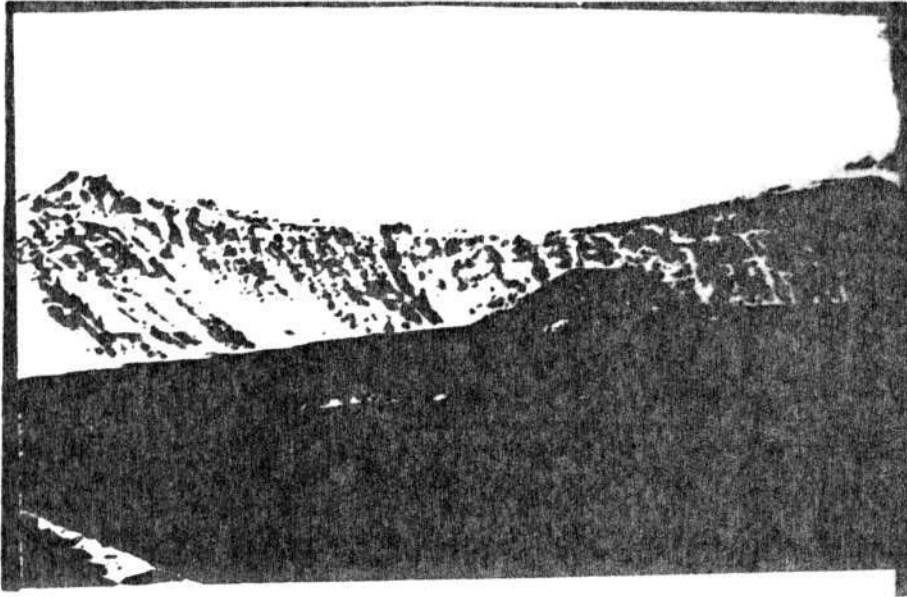


Figure 17. Wizard Island

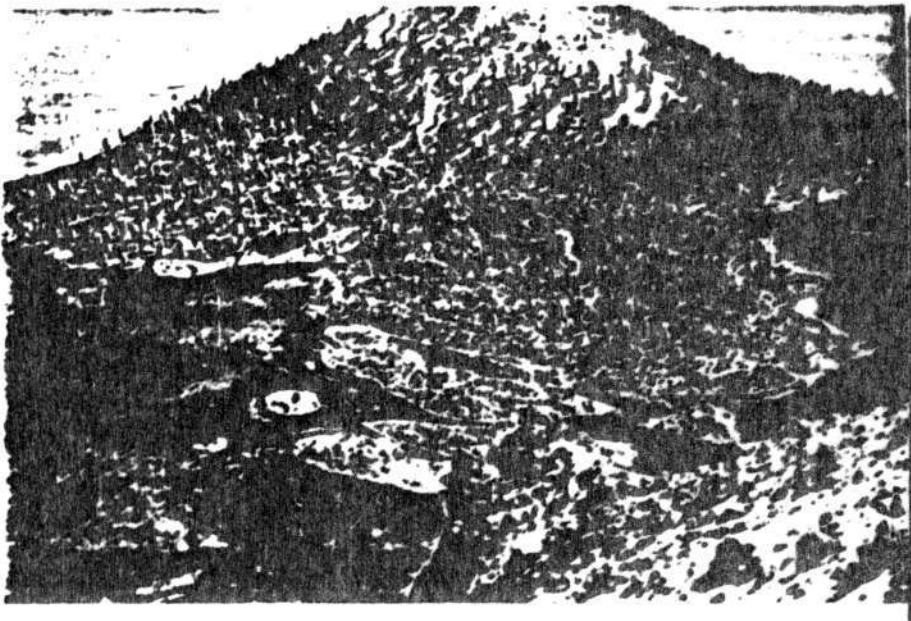


Figure 18. Lava flows extending from the western end of Wizard Island.

Mixed lavas, dacitic in composition, were erupted from the cinder cone, and east of the cone near the Rim Road. These lavas contain andesitic bands and basaltic inclusions. There is a question as to whether the lavas near the Rim Road are domes or parts of lava flows, but further work may resolve this question.

The cone is built on the western edge of Hillman Flow, an andesitic lava that issued from Hillman Peak. The summit of the cone is marked by a shallow crater that contains two shallow depressions that are separated by a small ridge. The rim of the crater is marked by a ridge of red scoria and agglutinate, except on the eastern side where the rim has been destroyed. The south side of the crater was breached by a dacitic lava flow (Figure 19).

The cone itself consists of ejecta and lava flows. The ejecta are red, scoriaceous bombs and lapilli, with agglutinate and smaller amounts of black scoria. A few bombs have cores of basalt, andesite, and dacite, some of which are pumiceous. Mixed lavas are also found as scoria-coated bombs or cores of bombs (Figure 20). Samples from Williams Crater contain 51 to 68% SiO_2 .



Figure 19. Williams Crater

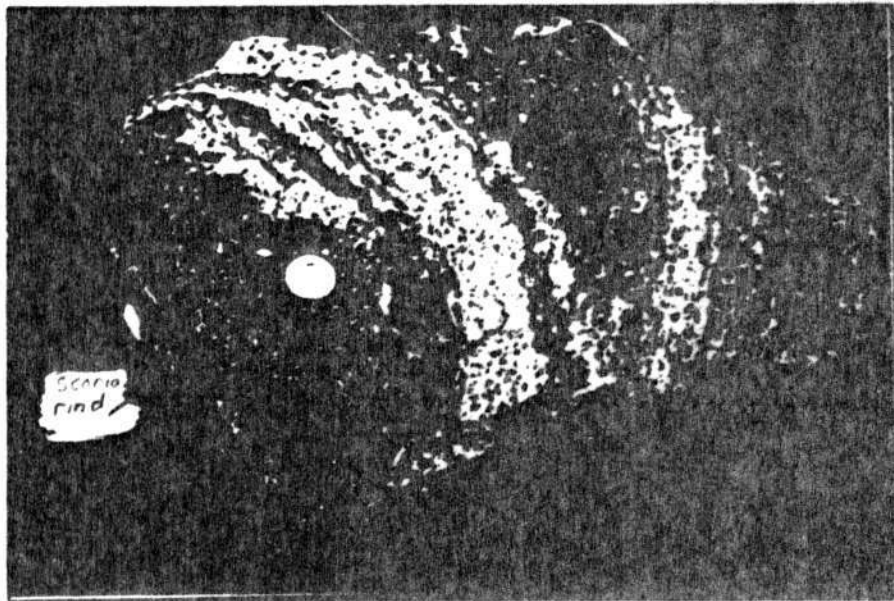


Figure 20. Bomb from Williams Crater. Note mixed lavas and scoria rind.

Bacon (1983) inferred that a normal fault with a trend of N10°E was buried by the products of the caldera-forming eruption. The beginning of the basaltic flow lies near the projection of this fault (Bacon, 1983). This structural intersection played an important part in the development of the Williams Crater Complex. Activity probably began with eruption of basaltic magma. A fracture system developed, or existing fractures radial to Mount Mazama reopened, after activity began. This led to tapping of the zoned magma chamber of Mount Mazama. The scoria-coated bombs of mixed magma are interpreted as evidence that the magma chamber was zoned when it was tapped. The interaction between the basaltic magmas and the zoned magmas produced the wide variety of complex lavas seen at Williams Crater.

Timber Crater Cinder Cones

Two cinder cones are associated with Timber Crater, Hill 6902 and an unnamed summit cinder cone. Activity at Timber Crater began at Hill 6902, then shifted southward to the summit of Timber Crater.

Hill 6902 (69)

Hill 6902 is a heavily wooded hill located on the northern flank of Timber Crater. Little of the cone is preserved, and no summit depression is visible. Red and

black scoria and agglutinate are exposed in a few places. A sample from Hill 6902 contains about 58% SiO_2 .

Summit Cinder Cone

This cone is located at the summit of Timber Crater. Most of the cone is covered by vegetation. A depression is present at the summit. The cone consists of black, scorificaceous bombs and lapilli, and a few lava flows. Samples from the cone range from 54 to 59% SiO_2 .

Union Peak Cinder Cones

Several cinder cones are associated with Union Peak (Williams, 1942). Two of these, Castle Point and the summit cinder cone, are included in this study.

Castle Point (CPT)

Castle Point is located on a ridge near the northern flank of Union Peak. The cone is heavily vegetated, partly destroyed, and has no summit depression. Near the summit, slides have exposed the underlying rock. The cone consists of red, black, and brown lapilli and bombs. A few bombs have rosy, iridescent rinds. Samples from Castle Point contain 50 to 54% SiO_2 .

Summit Cinder Cone

The summit cinder cone erupted into the crater of Union Peak, and consists of red and black ejecta with a few lava flows. The ejecta are mainly bombs and lapilli, with subordinate ash. Agglutinate becomes more abundant near the summit of the cone. After the cinder cone formed it was intruded by the plug that forms the summit pinnacle of Union Peak. The plug carried parts of the cinder cone with it as it moved upward. Patches of red and black scoria are visible in the plug. Samples from the cinder cone contain 53 to 55% SiO_2 .

Ages of Cinder Cones

Few ages have been determined for the Crater Lake cinder cones. The cones appear to be younger than about 50,000 years, judging from the amounts of weathering they have suffered, the amount of soil cover, and the material on which the cones stand. Mazama ash and pumice are found on most of the cinder cones. Therefore, activity at these cones ended before the climactic eruption of Mount Mazama. Two relative and four radiometric ages have been determined for the Crater Lake cinder cones (Table 4).

Table 4. Measured ages of Mount Mazama Cinder Cones

Cone	Age Reference	Method of determination
Wizard Island	6700 years Champion, 1983	paleomagnetism (tentative age)
Timber Crater	19,000 \pm 18,000 years Lanphere, 1984, personal communication	K/Ar
Williams Crater	22,000-30,000 years Bacon, 1983	glaciation, superposition, and paleomagnetism
Red Cone	36,000 \pm 12,000 years Lanphere, 1984, pers. comm.	K/Ar
Scoria Cone	< 45,000 years Mertzman, 1982, pers. comm.	K/Ar
Desert Cone	201,000 \pm 48,000 years Lanphere, 1984, pers. comm.	K/Ar

K/Ar ages for all samples except Scoria Cone determined by Lanphere (unpublished data) at the U.S.G.S in Menlo Park, CA.

Table 5. Morphological characteristics of Mount Mazama cinder cones. See Figure 4 for location. Measurements in meters.

Cone	Basal cone diameter (W_{co})	Cone height (H_{co})	Crater diameter (W_{cr})	Flank width	Slope angle (α)
BC	770	146	99	315	28
DC	926	138	130	391	22
RC	1387	266	152	694	23
65	610	90	nc	606	20
SC	625	113	152	381	19
CP	1295	241	152	619	24
MC	1219	208	nc	535	24
WI	1082	233	152	471	29

Table 5 continued.

Cone	Volume	H_{co}/W_{co}	r/H_{co}
BC	1.517×10^7	.19	2.64
DC	2.210×10^7	.15	3.36
RC	3.416×10^7	.19	2.61
65	0.750×10^7	.15	3.39
SC	1.718×10^7	.18	2.76
CP	9.670×10^7	.19	2.69
MC	6.235×10^7	.17	4.13
WI	5.413×10^7	.21	2.32

nc = no crater, nd = not determined.

Morphological Characteristics of the
Mount Mazama Cinder Cones

Morphometric measurements were determined for the eight cinder cones associated with Mount Mazama . Measurements were determined from the 1956 Crater Lake National Park and Vicinity topographic map. The map scale is 1:62500 and the contour interval 50 feet. The measurements were made in feet then converted to meters. A perfect cone shape was assumed for the volume calculations. The equation for the volume of a cone, $V = 1/3 \pi r^2 h$, where r = radius and h = height, was used to determine cone volume.

The pre-caldera Mount Mazama cones are found in three groups separated by thousands of meters. Measured cone height is the height of the cone above its base. Flank width is the cone radius. The values for these two parameters are presented as the average of the measurement of the long and short dimensions (Refer to Figure 8).

A plot of cone height (H_{co}) versus basal cone diameter (W_{co}) is plotted on Figure 21. The curves $H_{co} = 0.18 W_{co}$, reported for fresh cinder cones (Porter, 1972, Wood, 1980a) and $H_{co} = 0.20 W_{co}$, believed to represent the initial shape of a cinder cone (Settle, 1979), have also been plotted.

The values of H_{co}/W_{co} for the Mount Mazama cones range

from 0.14 to 0.21 (Table 5), and appear to fall between the two curves plotted on Figure 21, in agreement with other studies of young, less than 100,000 years, cinder cones. Wizard Island plots above both curves as is expected for a young, unweathered cinder cone. Desert Cone and Hill 6545 plot below both curves. These cones are heavily vegetated, and may be older and more degraded than the other cones. Desert Cone is known to be older than about 200,000 years (refer to Table 4), and would be expected to plot below both curves on Figure 21. However, Bald Crater and Maklaks Crater appear to be as vegetated, yet have greater ratios. Subsequent volcanic activity may have affected the H_{co}/W_{co} ratio. The flanks of some of the cones were undoubtedly buried by the pyroclastic flows from the climactic eruption of Mount Mazama.

Table 5 shows values of r/H_{co} and α for the Mount Mazama cinder cones. The values give some idea of the amount of degradation and relative age of the individual cones. Recall that values of r/H_{co} increase and values of α decrease as age increases. This can be seen in a general way in the Mount Mazama cones. Wizard Island is known to be the youngest cone, and has the smallest r/H_{co} value and the steepest slope. Red Cone and Scoria Cone, cones for which ages have been determined (refer to Table 4), have r/H_{co} values that are greater than that of Wizard Island,

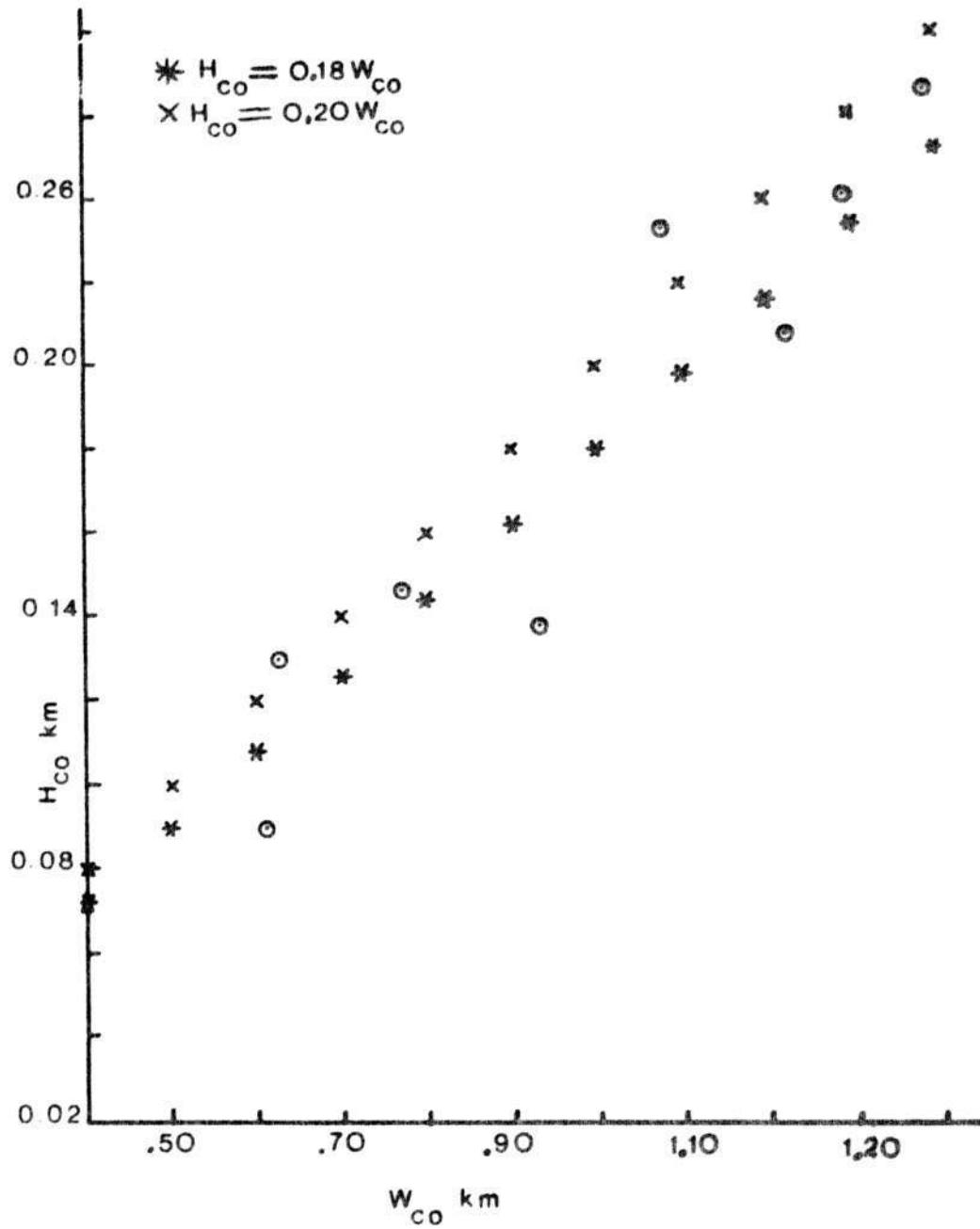


Figure 21. H_{co} versus W_{co} for eight Mount Mazama cinder cones. $H_{co} = 0.18 W_{co}$ and $H_{co} = 0.20 W_{co}$ plotted for reference.

and smaller angles, again in agreement with measured ages. The value for Desert Cone is greater than that of Red Cone and Scoria Cone, and Maklaks Crater has the greatest value of all of the Mount Mazama cinder cones. Desert Cone is known to be older than both Red Cone and Scoria Cone.

Relative ages of the Mount Mazama cinder cones can be inferred from consideration of the morphological characteristics and measured ages of the cinder cones. Based on the above discussion, the following relative ages are proposed:

Wizard Island	(youngest)
Williams Crater	
Bald Crater, Crater Peak	
Red Cone	
Scoria Cone, Hill 6545	
Desert Cone	
Maklaks Crater	(oldest)

CHAPTER 4

PETROGRAPHIC AND GEOCHEMICAL FEATURES

Petrography

The petrographic characteristics of the Mount Mazama cinder cones will be discussed first, followed by those of the Timber Crater and Union Peak cinder cones. In the following descriptions the phases are discussed in order of decreasing abundance. All mineral compositions were determined optically. Refer to Figure 11 for cinder cone location and Appendix A for thin section descriptions.

Mount Mazama Cinder Cones

In Chapter 3, the Mount Mazama cinder cones were classified according to chemical composition. The rocks can also be classified on the basis of their phenocryst phases. Figure 22 shows the agreement between the classification based on observed mineralogical composition and that based on chemical composition.

Basaltic samples contain phenocrysts of sodic to subcalcic labradorite, olivine, and magnetite, with lesser amount of hypersthene \pm augite. The phenocryst phases in the andesitic basalts are sodic labradorite, olivine,

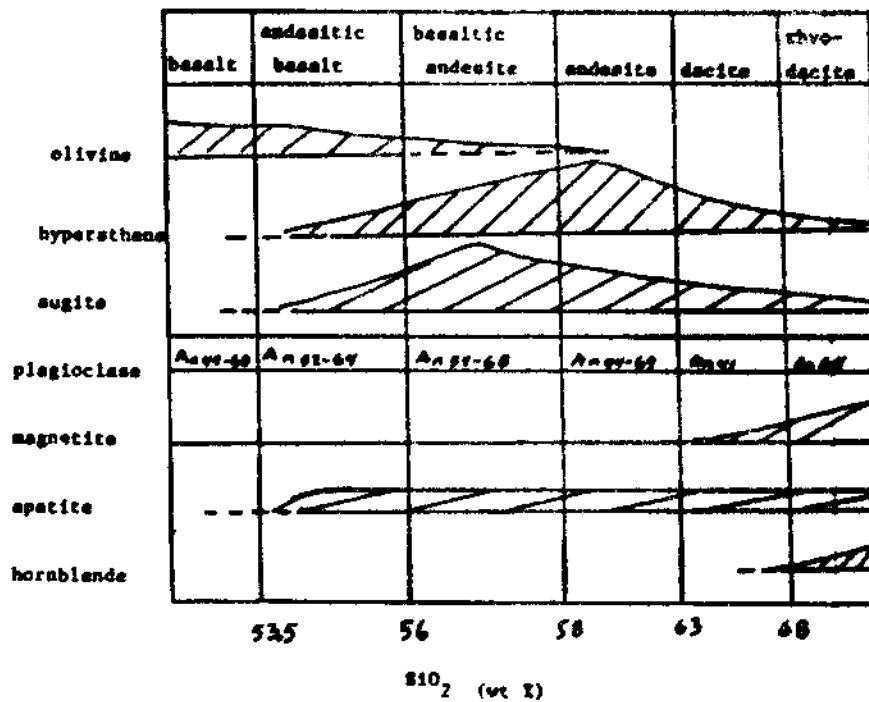


Figure 22. Relationship between rock name and abundance of phenocryst phases for the Mount Mazama cinder cones. Weight percent of SiO_2 and rock names as in Table 2.

hypersthene, augite, and magnetite. Apatite appears as an accessory mineral and persists through dacite. Hypersthene and augite begin to increase in abundance over olivine. Augite first increases, then decreases in abundance over hypersthene in andesitic basalt.

A definite change in phenocryst phases is seen in the transition from andesitic basalt to basaltic andesite. In basaltic andesite, the phenocryst phases are Ca-labradorite, hypersthene, augite, magnetite, and olivine. Olivine and augite decrease in abundance. Augite decreases to less than hypersthene, but remains greater than olivine.

Olivine disappears as a phenocryst phase in the andesitic rocks. The andesitic rocks contain andesine and calcic labradorite, hypersthene, magnetite, augite, and little or no olivine.

Dacites were collected only from Williams Crater. The samples contain phenocrysts of calcic labradorite, augite, magnetite, hypersthene, and hornblende. Magnetite appears as an euhedral phenocryst and is more abundant than in the other rock types.

The groundmass differs little in the samples studied. The samples are porphyritic with a range of groundmass textures from hyalophitic through hyalopilitic to intersertal, and the amount of glass decreases from eighty to five percent of the rock. The greatest variation is in

the amount of glass. The groundmass phases in the glass-rich samples are glass, opaques, plagioclase, and pyroxene. In a few cases, the order is glass, plagioclase, opaques, and pyroxene. In glass-free samples, plagioclase is the dominant mineral in the groundmass. Pyroxene is rarely observed in the groundmass of basaltic samples but increases in abundance as the amount of SiO_2 increases. In most samples the plagioclase microlites and pyroxene crystals are too small for optical determination of composition.

Mineralogic features

Olivine

Olivine is a euhedral to anhedral phenocryst in most of the samples studied (Figure 23). It is commonly altered to iddingsite, magnetite, and lesser amounts of hematite. The most extensive alteration of olivine is observed in the scoriaceous samples, where olivine is partly or totally replaced by granular magnetite. Olivine is unstable in most of the samples. Evidence for this includes embayed crystals, crystals with resorbed edges, and crystals rimmed with pyroxene and/or magnetite. Crystals larger than one millimeter are fractured, possibly as a result of pressure changes encountered as the crystal rose from depth

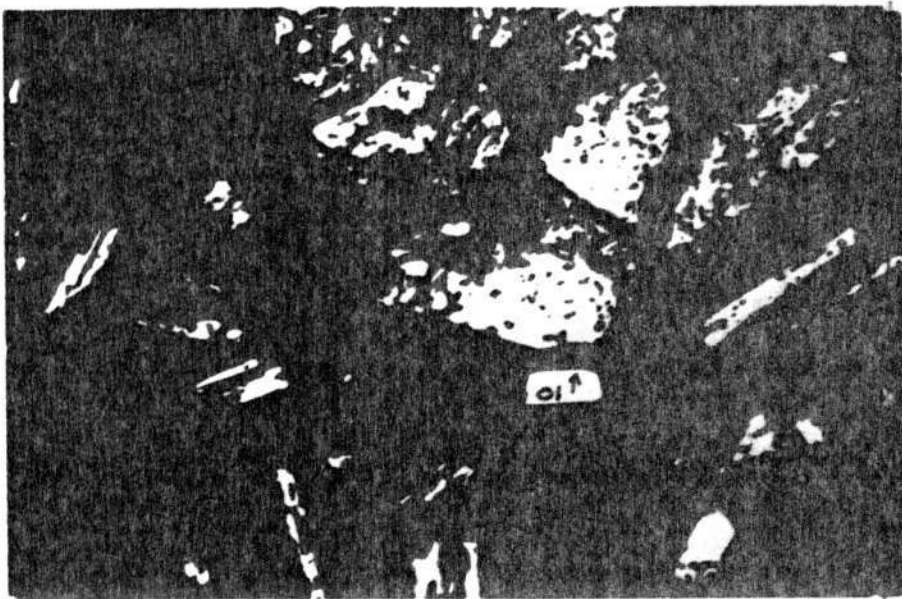


Figure 23. Photomicrograph of a euhedral olivine phenocryst. The long dimension of the photograph is 1.13 mm.

(Ritchey, 1979).

Normal zoning is observed in some crystals, and in a few crystals the rare olivine cleavage is observed. Measured compositions of olivine range from Fe_{85-90} . Euhedral olivine crystals are rare or absent in rocks with more than 56% SiO_2 . The larger euhedral and subhedral crystals are the most fractured and embayed, but the least altered. Inclusions of magnetite, hematite, pyroxene, and possibly spinel are found in the olivine crystals. Ritchey (1979) noted these spinels also, and Barnes (1978) noted the presence of spinel in olivine from Mount Bailey. Barnes suggests that they may indicate crystallization of olivine and spinel at pressures greater than seven kilobars.

Pyroxene

Hypersthene is present as a euhedral to anhedral phenocryst in all rock types studied (Figure 24). Euhedral hypersthene is absent in basaltic rocks. As the amount of SiO_2 increases from basalt to andesite, the abundance of euhedral hypersthene increases. In the dacites, hypersthene is less abundant than augite. In samples where the hypersthene is seriate in texture, the larger crystals are euhedral. The smaller, subhedral and anhedral crystals are resorbed and surrounded with a narrow rim of pyroxene,

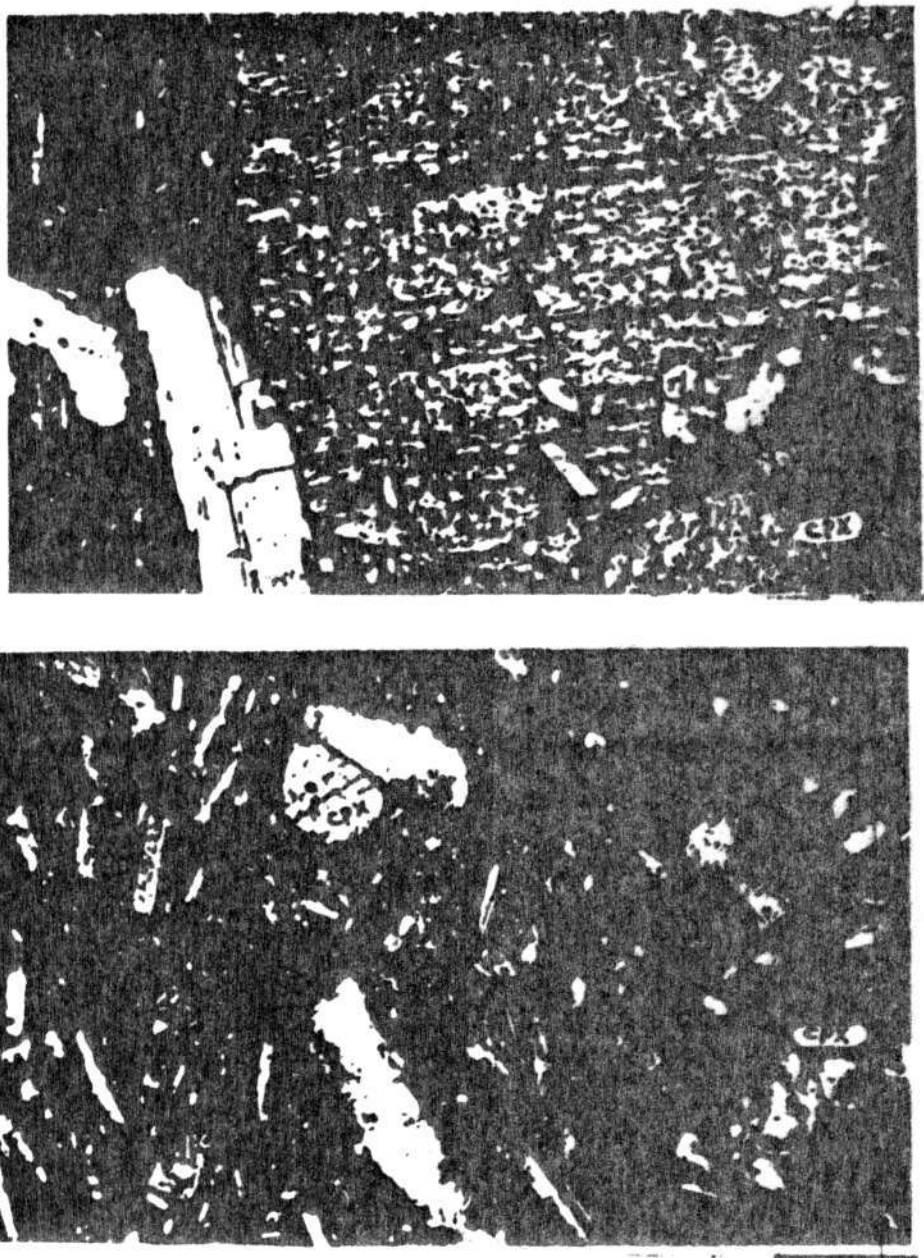


Figure 24. Photomicrographs of pyroxene phenocrysts. The long dimension of each photograph is 1.13 mm.
a. hypersthene. b. augite, denoted by cpx.

opaques, and plagioclase. In the scoriaceous samples, hypersthene is surrounded with a rim of opaques. Exsolution parallel to cleavage is observed in a few andesitic samples.

Augite is absent in basaltic samples but appears as a euhedral to anhedral phenocryst in andesitic basalt and persists to dacite (Figure 24). In andesitic basalt, the crystals are subhedral and embayed, and many crystals have resorbed edges or are surrounded by a narrow rim of pyroxene, opaques, and plagioclase. Augite is rimmed with opaques in the scoriaceous samples. Euhedral augite is abundant in samples with greater than 55% SiO₂, and is relatively fresh. The subhedral to anhedral crystals have resorbed edges and are surrounded by a narrow rim of pyroxene, opaques, and plagioclase. Twinning and zoning are observed in some of the euhedral crystals.

Plagioclase

Plagioclase is ubiquitous in the studied samples, constituting twenty to forty percent of the rock. Measured compositions of groundmass plagioclase range from An₅₁₋₆₆.

Two types of phenocrysts are found in the samples. Type 1 has been named macrophenocryst (Figure 25). Plagioclase macrophenocrysts are present in all the rock types studied. The crystals have a size range of 3-10mm

and are subhedral to anhedral with the majority retaining the characteristic lath shape. The majority of crystals are twinned and exhibit normal, reverse, and oscillatory zoning, often in the same rock. Measured compositions are An_{44-56} . The crystals are rounded, embayed, and many have resorbed edges. Inclusions of glass, opaques, dust, pyroxene, olivine, hematite, and apatite are found in the macrophenocrysts. In some cases, the inclusions are controlled by cleavage or twin planes, or the edges of an earlier crystal.

Four types of inclusions are observed (Figure 26). Inclusions of Type 1 comprise a small part of the crystal, and are scattered randomly throughout the crystal. Type 2 inclusions are found as a ring of fine, "dusty" inclusions surrounded by an inclusion-free rim and core.

In crystals with Type 3 inclusions the inner part of the crystal contains numerous inclusions, surrounded by a thin, inclusion-free rim. The inner, inclusion-rich part appears to be an earlier, partly resorbed crystal, surrounded with a later, inclusion-free overgrowth (Bottlinga, Kudo, and Weill, 1966). The dusty appearance of the Type 2 and 3 inclusions suggests rapid growth of the crystal. Liquid was incorporated in the rapidly growing crystal and subsequently crystallized to form the inclusions.

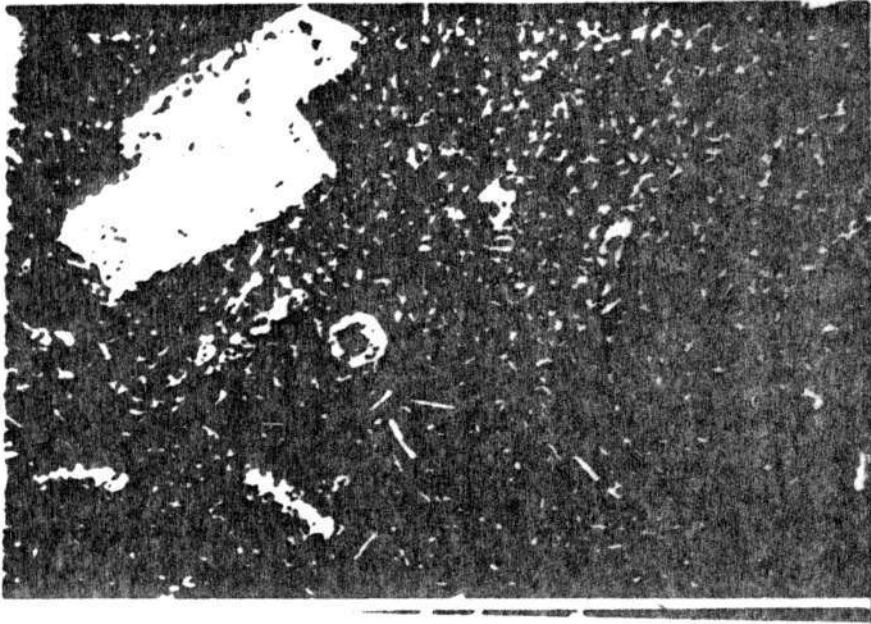


Figure 25. Photomicrograph of a plagioclase macrophenocryst. The long dimension of the photograph is 1.13 mm.

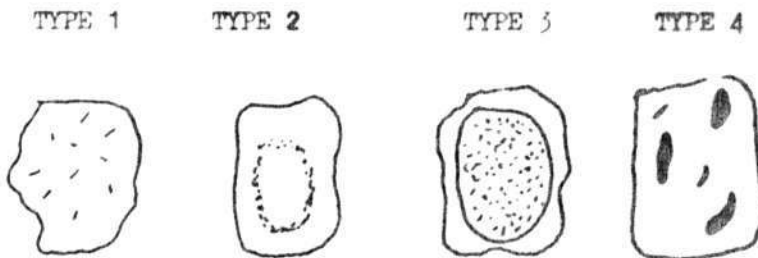


Figure 26. Sketch of types of inclusions found in plagioclase macrophenocrysts.

Type 4 inclusions are "blebs" of dark-brown glass. These inclusions are larger in size than the three other types. Plagioclase crystals with Type 3 and 4 inclusions have a spongy or moth-eaten appearance as a result of the large abundance of inclusions.

Phenocrysts of the second type are smaller, 1.0mm-0.05mm, and are euhedral to anhedral, with lath shaped crystals common. Labradorite is the dominant feldspar, the measured composition being An_{70-36} . Zoning is less prevalent in these crystals and is normal. Inclusions of glass, opaques, pyroxene, olivine, hematite, and apatite are observed. The inclusions occur as patches or small rings, or scattered randomly throughout the crystal. The abundance of inclusions is less than that observed in the macrophenocrysts.

Differences in size, inclusion habit, zoning, and resorption features suggest different origins for the two types of plagioclase phenocrysts. The macrophenocrysts are clearly not in equilibrium with

the liquid (groundmass) in which they now occur. The crystals have rounded and resorbed edges, and most are rimmed with an inclusion-free overgrowth. These observations suggest that these crystals were transported into the melt where they now reside.

Hornblende

Hornblende is present as phenocrysts in dacites from Williams Crater and as xenocrysts in a lava flow from Wizard Island. The most mafic rock in which hornblende first appears is a dacite with 64% SiO_2 from Williams Crater. The hornblende is unstable as evidenced by the rim of opaques that surround the crystals. Hornblende is a stable phase in the sample with 68% SiO_2 . The crystals are nearly euhedral and are not rimmed with opaques.

Apatite

Apatite appears as an accessory mineral in andesitic basalt and persists to dacite. The crystals are euhedral to subhedral and have the characteristic high relief and needle shape.

Magnetite

Magnetite is ubiquitous in the rocks of the cinder cones. It is found as a phenocryst and in the groundmass. The crystals are euhedral to anhedral with a size range of about 0.50-1.0mm. The size and abundance of the magnetite phenocrysts increase as the amount of SiO_2 increases. Magnetite is also present as an inclusion in each of the other phenocryst minerals, suggesting that magnetite is an early phase.

Cinder Cones of Timber Crater and Union Peak

Samples from the cinder cones of Timber Crater and Union Peak are similar in appearance to the cinder cones of Mount Mazama. Therefore, the mineral descriptions presented above will not be repeated. Differences are observed between the rocks of the two groups of cinder cones, particularly in texture and phenocryst size and abundance. These differences will be discussed below.

The Union Peak cinder cones are basalt to andesitic basalt in composition. Plagioclase, olivine, augite, and hypersthene are present as phenocrysts. Pyroxene is more abundant than olivine in all rocks that are more silica rich than the

andesitic basalt. The pyroxene and olivine phenocrysts are altered to a red, iron-oxide phase, probably iddingsite. Plagioclase is more abundant than in the rocks of the Mazama cinder cones. Textures observed in the groundmass are intergranular and pilotaxitic to trachytic.

Samples from the Timber Crater cinder cones are basaltic andesite to andesite in composition. Plagioclase, augite, hypersthene, and olivine are present as phenocrysts. Olivine is absent or present in only small amounts. The olivine abundance decreases, and the hypersthene abundance increases from basaltic andesite to andesite. The groundmass texture is interstitial to intergranular, and pilotaxitic to trachytic. The Timber Crater cones differ from those of Mount Mazama in their smaller modal proportion of phenocrysts, larger abundance of hypersthene, and the intergranular and trachytic groundmass.

Chemical Variation

For the purposes of this discussion, the cinder cones have been divided into two groups, the cinder cones of Mount Mazama, and the cinder cones of Timber Crater and Union Peak.

A plot of total alkalies versus SiO_2 for the Crater Lake cinder cones is presented in Figure 27. The rocks plot within the high-alumina field of Kuno (1964).

Cinder Cones of Mount Mazama

Twenty-nine samples were analyzed for major and trace-element composition by use of the Atomic Absorption method at the University of Oregon by Christine McBirney. Nine samples were analyzed for trace and minor-element composition at the University of Oregon using the Instrumental Neutron Activation Analysis method. Chemical analyses are presented in Appendix B, major-element variation diagrams in Figure 28, and trace-element variation diagrams in Figure 29.

Major elements

The major-element trends are linear, typical of the calc-alkaline rock series. The plot for Al_2O_3 is the exception. This scatter is thought to be important and will be discussed later.

INDEX

- Bald Crater
- ⊙ Crater Peak
- ▲ Desert Cone
- × Maklaks Crater
- Hill 6545
- ▣ Scoria Cone
- + Williams Crater
- △ Wizard Island
- ⊖ Red Cone

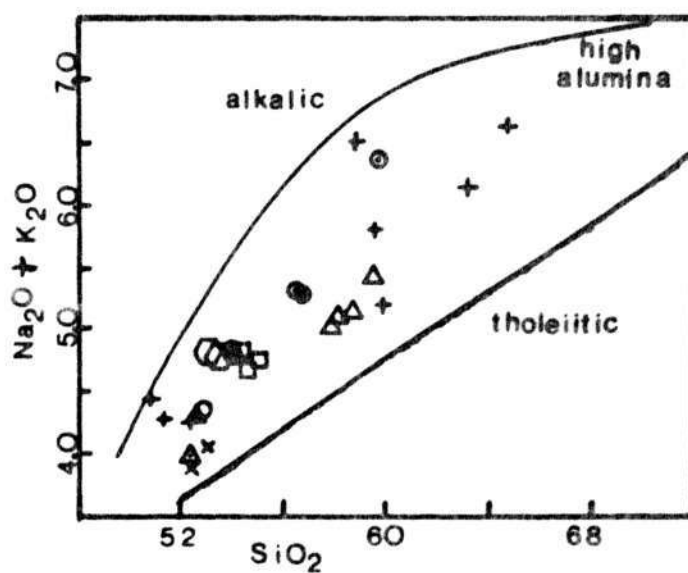


Figure 27. Plot of $\text{Na}_2\text{O} + \text{K}_2\text{O}$ versus SiO_2 for the Crater Lake cinder cones. Fields after Kuno (1964).

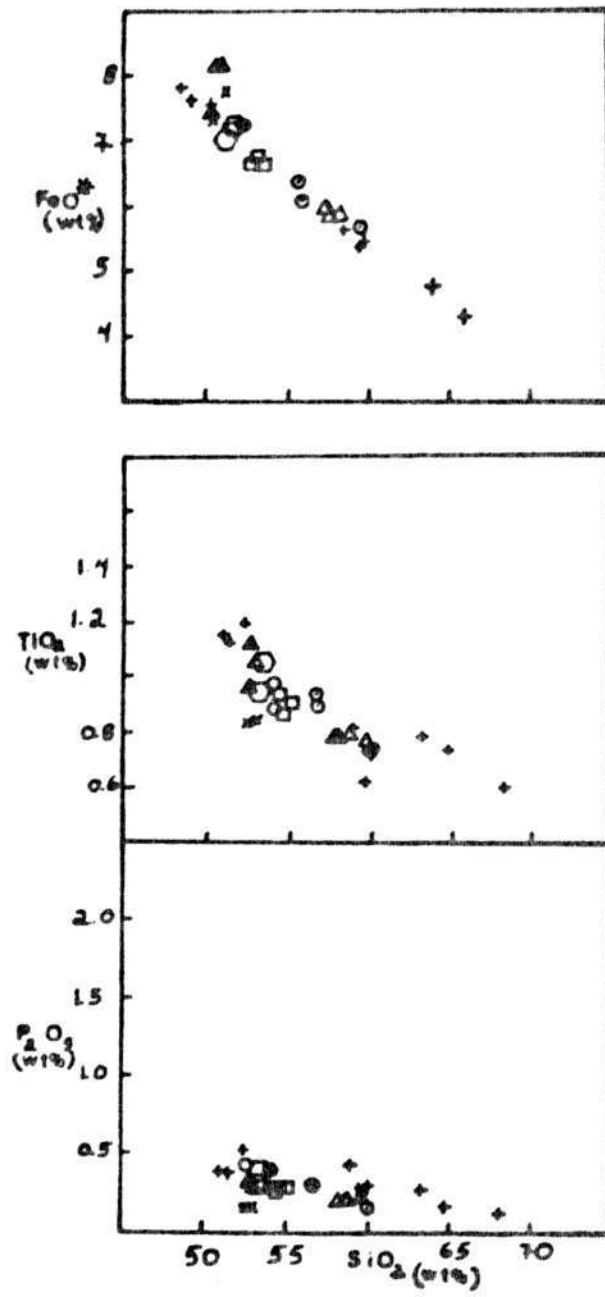


Figure 28. Harker diagrams for the Mount Mazama cinder cones. Symbols as in Figure 27.

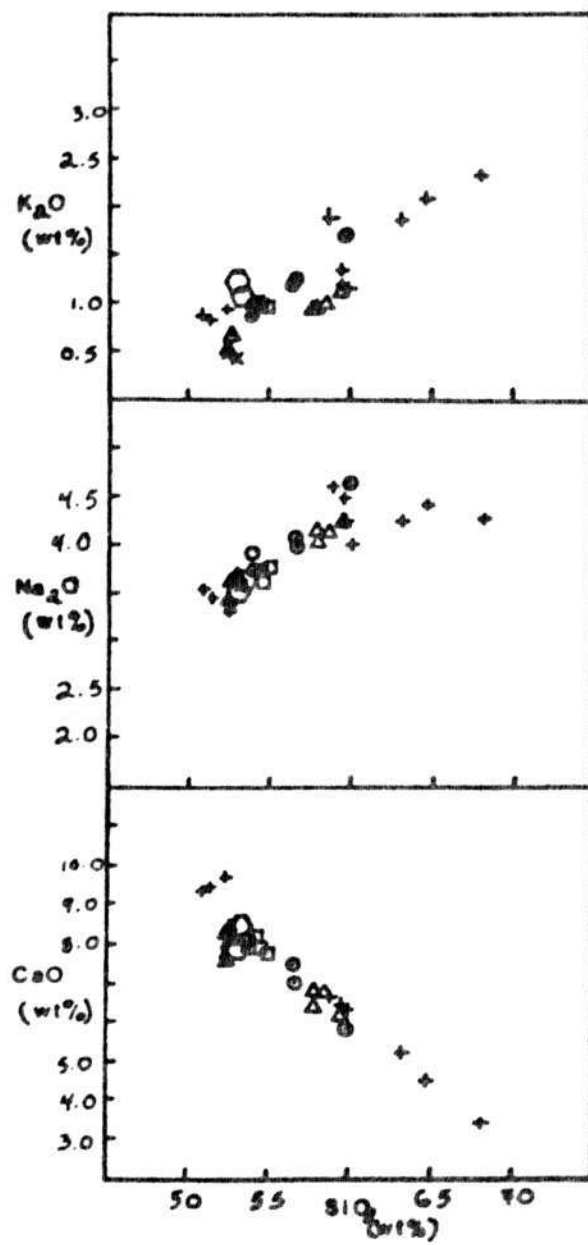


Figure 28 continued.

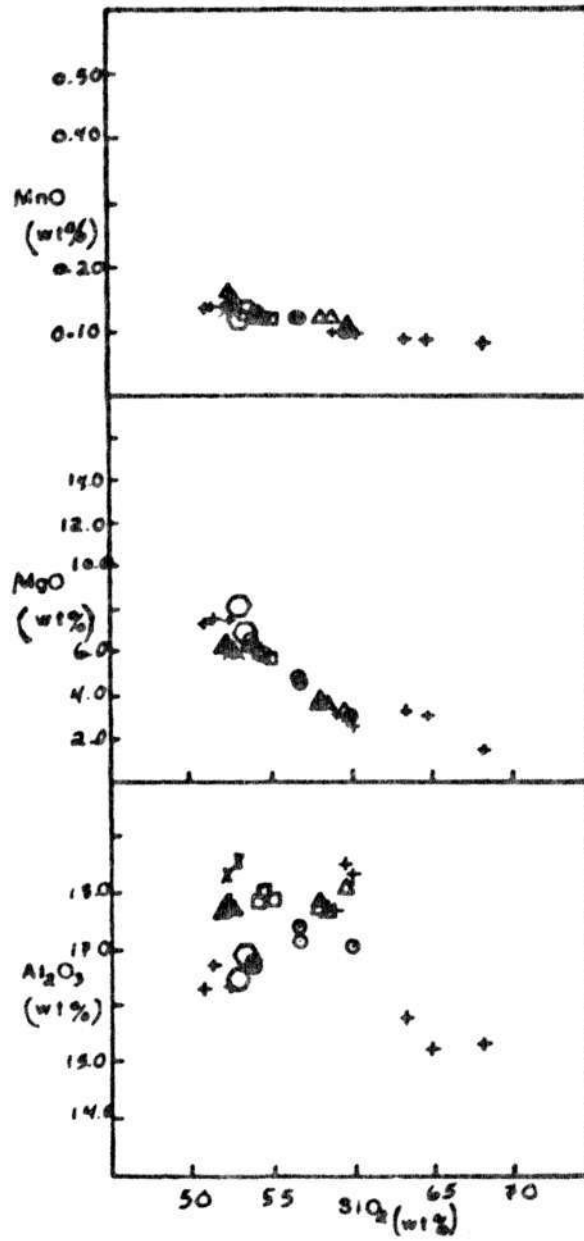


Figure 28 continued.

The different rock types exhibit coherent trends for most of the elements. The widest compositional variation is observed in the basalts and basaltic andesites. On many of the diagrams, there appears to be more than one trend. This is most evident on the plots of MgO, MnO, TiO₂, and FeO^{*}.

Samples from Maklaks Crater and Desert Cone plot below the main trend on the diagrams of P₂O₅, K₂O, CaO, MgO, and TiO₂, and above the trend on the FeO^{*} diagram.

Trace elements

The trends on the trace-element variation diagrams are nearly linear for most of the elements considered. Again, the widest range in composition is observed in the basalts and andesitic basalts. This is most evident on the plots of Ba, Sr, and Ca. As in the major-element diagrams, there appears to be more than one trend on some of the diagrams, particularly Ni and Rb. The observed abundances for Ni and Cr in the cinder cones are lower than typical mantle values, i. e. 250-450ppm for Ni and >500 ppm for Cr, suggesting that these magmas are not primitive.

Samples from Maklaks Crater plot below the general trend on the diagrams of Sr, Ba, and Rb. Desert Cone samples plot below the trend on the Sr and Ba diagrams. RC-12 plots above the trend on the plots of Cr and Ni, and

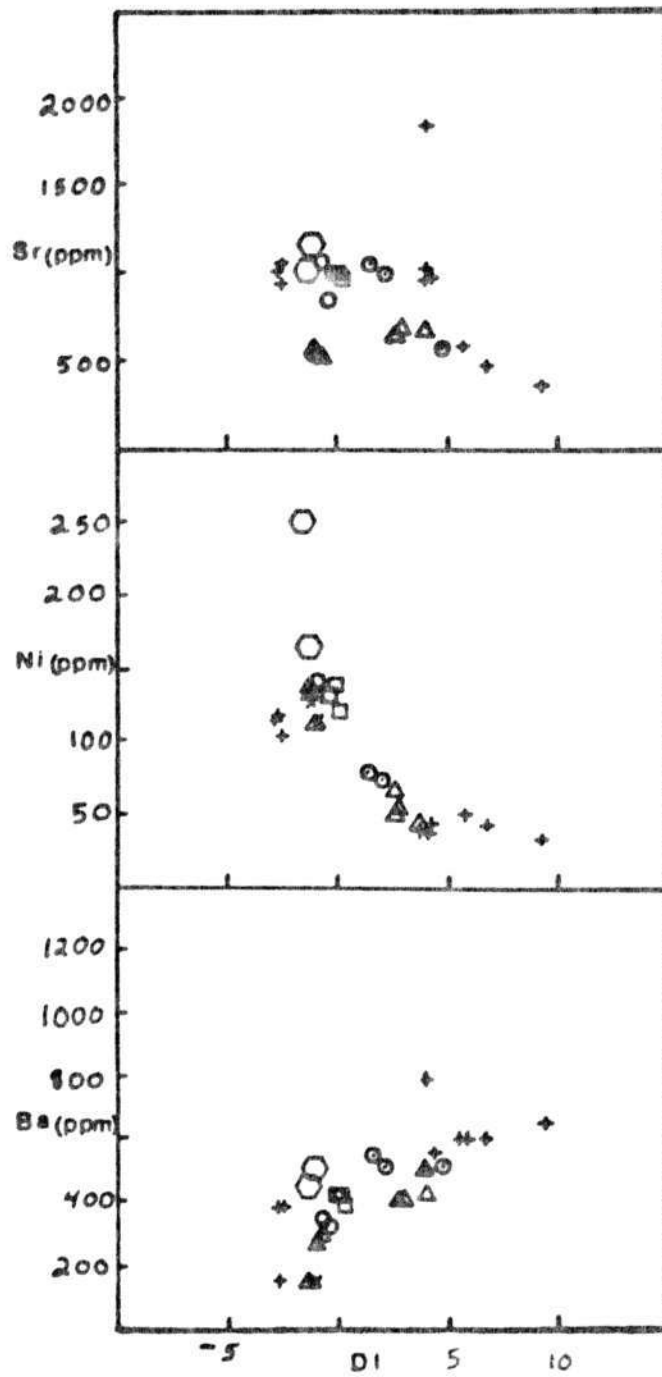


Figure 29. Trace element versus differentiation (DI) for the Mount Mazama cinder cones. Symbols as in Figure 27.

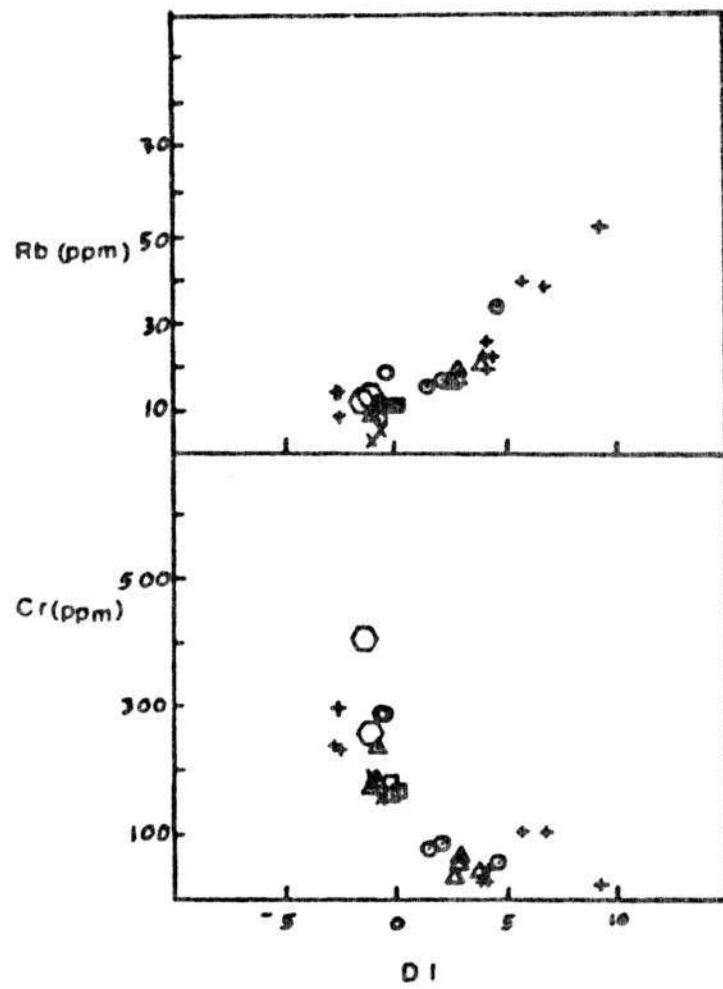


Figure 29 continued.

the abundances approach mantle abundances for these minerals.

Cinder Cones of Timber Crater and Union Peak

Major elements

Major-element diagrams for the Timber Crater and Union Peak cinder cones are presented in Figure 30. The samples from the two cinder cones of Timber Crater plot together, with the exception of TC-5, which plots with the Union Peak samples, and the samples from the two cinder cones of Union Peak plot together as expected. The trends are less coherent than those of the Mount Mazama cinder cones, possibly because of the smaller number of samples. Again, it is possible to distinguish more than one trend on many of the diagrams, particularly those for FeO^+ , TiO_2 , Al_2O_3 , and MnO .

Trace elements

Plots of trace-element variation are presented in Figure 31. The trends are less coherent than those of the Mazama cinder cones. For most of the elements, particularly Ni and Cr, the trends for the Timber Crater cones are distinct from those of the Union Peak cones. Again, TC-5 plots with the Union Peak cinder cones. The abundances of Ni and Cr are less than typical mantle values.

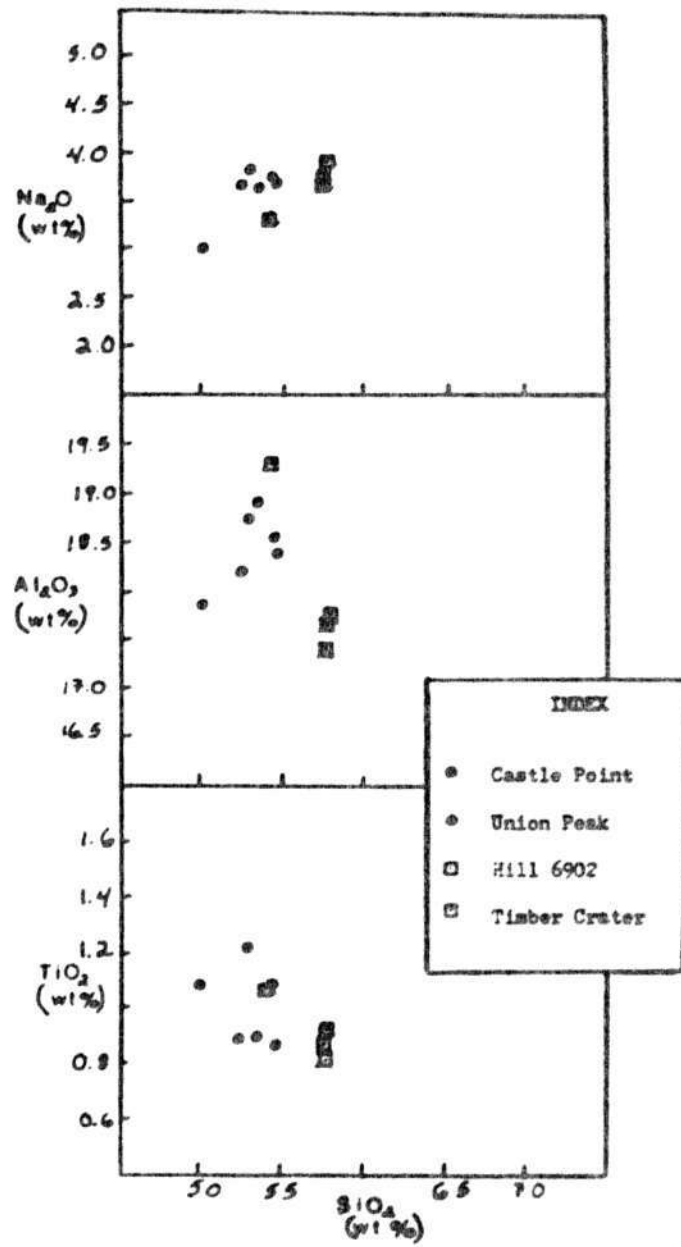


Figure 30. Harker diagrams for the Timber Crater and Union Peak cinder cones.

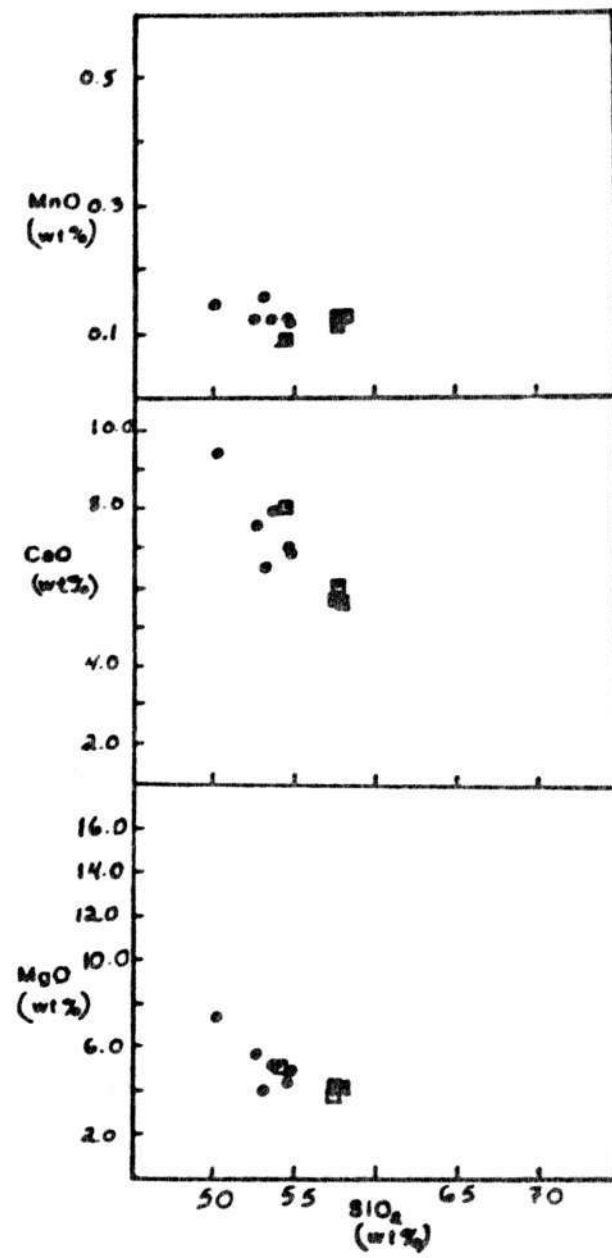


Figure 30 continued.

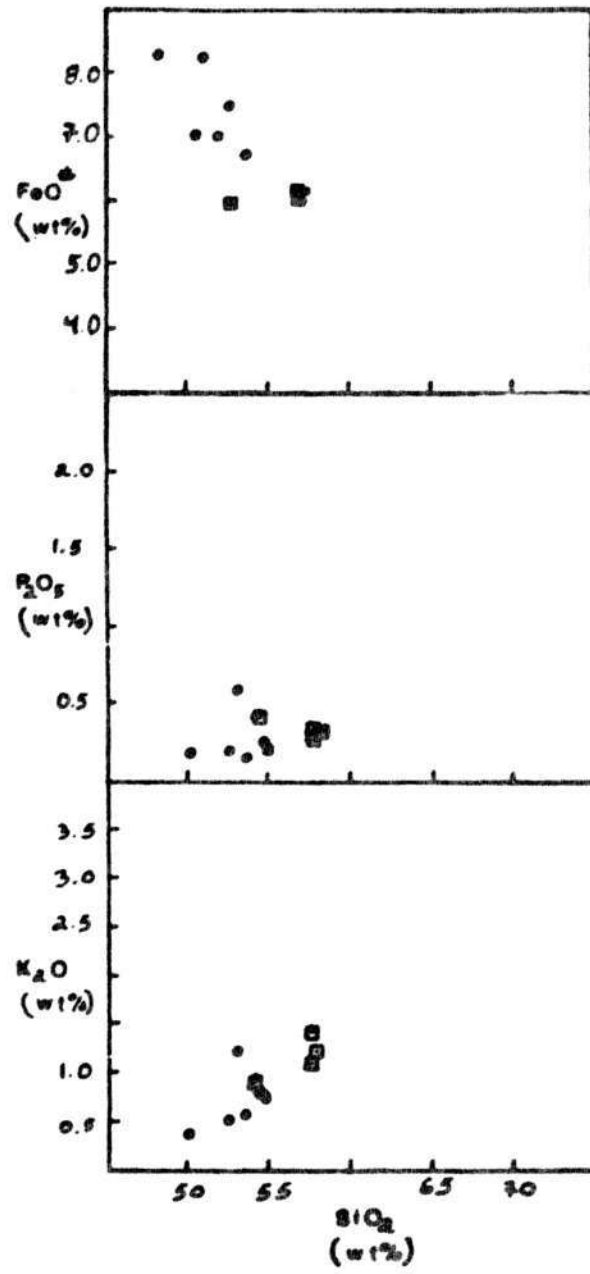


Figure 30 continued.

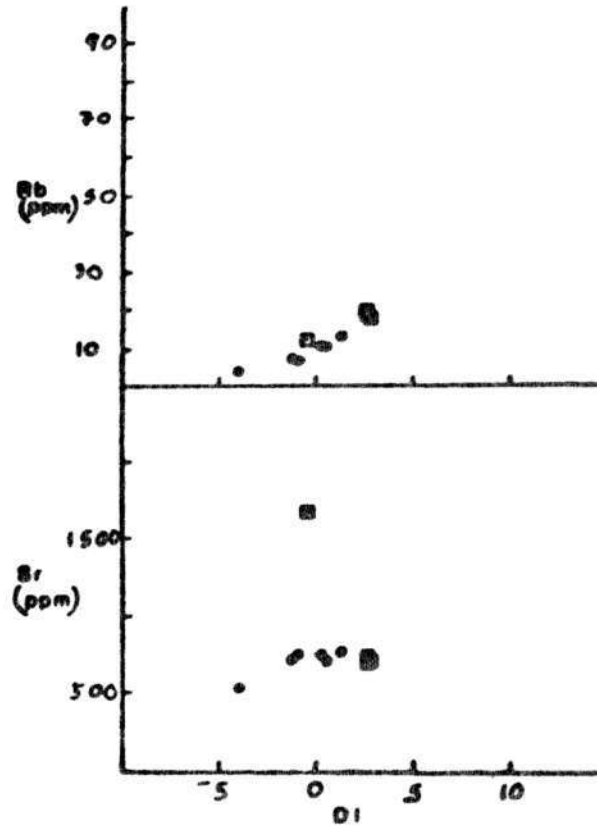


Figure 31. Trace element versus differentiation index (DI) for the Timber Crater and Union Peak cinder cones. Symbols as in Figure 30.

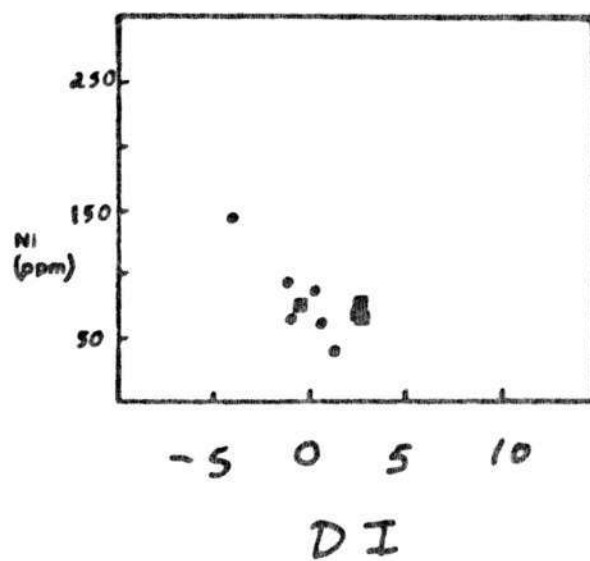


Figure 31 continued.

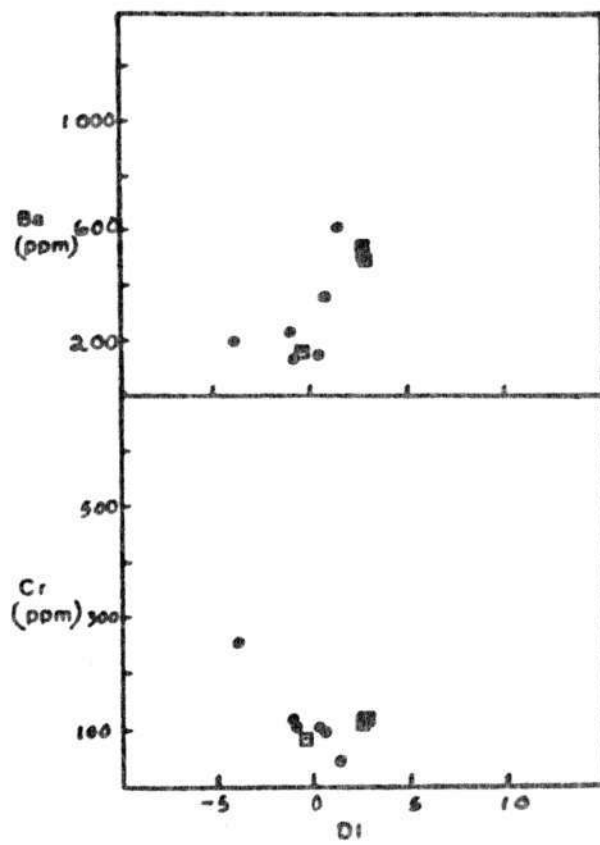


Figure 31 continued.

Discussion

Major and trace-element variation and petrographic evidence suggest the Mazama cinder cones are related by fractionation of plagioclase, magnetite, olivine, clinopyroxene, and orthopyroxene. Plagioclase and magnetite are phenocryst phases in all of the rock types studied (Refer to Figure 22). Olivine is present in basalt and decreases in abundance with increasing SiO_2 content. Clinopyroxene and orthopyroxene are present in andesitic basalt and persist to dacite.

Fractionation of these minerals will produce the observed depletion in included elements. Ni is included in olivine and, to a lesser extent, in magnetite. Sr is included in plagioclase and clinopyroxene, and Cr is included in clinopyroxene, orthopyroxene, and magnetite.

Samples from the Williams Crater Complex bracket those of the Mazama cinder cones on the variation diagrams (Refer to Figures 28 and 29). The continuity of the trends suggests that the Williams Crater cinder cone is similar in origin to the other Mazama cinder cones. The dacitic samples are thought to be a result of magma mixing that took place when the zoned magma chamber of Mount Mazama was tapped.

Comparison of the variation diagrams for the Timber

Crater and Union Peak cinder cones with those for the Mazama cinder cones reveals several similarities. If the diagrams are overlain (Figure 32), the Timber Crater and Union Peak samples fall along the trend of the Mazama cones.

The fact that the Union Peak cinder cones and the Timber Crater cinder cones plot with the Mount Mazama cinder cones suggests a similar history for the three groups of cinder cones. The Union Peak cinder cones stand on lavas from Union Peak. The lavas of the cinder cones could have undergone contamination by the Union Peak lavas. The similarity in chemical composition between the cinder cones of Union Peak and Mount Mazama, suggests that contamination has not occurred or has been minimal. The lavas of the Timber Crater cinder cones also do not appear to have suffered contamination for the reasons outlined above. Therefore, an origin and crystallization history similar to that of the Mazama cones is proposed for the Timber Crater and Union Peak cinder cones.

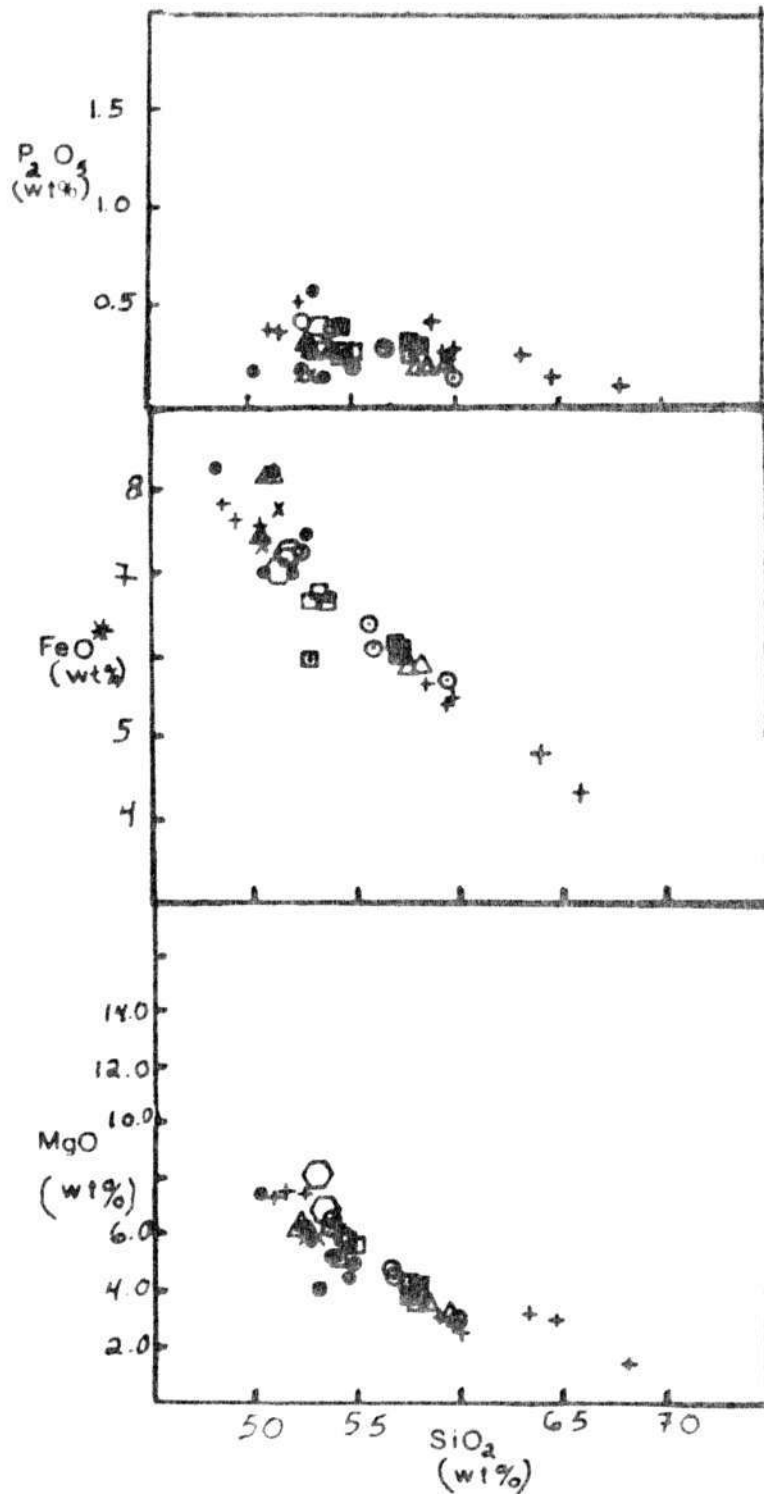
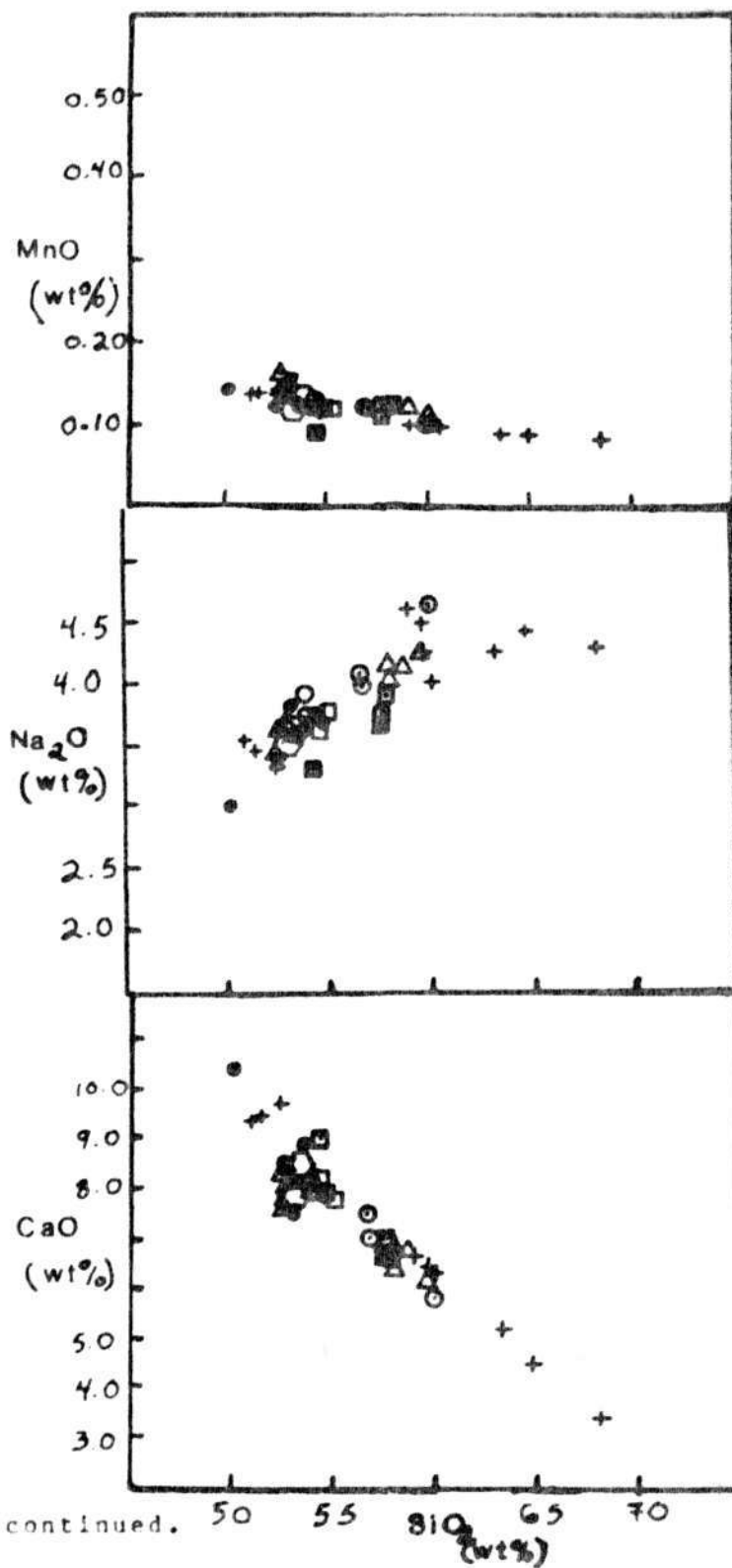


Figure 32. Comparison of variation diagrams for the cinder cones of Mount Mazama, Timber Crater, and Union Peak. Symbols as in Figures 27 and 30.



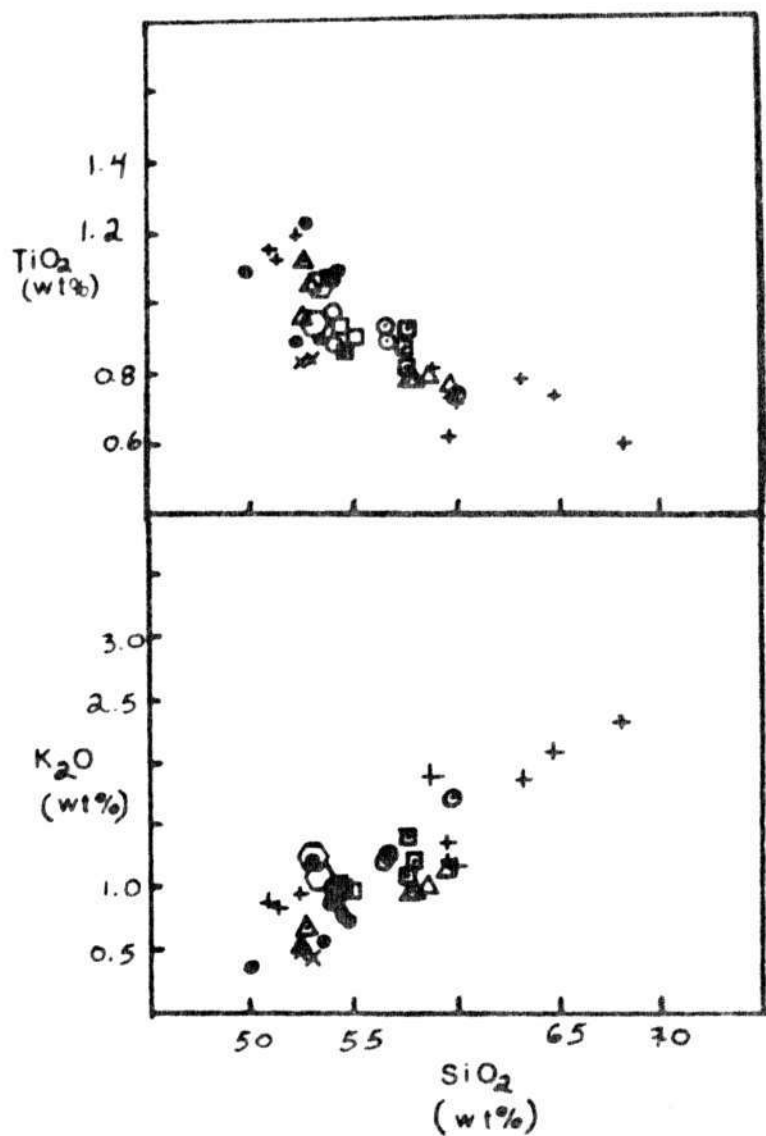


Figure 32 continued.

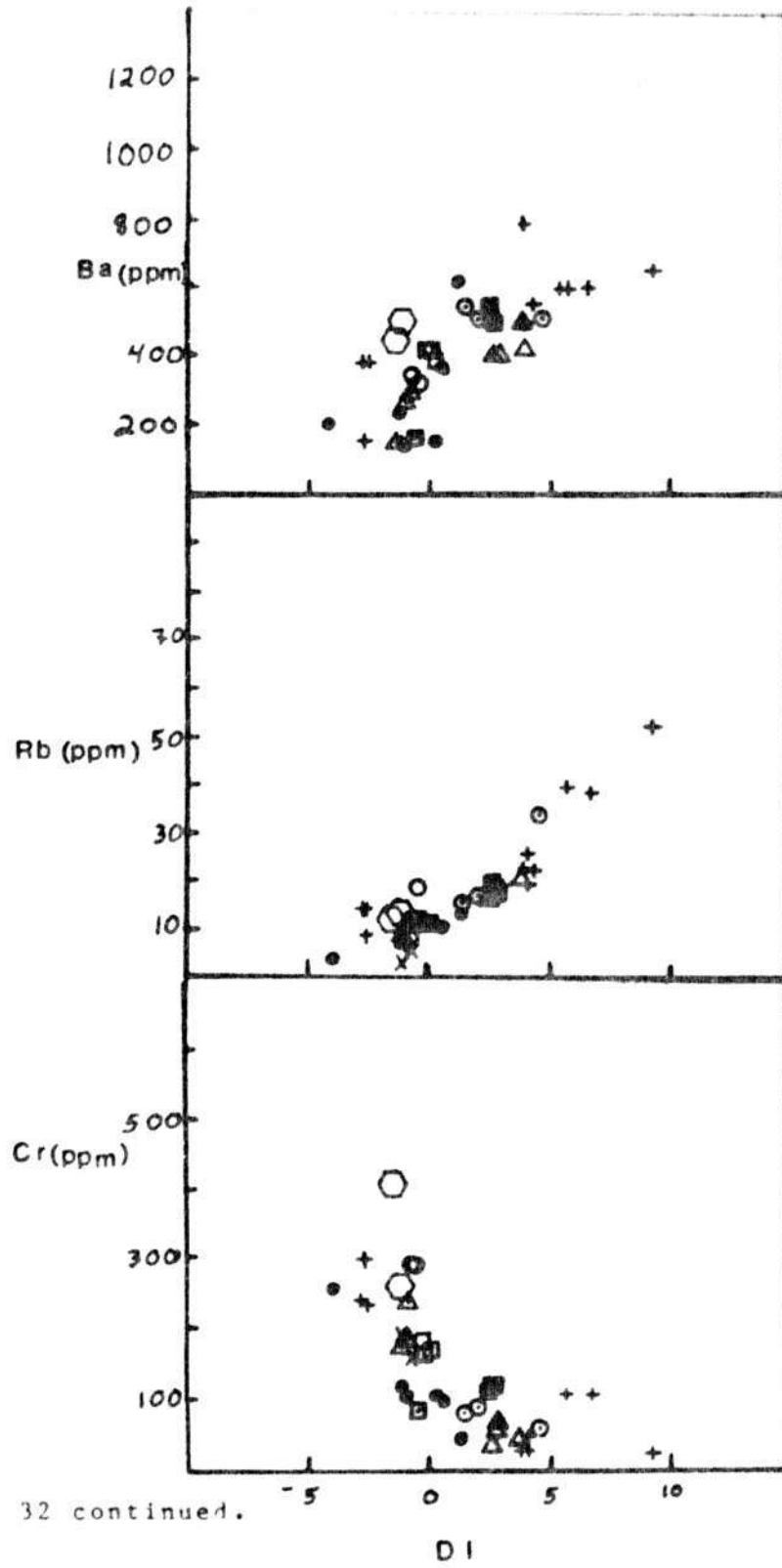


Figure 32 continued.

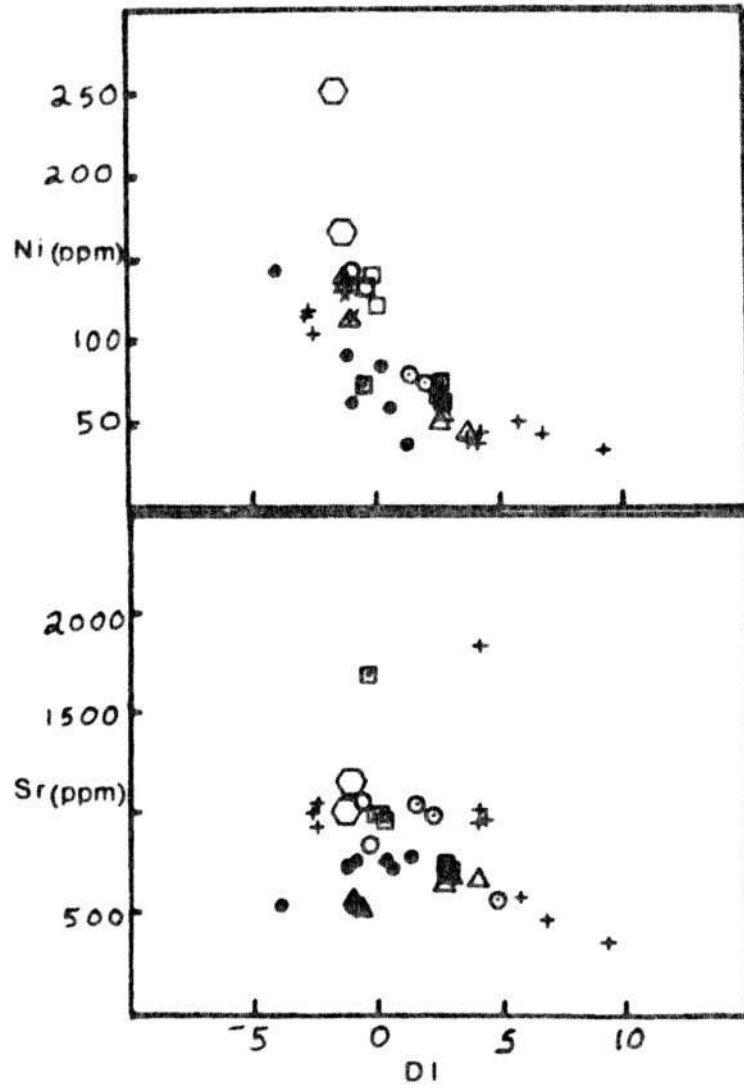


Figure 32 continued.

Mass-balance Calculations

Crystal fractionation is proposed as the dominant mechanism responsible for the observed range in composition in the cinder cones at Crater Lake. In order to test this theory, mass-balance calculations were performed, using a least-squares program developed at the University of Oregon by B. Baker, D. Geist, and A. R. McBirney. Very simply, the program involves subtraction of minerals from a parental liquid to produce a chosen daughter. The success of the calculation is judged by the size of the residual for each major-element oxide and the sum of the squares of the residual, $\sum r^2$. A residual is the difference between the actual and calculated values of an oxide in the daughter analysis. $\sum r^2$ should be less than or equal to 0.10 for a satisfactory solution. It should be noted that these calculations ignore petrologic constraints and therefore can only be considered as permissive evidence.

Mineral phases used in the calculation are those observed in the rock. Chemical compositions of the minerals used are from Ritchey (1979) and McBirney (unpublished data).

The object of the calculations was to start with a basalt and through successive calculations, produce the Wizard Island andesite. Calculations were performed

starting with the most mafic basalt as the parent and an andesitic basalt as the daughter. Each successive calculation used the daughter of the previous run as the parent for the next. Satisfactory results were obtained for these calculations (Table 6).

Ritchey (1979) proposed that the products of the climactic eruption of Mount Mazama were derived from magmas similar to the Red Cone lavas. In order to test this theory, calculations were performed using a Red Cone sample as a parent and samples from the climactic ash-flows as daughters. Satisfactory results were obtained (Table 6).

To take this one step further, calculations were performed to see if the climactic samples (analyses taken from Ritchey, 1979) could be derived from basalts of any other cinder cone. Again, satisfactory results were obtained. Therefore, mass-balance calculations with major-element oxides support the conclusion that crystal fractionation was an important process in the genesis of the Mazama cinder cones, and that the products of the climactic eruption were derived from the cinder cone magmas by fractional crystallization.

When trace elements are included in the mass-balance calculations, however, the solutions are less satisfactory. The success of this calculation is judged by a weighted residual, calculated as the difference between the actual

and calculated abundance of the trace element in the daughter sample. Two of the mass-balance calculations are presented in Table 7. Although the $\sum r^2$ is good for the major elements, there are large weighted residuals for the trace elements, particularly Sr and Ba. In fact, the weighted residuals for Sr and Ba are large for all the calculations. Also, for some of the calculations, the included elements increased and the excluded elements decreased. This is the opposite of the expected result if the rocks were related by crystal fractionation alone. Therefore, crystal fractionation cannot have been the only process involved. The possible effects of partial melting and magma mixing will be considered below.

Table 6. $\sum r^2$ for mass-balance calculations where $\sum r^2 < 0.10$.

Parent	WC18	WC18	WC18	MC1	MC1	DC4
Daughter	WC175	WC110	DC5	RC7	WC110	RC7
$\sum r^2$	0.03	0.03	0.02	0.05	0.06	0.05
Parent	DC4	RC7	RC7	CP1	MC1	DC4
Daughter	WC110	CP1	WI12	WC110	WC175	CP7
$\sum r^2$	0.10	0.00	0.08	0.00	0.04	0.05

WC110 and WC175 are samples of the Pinnacles section (Ritchey, 1979). The numbers refer to stratigraphic height. WC175 is a basaltic andesite and WC110 is an andesite.

Table 7. Examples of two mass-balance calculations.
 a. Satisfactory results when trace elements considered.

Parent: RC-7
 Daughter: CP-1

	SOL'N	% CUMULATE
RC-7	1.000	
OLPL2	-0.126	67.422
CPXLR6	-0.079	42.288
PL110C	-0.094	50.133
OPXLR6	0.132	-70.556
MGT-2	-0.020	10.714
CP-1	0.813	

R Square = 0.000

	Parent Analysis	Daughter Analysis	Daughter Calc	Weighted Resid
SiO ₂	52.83	56.78	56.75	0.03
TiO ₂	1.05	0.90	0.92	-0.02
Al ₂ O ₃	16.75	17.20	17.20	-0.00
FeO	7.13	6.09	6.07	0.01
MnO	0.13	0.12	0.18	-0.03
MgO	6.94	4.64	4.62	0.03
CaO	8.45	7.08	7.08	0.00
Na ₂ O	3.64	4.00	3.97	0.03
K ₂ O	1.09	1.29	1.33	-0.03

Bulk D

Ba	511.00	516.00	609.86	-93.86	0.147
Co	48.00	24.00	38.11	-14.11	2.113
Cr	260.00	92.00	6.90	85.10	18.516
Cu	73.00	35.00	ND	ND	ND
Li	13.00	16.00	ND	ND	ND
Ni	164.00	74.00	22.85	51.15	10.512
Pb	14.00	18.00	17.08	0.92	0.041
Sr	1147.00	994.00	1200.78	-206.28	0.781

ND-not determined

Table 7 continued.

b. Less satisfactory results when trace elements considered. Notice the large weighted residual for Ba and Sr, and the increase in some included elements, i. e. Cr, Ni, Sr.

Parent: DC-4
Daughter: RC-7

	SOL'N	% CUMULATE
DC-4	1.000	
CLRC3C	0.030	-19.225
CPXPL2	0.019	-11.977
AN65	-0.114	72.317
OPXPL2	-0.074	46.798
MGT-2	-0.019	12.087
RC-7	0.842	

R Square = 0.05

	Parent Analysis	Daughter Analysis	Daughter Calc	Weighted Resid
SiO ₂	52.18	52.89	52.89	0.00
TiO ₂	1.12	1.05	1.00	0.05
Al ₂ O ₃	17.65	16.77	16.76	0.01
FeO	8.09	7.14	7.15	0.01
MnO	0.15	0.13	0.16	-0.01
MgO	6.16	6.95	6.95	-0.00
CaO	8.30	8.46	8.47	-0.00
Na ₂ O	3.60	3.65	3.75	-0.09
K ₂ O	0.67	1.09	0.80	0.20

					Bulk D
Ba	156.00	511.00	178.36	332.64	0.221
Co	50.00	48.00	47.54	0.64	1.293
Cr	181.00	260.00	2.18	257.82	26.694
Cu	58.00	73.00	ND	ND	ND
Li	12.00	13.00	ND	ND	ND
Ni	133.00	164.00	154.98	9.02	0.111
Rb	9.40	14.00	1.05	2.95	0.058
Sr	571.00	1147.00	563.26	583.74	1.079

ND-not determined.

Rare-earth Elements (REE)

A plot of REE abundances, normalized to chondritic meteorites, versus ionic radius is shown in Figure 33. Two interesting features are apparent. First, a large, positive Eu anomaly appears in basalt, andesitic basalt, and basaltic andesite, with a smaller anomaly in the andesite, and second, the andesitic basalt and andesite are depleted in LREE relative to basalt.

The positive Eu anomaly is unexpected in light of the demonstrated plagioclase fractionation. Eu is strongly included in plagioclase, and plagioclase fractionation is expected to produce a negative Eu anomaly. One possible explanation for the observed anomaly is plagioclase contamination of the magma.

The second observation is more difficult to explain. Closer examination of the REE plot reveals a repeated pattern in the light rare-earth elements (LREE). Starting at the bottom of the plot and moving upward, to increasing REE contents, the following sequence is encountered: basalt-andesitic basalt-andesite, andesitic basalt-andesite, basalt-basaltic andesite-andesite, and finally, basalt that is enriched in LREE relative to all other samples. Obviously, more than simple crystal fractionation is involved. First of all, the LREE elements are strongly

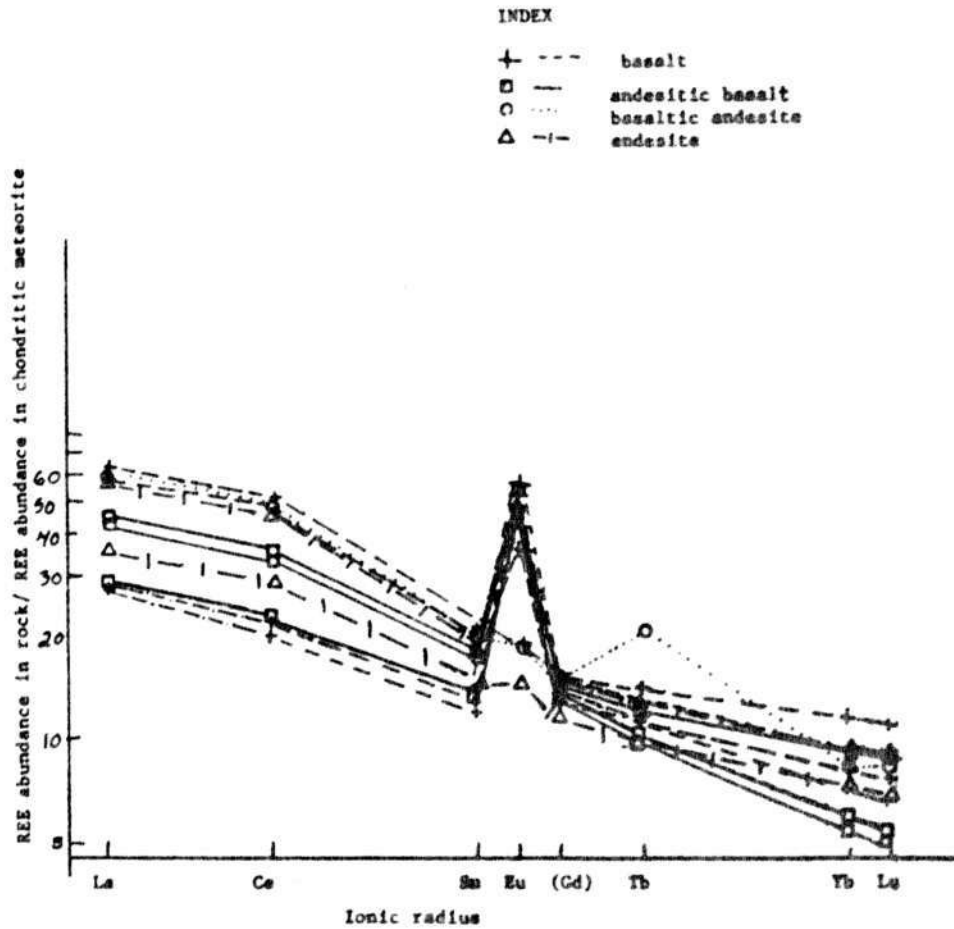


Figure 33. REE abundance versus ionic radius for the Crater Lake cinder cones. REE values normalized to chondritic values after Masuda, Nakamura, and Tanaka, 1973.

excluded elements and should increase with fractionation. In other words, basalt should be depleted in LREE relative to andesitic basalt and andesite. Second, the sequence of basalt-andesite could not be a result of fractionation within a single magma, because the basalt of the next sequence is LREE enriched relative to the andesite of the previous one. Therefore, each group probably represents fractionation operating on parental magmas of a separate partial melt episode.

Robyn (1977) calculated REE patterns for different degrees of partial melting of various mantle source rocks (Figure 34). The REE pattern for the Crater Lake cinder cones were compared with these calculated patterns. Robyn notes that interpretation of the calculations should be made with caution because errors may be introduced by imprecise values of the distribution coefficients which may vary with bulk composition and degree of partial melting. Also, it is more difficult to model the source region because the compositions of the bulk rock and individual phases are poorly known, and because parameters which may affect the melt composition, such as temperature, pressure, water pressure, and f_{O_2} are not well constrained. However, the calculations can be used to infer the mineralogy of the source region if the above restrictions are kept in mind, and certain trace-element trends can be used as well

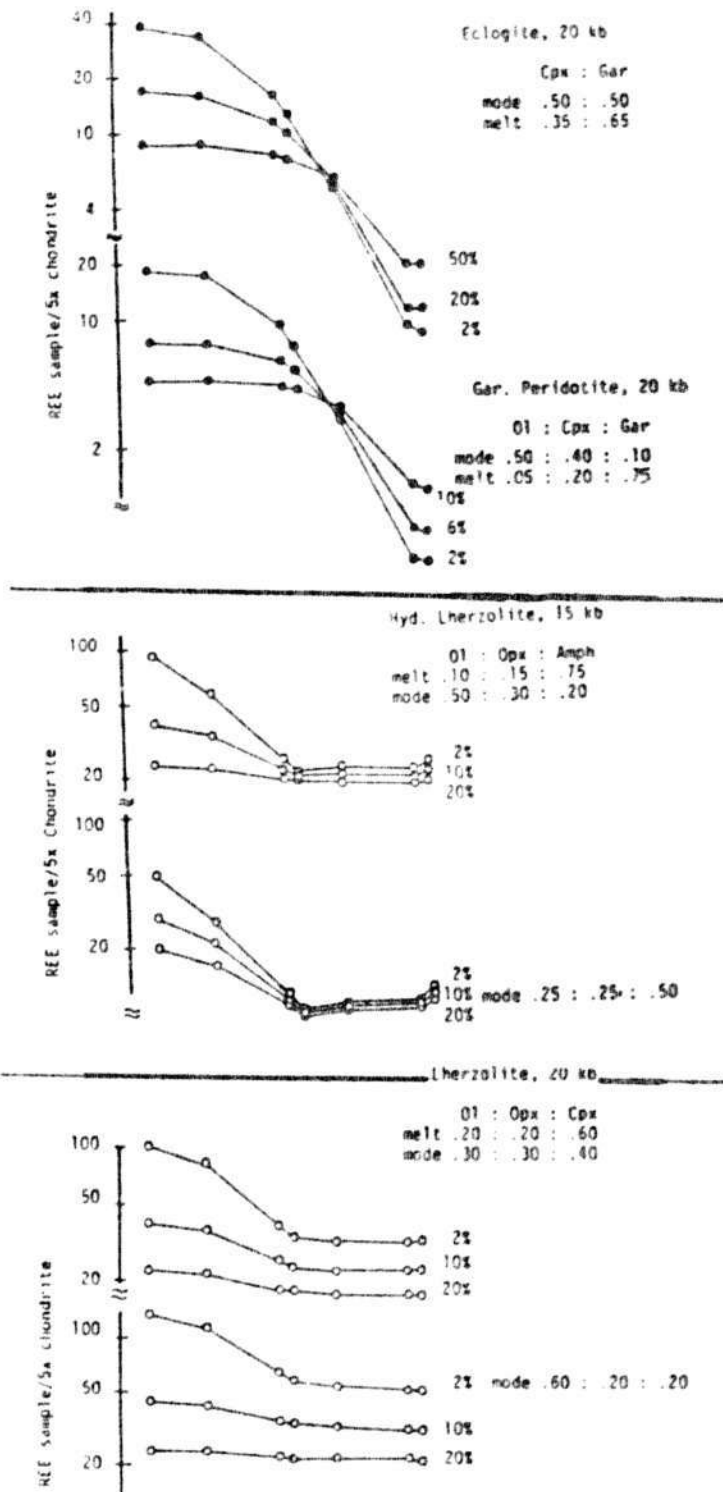


Figure 34. Calculated REE patterns from Robyn, 1977.

(as will be seen in the following section).

The REE patterns of the Crater Lake cinder cones are similar to that of a dry peridotite source that underwent less than about 20% partial melting (Figure 34). The magmas were not in equilibrium with residual garnet because the garnet signature (extreme LREE enrichment relative to the HREE) is absent. The hornblende signature (a concave-upward pattern, with a kink at or near Eu) and the spinel signature (a convex pattern) are also not observed in the REE patterns of the Crater Lake cinder cones (Figure 34). It is likely that not much was left behind in the source rock as residual after partial melting occurred. Therefore, the magmas probably represent separate partial melts as opposed to different degrees of partial melting of the same source.

Fractional Crystallization and Partial Melting

Recent workers have published chemical diagrams that can be used to distinguish between the effects of partial melting and fractional crystallization on magma genesis. Refer to Hering (1981) and Clark (1983) for comprehensive discussions of the methods described below.

Hanson (1978) observed the effects of fractional crystallization and partial melting on the behavior of

included and excluded elements. For partial melting a relatively large variation in excluded elements and a relatively small variation in included elements is observed. The opposite is observed for fractional crystallization. Figure 35 shows Hanson's predicted effects of partial melting and fractional crystallization. Figure 36 is a plot of Rb versus Ni for the Crater Lake cinder cones. No definitive trend is seen on this diagram, although the steep trend on the left-hand side of the plot seems indicative of partial melting, while the more gently sloping curve near the center seems indicative of fractional crystallization (refer to Figure 35 for comparison of the curves). Therefore, both partial melting and fractional crystallization may have been involved.

Hering (1981) used diagrams of a strongly excluded element, H or hygromagmatophile (after Allegre and Minster, 1978) and a moderately excluded element, M or magmatophile, to distinguish between the effects of partial melting and fractional crystallization. The diagrams will be referred to as H/M versus H plots. Typical H elements are Rb and Th, and typical M elements are Zr, Ba, Hf, and K.

Figure 37 shows H/M versus H plots for the Crater Lake cinder cones. Plots of Rb/Ba vs. Rb and Rb/Zr vs. Rb show scatter but suggest a fractional crystallization component. A plot of Th/Hf vs. Th suggests a partial melting

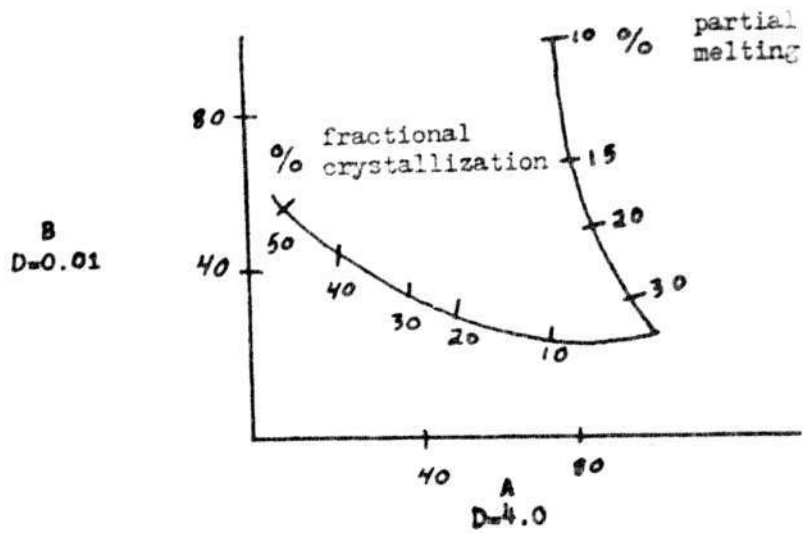


Figure 35. Fractional crystallization versus partial melting. Predicted trends for a strongly excluded trace element ($D = 0.01$) and a strongly included trace element ($D = 4.0$). After Hanson, 1978.

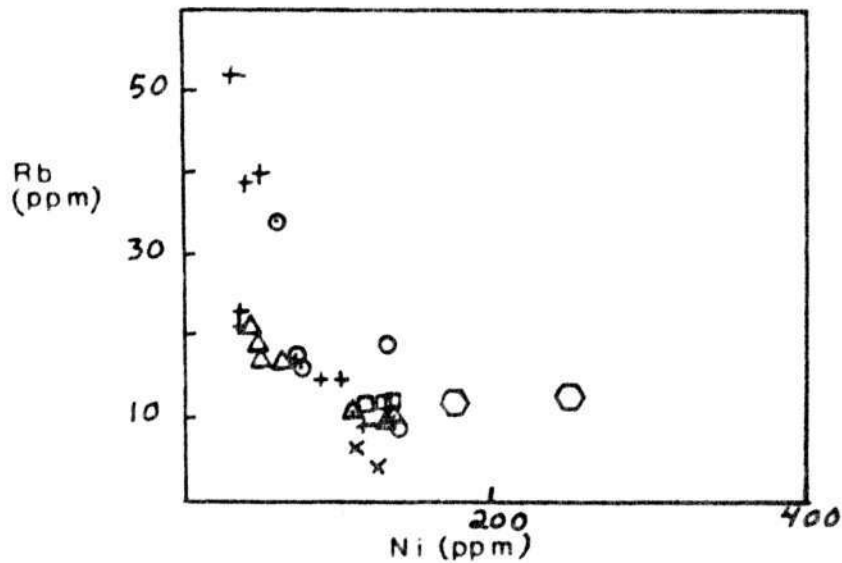


Figure 36. Rb versus Ni for the Crater Lake cinder cones. Symbols as in Figure 27.

component. Therefore, both partial melting and fractional crystallization may have been important in the genesis of the Crater Lake cinder cones.

In order to obtain a further test of the assumption that discrete batches of partial melt are involved, plots of excluded elements versus SiO_2 and MgO were considered (Figure 38). The cinder cones plot in three groups on the diagrams of Ce/Yb versus SiO_2 and Th versus SiO_2 . This pattern is reflected in the Ce versus MgO diagram. No samples fall between 55% to 57% SiO_2 ; the existence of samples in that range could better define a trend on these diagrams. Again, the existence of discrete batches of partial melt is indicated.

Spatial Distribution of Vents

Radial distance, defined as the distance of each cinder cone from the geographic center of Crater Lake, was determined for each cone. A plot of the radial distance versus age for the Crater Lake cinder cones is presented in Figure 39. Two weak linear trends are suggested.

Radial distance versus major- and trace-element abundances were also considered. Radial distance versus weight percent SiO_2 is presented in Figure 40 and radial distance versus Rb is presented in Figure 41. A definitive trend is absent on these diagrams.

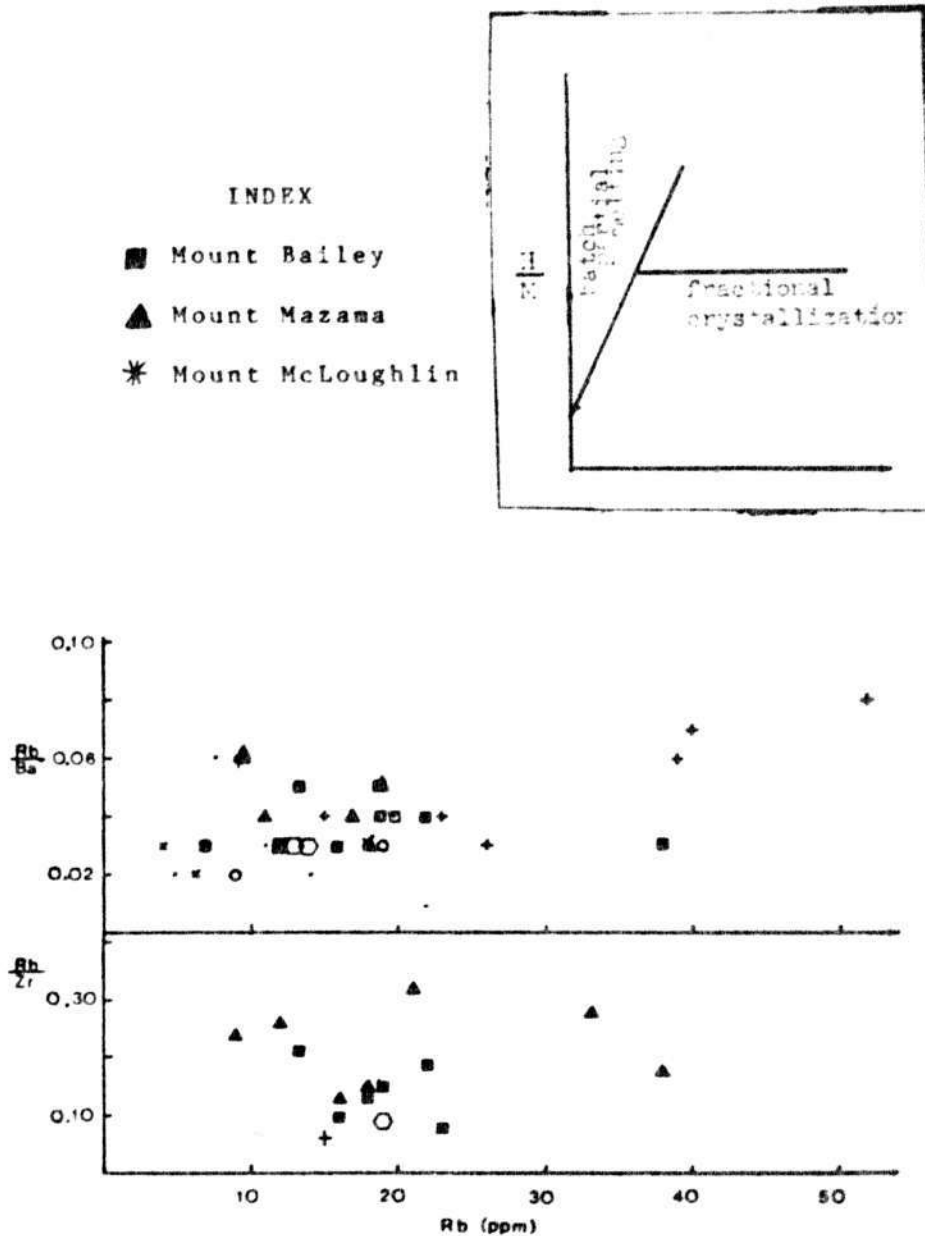


Figure 37. H/M versus H diagrams for the Crater Lake cinder cones, Mount Mazama, Mount Bailey, and Mount McLoughlin. Refer to text for explanation. Refer to Figure 27 for symbols not in Index. Inset shows predicted curves (After Hering, 1981).

a. Rb/Ba vs Rb.
b. Rb/Zr vs. Rb.

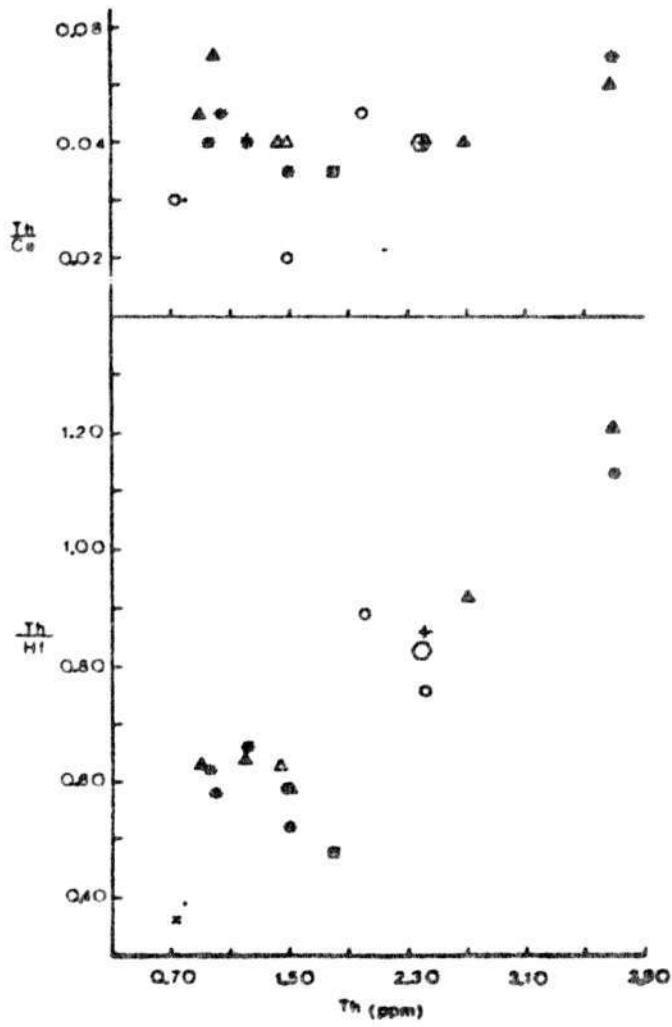


Figure 37 continued. c. Th/Ce vs Th.
d. Th/Hf vs Th.

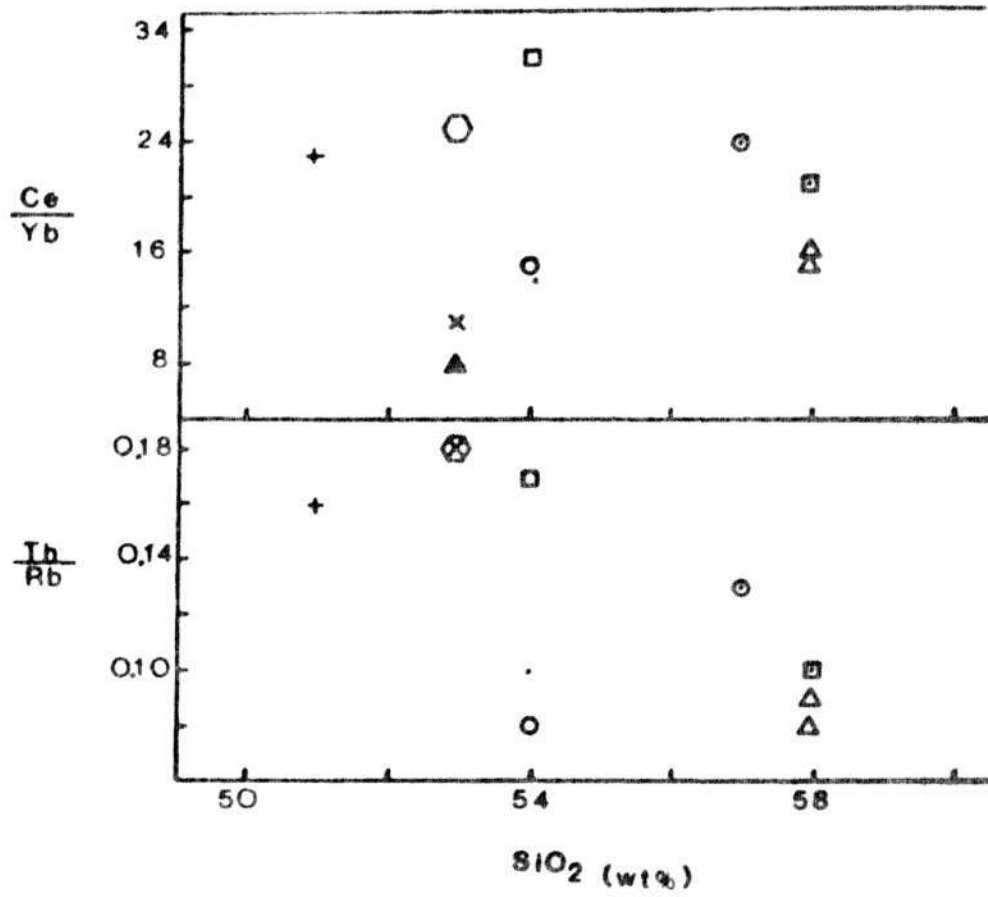


Figure 38. Excluded elements versus SiO₂ and MgO.

a. Ce/Yb vs SiO₂

b. Th/Rb vs SiO₂

Symbols as in Figures 27 and 37.

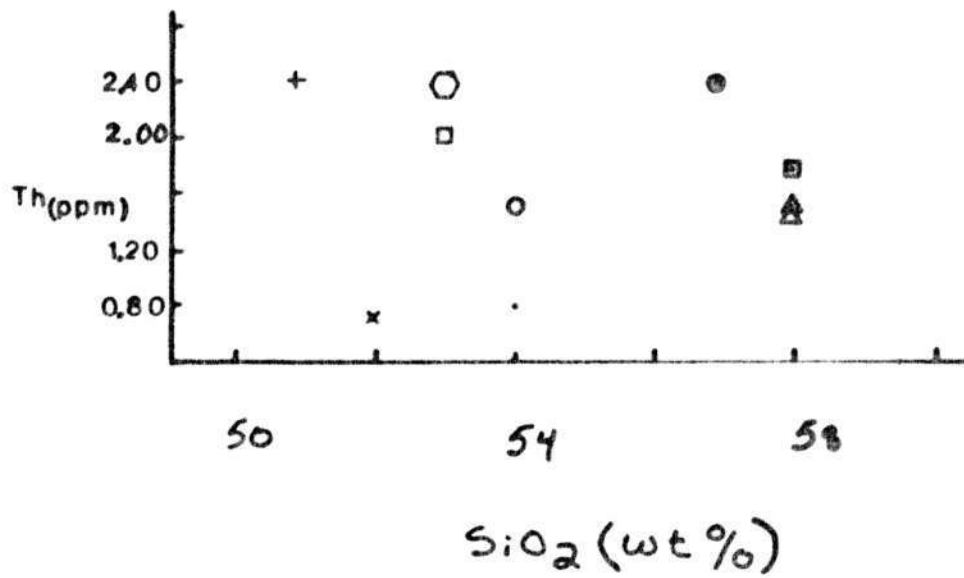


Figure 38 continued.
c. Th vs SiO₂.

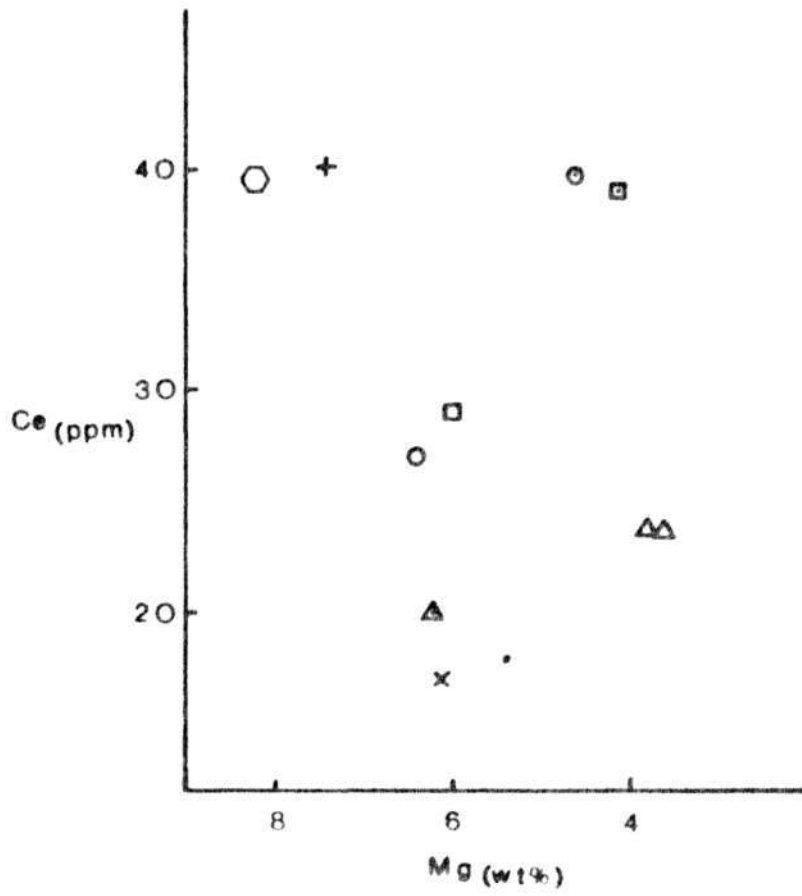


Figure 38 continued.
d. Ce vs MgO.

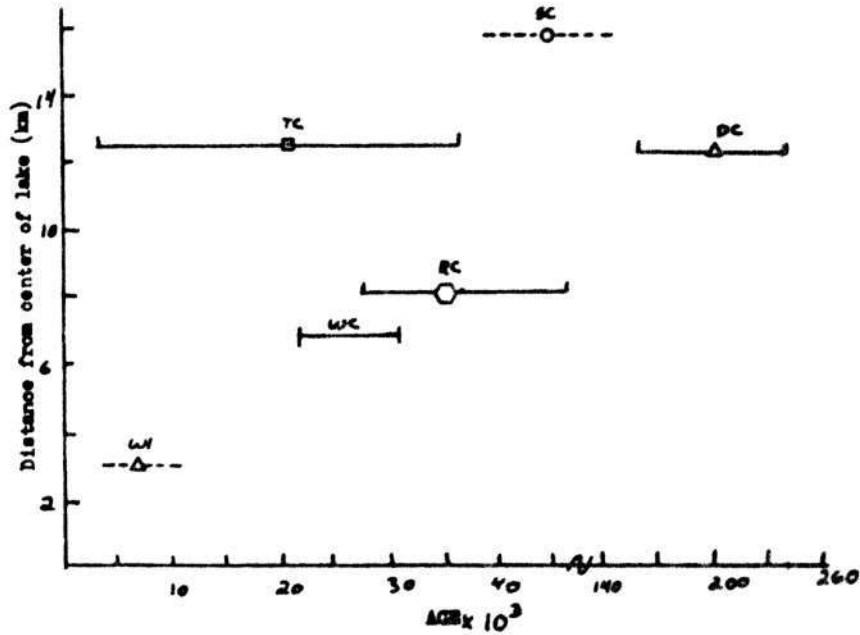


Figure 39. Spatial distribution of vents versus age for the Crater Lake cinder cones. Note break in age scale. Symbols as in Figure 29. Solid lines denote error bars, dashed lines represent approximate ages.

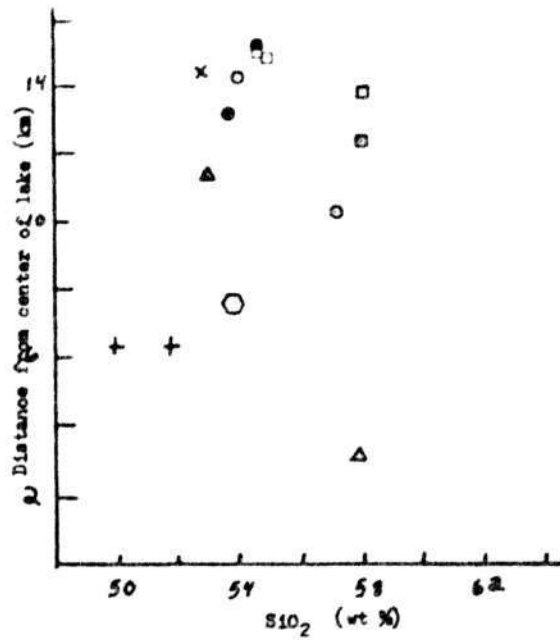


Figure 40. Vent distribution versus SiO₂ for the Crater Lake cinder cones. Symbols as in Figure 39.

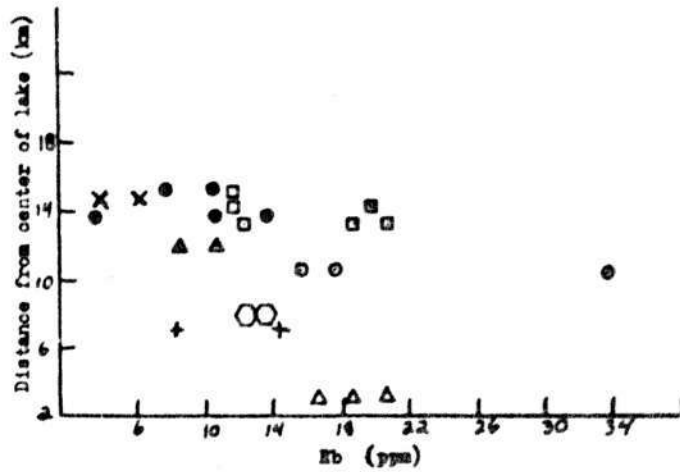


Figure 41. Vent distribution versus Rb for the Crater Lake cinder cones. Symbols as in Figure 39.

AFM Diagram

An AFM diagram for the Crater Lake cinder cones is presented in Figure 42. The rocks plot within the calc-alkaline field and lack iron enrichment, as is characteristic of the calc-alkaline series.

Magnetite or amphibole fractionation is often proposed to account for the lack of iron enrichment. Magnetite phenocrysts are ubiquitous in the cinder cone samples, evidence that fractionation of magnetite is the mechanism responsible for the lack of iron enrichment. However, early fractionation of hornblende should also be considered.

Hornblende is present in the dacites from Williams Crater and certainly played a role in the fractionation of the more siliceous rocks. Early hornblende fractionation cannot be ruled out on the basis of petrographic evidence because hornblende formed at depth would probably break down before reaching the surface. Sc is strongly included in hornblende, and less strongly included in clinopyroxene, and would be a good indicator of hornblende fractionation. Sc abundances are similar in the basalts and basaltic andesites, indicating that early hornblende fractionation was not significant. Hornblende fractionation would also affect the REE abundances, resulting in a concave-upward

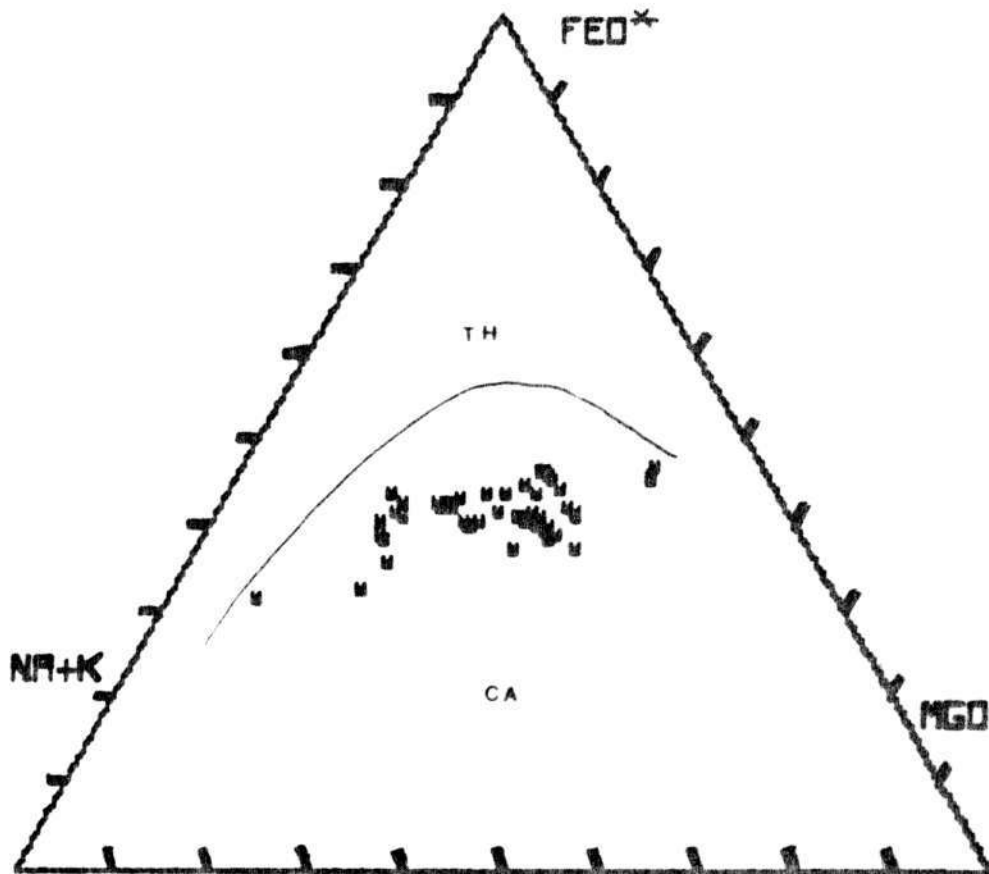


Figure 42. AFM diagram for the Crater Lake cinder cones. Solid line separating the tholeiitic (TH) and calc-alkaline (CA) fields after Kuno, 1968.

REE pattern and some flattening of the heavy REE pattern (Robyn, 1978). The REE patterns for the Crater Lake cinder cones do not show this, suggesting that early fractionation of hornblende was not significant.

Comparisons with Other Cascade Volcanoes

The question arises as to whether the observed relationships for the cinder cones are unique to Mount Mazama. Comparisons were made between the Crater Lake cinder cones, Mount Mazama (data from Ritchey, 1979), Mount Bailey (Barnes, 1978), and Mount McLoughlin (Maynard, 1974). Using samples with less than 55% SiO_2 , various combinations of elements and element ratios were plotted on variation diagrams. The most revealing of these are presented in Figures 37 and 43. Although the four groups are similar, some differences are observed. On a plot of Rb versus Ni, the Crater Lake cinder cones plot slightly below the cluster of samples, possibly a reflection of differences in partial melting. Some separation of Mount Bailey and Mount Mazama samples is observed on the plot of Rb/Zr versus Rb, suggesting different partial melts or a slight difference in degree of melting. Plots of Th are most distinctive. Samples from the Crater Lake cinder cones, Mount Mazama, and a few from Mount McLoughlin fall

along a nearly straight line, with a slope indicative of partial melting. Samples from Mount McLoughlin and a few from Mount Mazama plot in a second group, slightly above the linear trend, indicative of different degrees of partial melting. Therefore, the following conclusion is drawn: the cinder cones at Crater Lake are derived from partial melts that are not necessarily unique to Mount Mazama. Differing degrees of partial melting and fractional crystallization produced the observed differences, and the more differentiated magmas may be unique to Mount Mazama.

Hering (1981) compared Rb/Hf and Rb/Zr ratios in mafic rocks from Mount Hood, Mount Jefferson, Three Fingered Jack, South Sister, Mount Thielsen, Mount Bailey, and Newberry Volcano, and found that these ratios increase rapidly in basaltic andesite and andesitic samples. He concluded that the basaltic andesite and andesitic magmas of Mount Hood, Mount Jefferson, and Three Fingered Jack were products of discrete batches of partial melt, which may have undergone some fractionation.

Rb/Hf ratios for the Crater Lake cinder cones (not shown) do show an increase with an increase in percent SiO_2 . Zr data for the cinder cones are limited and were not considered.

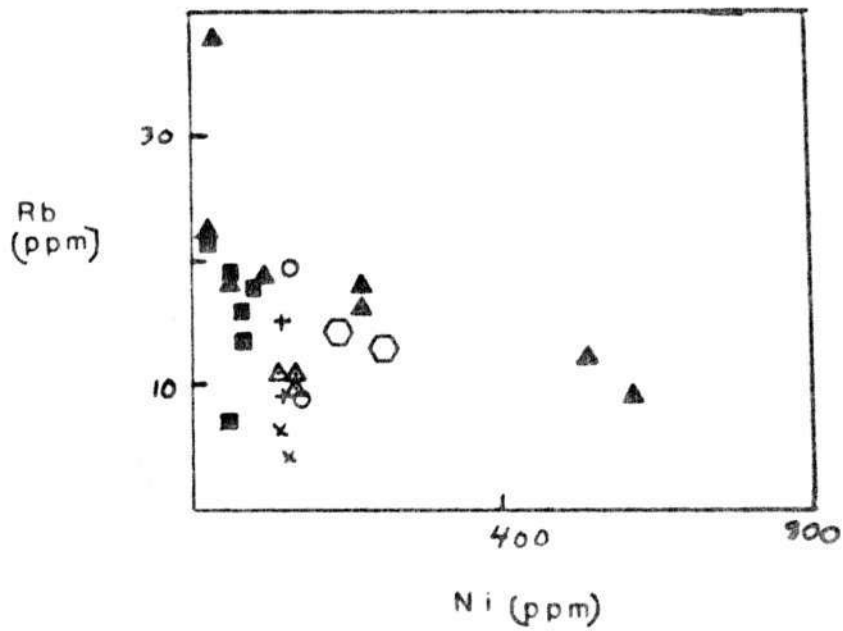


Figure 43. Comparison diagram for the Crater Lake cinder cones, Mount Mazama, Mount Bailey, and Mount McLoughlin. Symbols as in Figures 27 and 37.

Summary

Petrographic and geochemical evidence suggests that crystal fractionation of plagioclase, magnetite, olivine, augite, and hypersthene was involved in the genesis of the magmas of the Crater Lake cinder cones. However, crystal fractionation was not the only mechanism. The following observations need to be considered when formulating a model for the origin of the cones. First, the irregular pattern of basalts and andesites observed for the LREE, and the LREE enrichment in basalt relative to other members of the suite. Second, the satisfactory solutions obtained for mass-balance calculations when only major-elements are considered, but the less satisfactory solutions obtained when trace elements are considered, and the observed increase in included elements and the decrease in excluded elements in the daughter products of some of the calculations. Third, the appearance of two trends on many of the variation diagrams, and the observed scatter on the plot of Al_2O_3 . Fourth, the magmas are not primary. The contents of Ni, Cr, and MgO are too low for the magmas to be in equilibrium with mantle values.

From consideration of the LREE data, it is apparent that the Crater Lake cinder cones were derived from more than one partial melt, probably a distinct melt for each of

the groups observed. The data require at least four, distinct partial melts, which underwent various degrees of mixing and fractional crystallization to produce the lavas of the cinder cones. If this is true, then the trend is correct for fractional crystallization. In other words, for each pair, the andesite is enriched in LREE relative to the basaltic andesite as is expected. A separate partial melt is implied for the Williams Crater basalt.

Magma mixing and subsequent fractional crystallization may explain the observed patterns in the variation diagrams, and the discrepancies in the mass-balance calculations. The fact that the magmas are not primary indicates that the partial melts underwent differentiation to produce cinder cone magmas. The hypothesis of more than one partial melt would explain the presence of the two trends observed on some variation diagrams. Distinct trends for neither partial melting or fractional crystallization appear on plots of highly excluded versus highly included elements, or on H/M versus H diagrams. Thus, both processes were probably involved in the genesis of the cinder cone lavas.

The increase in included elements from parent to daughter, particularly for Ni, Cr, and Sr, can be explained by the addition of olivine, clinopyroxene, and plagioclase, possibly during magma mixing. Plagioclase contamination is

further indicated by the large weighted residuals for Sr and Ba, the scatter on the Al_2O_3 versus SiO_2 diagram, the positive Eu anomaly, and the presence of plagioclase macrophenocrysts in the samples.

CHAPTER 5

CONCLUSIONS

Twenty cinder cones are located within the boundaries of Crater Lake National Park. The thirteen cinder cones in this study have been divided into two groups, the cinder cones associated with Crater Lake, and the cinder cones associated with Mount Mazama. The Crater Lake cinder cones consist of two cinder cones associated with the Timber Crater volcano, two cinder cones associated with the Union Peak volcano, and nine cinder cones associated with Mount Mazama (refer to Figure 4 for location). The nine Mount Mazama cinder cones can be divided into two groups: eight pre-caldera cinder cones, Bald Crater, Crater Peak, Desert Cone, Hill 6545, Maklaks Crater, Red Cone, Scoria Cone, and Williams Crater; and, one post-caldera cone, Wizard Island.

Most of the cinder cones associated with Mount Mazama are located on or near the flanks of the volcano. The only exceptions are Wizard Island and Merriam Cone, located within the caldera. The cinder cones are composed of high-alumina basaltic to andesitic scoria and lavas. Mount Mazama ash and pumice are found at or near the summit of the pre-caldera cones. Therefore, the volcanic activity of the cones had ended before the climactic eruption of Mount

Mazama began. The Williams Crater Complex, a basaltic cinder cone and associated andesitic to dacitic lavas, stands on the western edge of the caldera, against an andesitic flow from Mount Mazama.

The Mount Mazama cinder cones have a range in height of 90 to 260m, basal diameter of 610 to 1295m, and ratio of cone height to basal diameter of 0.14 to 0.21. Measured ages of four Crater Lake cinder cones have a range of about 200,000 to 6700 years BP. Using morphological characteristics and measured ages, the following relative ages are proposed for the Mount Mazama cinder cones:

Wizard Island	youngest
Williams Crater	
Bald Crater, Crater Peak	
Red Cone	
Scoria Cone, Hill 6545	
Desert Cone	
Maklaks Crater	oldest

Compositional variations in the magmas of the cinder cones support the conclusion that they were generated by more than one partial melting event. Partial melting of a mantle source region with the composition of peridotite could have produced the primitive basaltic magmas.

Subsequent mixing and fractional crystallization produced the more differentiated basaltic to andesitic magmas of the cinder cones. Fractionation continued after the eruption of the cinder cones, with larger amounts of plagioclase, and eventually hornblende (Ritchey, 1979) fractionated to produce the products of the climactic eruption of Mount Mazama.

The genesis of the Williams Crater cinder cone is similar to that of the other Mazama cinder cones. The dacitic magmas are proposed to be a result of mixing that occurred when Williams Crater tapped the same magma chamber as the climactic eruption of Mount Mazama. The similarity between the composition of the cinder cones of Union Peak and Timber Crater and those of the Mazama cinder cones suggests a similar origin.

A schematic representation of the proposed evolution of the Crater Lake cinder cones is presented in Figure 44. The following model is proposed for the evolution of the Crater Lake cinder cones:

1. Generation of discrete partial melts in the mantle from a peridotitic source region.
2. Injection of these melts into the base of the crust, where initial fractional crystallization and magma mixing may have occurred.
3. Injection of magma into the crust and the base of

the Mount Mazama chamber. Magma mixing and fractionation of olivine, clinopyroxene, orthopyroxene, and plagioclase produced the basaltic to andesitic magmas of the cinder cones.

- a. The Mount Mazama magma chamber was compositionally zoned at this time, and the denser, basaltic magma could not rise through the overlying, less dense magma.
4. Eruption of the cinder cones on the flanks of Mount Mazama.
5. Fractionation of plagioclase and hornblende.
6. Eruption of 60 km^3 of zoned magma and the formation of the Crater Lake caldera.
7. Eruption of Merriam Cone, Wizard Island, and lavas onto the floor of the caldera.

The cinder cones at Crater Lake are part of the magmatic system that produced the main cone of Mount Mazama and represent magmas that were parental to the differentiated magmas of Mount Mazama.

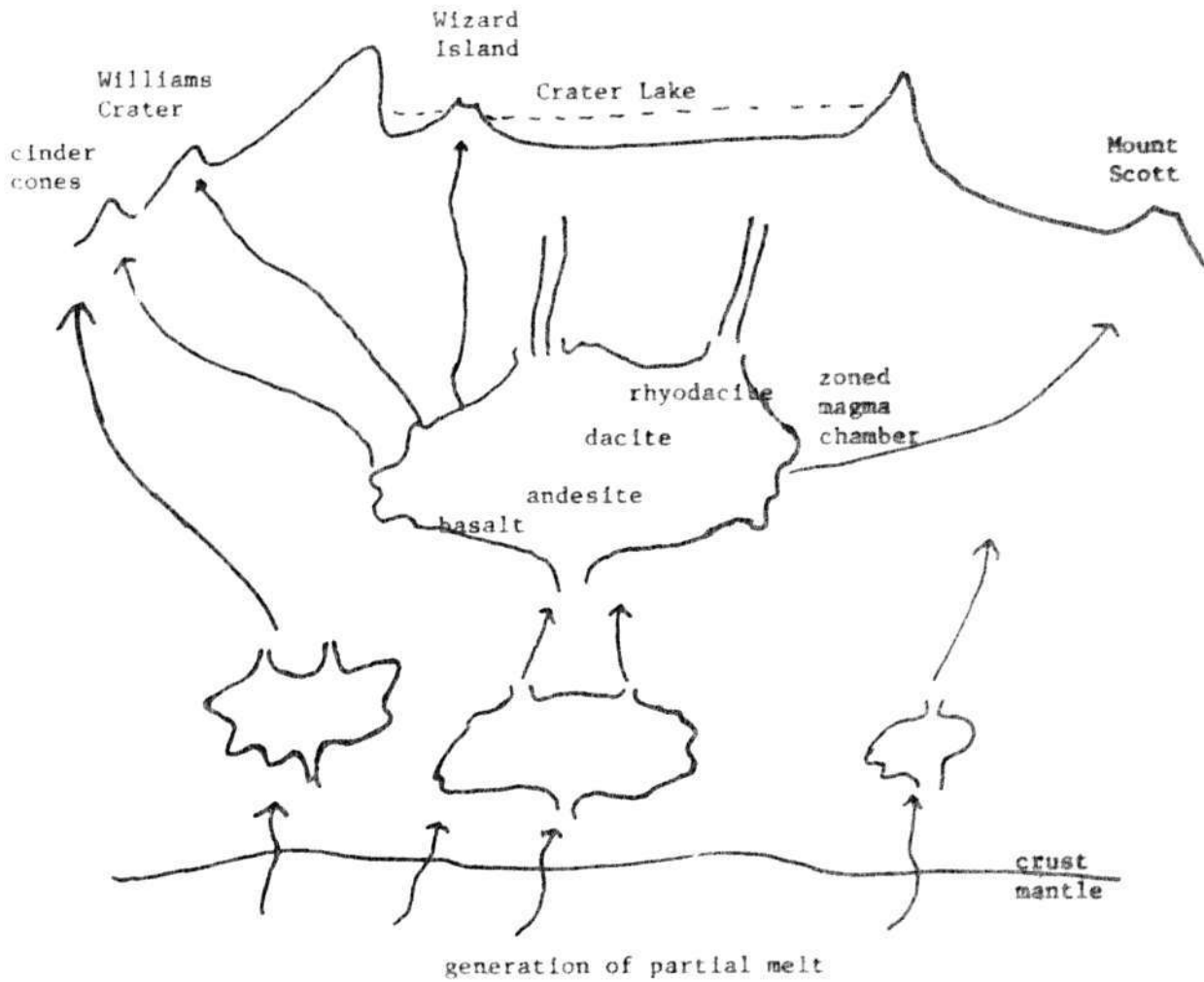


Figure 44. Schematic representation of the evolution of the Crater Lake cinder cones.

APPENDIX A

DESCRIPTIONS OF REPRESENTATIVE THIN SECTIONS

Phenocryst and groundmass phases listed in order of decreasing abundance. Phase abundances are given as the percent of the phase in the whole rock. Mineral compositions were determined optically. In some samples, the number of macrophenocrysts that could be used to determine composition were small. In these cases, less than 10 crystals were used to determine the composition. The number of crystals used is indicated in the description.

Basalt

Scoria

Sample name: MC-3

Texture: vesicular, porphyritic, hyalophitic

Phenocrysts: plagioclase, olivine, opaques

Groundmass: glass, opaques, plagioclase

Mineral description and percentages:

40% Glass-red.

30% Plagioclase-An₄₈, euhedral to subhedral, some resorbed edges.

20% Opaques-anhedral.

10% Olivine-Fo₈₀, anhedral, most crystals rimmed with and contain inclusions of opaques, many crystals partially or completely altered to granular opaques.

Lava flow

Sample name: WC-13

Texture: vesicular, porphyritic, hyalophitic

Phenocrysts: plagioclase, augite, hypersthene, olivine

Groundmass: glass, opaques, plagioclase

Mineral description and percentages:

25% Glass-red.

25% Plagioclase

macrophenocrysts-An₄₄ (less than 10 crystals), subhedral to anhedral, contain inclusions of Types 2 and 3, rounded crystals, crystals contain normal and oscillatory zoning, most crystals have

- resorbed edges.
 smaller phenocrysts-An₅₄, subhedral, most
 crystals are lath shaped, a few crystals
 contain inclusions, crystals are zoned.
- 20% Opaques-anhedral.
- 10% Hypersthene-subhedral, some crystals contain
 inclusions of opaques.
- 10% Augite-subhedral to anhedral, some crystals
 are twinned.
- 5% Olivine-Fo₈₅, subhedral, many crystals corroded,
 some crystals are rimmed with glass.

Andesitic Basalt

Lava flow

- Sample name: RC-14
 Texture: vesicular, porphyritic, intergranular groundmass
 Phenocrysts: plagioclase, augite, hypersthene, olivine,
 opaques
 Groundmass: plagioclase, pyroxene, opaques
 Mineral description and percentages:
- 40% Plagioclase-An₅₄, rim An₆₀, core An₅₂,
 euhedral to anhedral, most of the crystals
 are lath shaped, forms glomerocrysts with
 pyroxene, crystals contain inclusions of
 opaques and apatite, crystals are zoned.
 groundmass-An₅₁, rim An₆₀, core An₄₆.
- 20% Augite-subhedral to anhedral, some crystals are
 twinned, crystals contain opaque inclusions.
- 10% Hypersthene-euhedral to anhedral, crystals contain
 inclusions of opaques and clinopyroxene, the
 larger, euhedral crystals appear to be breaking
 apart.
- 15% Opaques-anhedral.
- 5% Olivine-Fo₈₅ subhedral, crystals contain
 inclusions of opaques, edges of crystals
 altered to a greenish material, possibly
 serpentine.
- 1% Apatite-euhedral.

Basaltic andesite

Scoria

- Sample name: CP-7
 Texture: vesicular, porphyritic, hyalophitic

Phenocrysts: plagioclase, augite, hypersthene, olivine

Groundmass: glass, opaques, minor plagioclase

Mineral description and percentages:

35% Glass-red to reddish brown.

25% Plagioclase-

macrophenocrysts-An₄₅, rim An₇₁,
core An₆₂ (five crystals), subhedral to
anhedral, inclusions of Type 3, most crystals
have rounded edges, crystals exhibit normal,
reverse, and oscillatory zoning.

smaller phenocrysts-An₆₈, euhedral to
subhedral, some crystals have resorbed edges,
crystals form plagioclase glomerocrysts,
apatite inclusions.

15% Opaques-anhedral.

10% Augite-subhedral to anhedral, crystals contain
inclusions of opaques and hematite.

10% Hypersthene-subhedral to anhedral, crystals
contain inclusions of opaques and hematite.

5% Olivine-Fo₈₀, subhedral, crystals contain
inclusions of opaques and hematite.

<5% Hematite-anhedral.

1% Apatite-euhedral to subhedral.

Andesite

Scoria

Sample name: CP-4

Texture: porphyritic, pilotaxitic

Phenocrysts: plagioclase, hypersthene, augite, olivine,
opaques

Groundmass: plagioclase, opaques, glass, pyroxene

Mineral description and percentages:

30% Plagioclase-

macrophenocrysts-An₅₆, rim An₃₇, core An₅₂,
subhedral to anhedral, crystals are twinned,
and zoned, with normal, reverse, and
oscillatory zoning, crystals are rounded,
many with resorped edges, crystals contain
inclusions of glass, apatite, groundmass,
inclusions of Types 2 and 3.

smaller phenocrysts-An₅₆, subhedral, crystals
contain twinning and zoning.

20% Hypersthene-euhedral to anhedral, some crystals
are fractured and broken apart along the
fractures, crystals contain inclusions of
pyroxene and opaques, a few crystals contain

- exsolution parallel to cleavage.
- 15% Augite-euhedral to anhedral, crystals contain inclusions of pyroxene and opaques, some crystals are twinned, some crystals have resorbed edges.
 - 15% Opaques-subhedral to anhedral.
 - 10% Glass-clear with a greenish tint.
 - 5% Olivine-Fo₇₇, subhedral to anhedral, crystals contain opaque inclusions.
 - 1% Apatite-euhedral.

Lava flow

- Sample name: WI-14
 Texture: vesicular, porphyritic, intersertal, seriate, glomerocrystic
 Phenocrysts: plagioclase, hypersthene, augite, olivine, opaques, hornblende
 Groundmass: plagioclase, opaques, glass
 Mineral description and percentages:
- 35% Plagioclase-forms glomerocrysts with pyroxene and hornblende.
 macrophenocryst-An₄₉, rim An₅₄, core An₆₂, rim An₃₈, core An₃₄, euhedral to anhedral, inclusions of opaques, pyroxene, dust, glass, apatite, inclusions of Types 1, 2, 3, and 4, normal, reverse, and oscillatory zoning present.
 smaller phenocrysts-An₃₆, euhedral to subhedral, many crystals have resorbed edges.
 - 20% Glass-gray.
 - 20% Opaques-anhedral.
 - 10% Hypersthene-euhedral to anhedral, inclusions of opaques and apatite, anhedral crystals have resorbed edges.
 - 8% Augite-euhedral to anhedral, inclusions of opaques and apatite, some crystals are twinned, many crystals rimmed with opaques or pyroxene.
 - 5% Olivine-Fo₈₈, subhedral, inclusions of opaques, and orthopyroxene.
 - 1% Hornblende-oxyhornblende, subhedral to anhedral, inclusions of opaques, clinopyroxene, orthopyroxene, and plagioclase, crystals rimmed with opaques surrounded by a rim of plagioclase, pyroxene, and opaques.
 - 1% Apatite-euhedral to subhedral, occurs as inclusions in other minerals.

Dacite

Lava flow

Sample name: WC-16 (dark band)

Texture: slightly vesicular porphyritic, hyalophitic

Phenocrysts: plagioclase, hypersthene, augite, opaques, hornblende

Groundmass: glass, plagioclase, opaques

Mineral description and percentages:

30% Plagioclase-

macrophenocrysts-An₆₅, subhedral to anhedral, crystals fresher, less corroded than those in rocks with less than 63% SiO₂, oscillatory zoning, inclusions of Types 2 and 4.

smaller phenocrysts-An₅₃, subhedral to anhedral, normal and oscillatory zoning present, inclusions of pyroxene and opaques.

30% Glass-light brown to clear.

20% Opaques-euhedral to anhedral, opaque phenocrysts become more abundant in this rock type.

10% Hypersthene-euhedral to subhedral.

10% Augite-euhedral to subhedral.

1% Hornblende-anhedral.

1% Apatite-euhedral.

Sample name: WC-16 (light band)

Texture: porphyritic, intersertal, seriate

long, slender crystals of pyroxene radiating from plagioclase crystals are found at the contact between the light and dark bands.

Phenocrysts: plagioclase, hypersthene, augite, opaques

Groundmass: glass; pyroxene, glass, and opaques occupy the interstices between the plagioclase crystals

Mineral description and percentages:

30% Plagioclase-

macrophenocrysts-subhedral to anhedral, normal, oscillatory, and possibly reverse zoning, inclusions of opaques, pyroxene, and glass, inclusions of Types 2 and 4.

smaller phenocrysts-An₄₁, rim An₄₂, core An₃₁, subhedral to anhedral, normal, oscillatory, and possibly reverse zoning present, inclusions of opaques and pyroxene.

30% Glass-light brown.

15% Hypersthene-subhedral to anhedral, crystal edges are embayed.

15% Augite-subhedral to anhedral, crystal edges are embayed.

10% Opaques-subhedral to anhedral.

Rhyodacite

Lava flow

Sample name: WC-24

Texture: porphyritic, hyalophitic

Phenocrysts: plagioclase, augite, hornblende, hypersthene, opaques

Groundmass: glass, plagioclase

Mineral description and percentages:

30% Plagioclase

macrophenocrysts-An₇₁, euhedral to anhedral, oscillatory zoning with some normal zoning, only a few crystals have inclusions of opaques, pyroxene, hornblende, and apatite, inclusions of Types 2 and 4, crystals relatively fresh, most are nearly euhedral, forms plagioclase glomerocrysts.

smaller phenocrysts-An₆₄, euhedral to subhedral, some crystals have resorped edges, inclusions of opaques.

20% Glass-clear.

15% Hornblende-oxyhornblende, euhedral to anhedral, inclusions of opaques.

15% Augite-euhedral to anhedral, opaque inclusions.

15% Opaques-magnetite, euhedral to anhedral.

5% Hypersthene-euhedral to anhedral, opaque inclusions.

APPENDIX B

CHEMICAL ANALYSES

AA Analyses

Mount Mazama Cinder Cones

<u>Major Elements</u>	<u>Values in weight percent.</u>						
	CP-1	CP-7	WI-1	WI-8	WI-12	RC-7	BC-4
SiO ₂	56.72	56.55	57.99	58.10	58.68	53.50	54.04
TiO ₂	0.90	0.94	0.79	0.78	0.80	1.06	0.99
Al ₂ O ₃	17.18	17.46	17.80	17.89	17.73	16.96	16.74
Fe ₂ O ₃	3.05	2.72	1.42	5.15	1.32	4.19	3.36
FeO	3.34	3.94	4.65	1.22	4.66	3.45	4.22
MnO	0.12	0.12	0.12	0.12	0.12	0.13	0.14
MgO	4.64	4.93	3.80	3.73	3.62	7.03	6.68
CaO	7.07	7.57	6.51	6.85	6.81	8.56	8.31
Na ₂ O	4.00	4.08	4.05	4.16	4.15	3.69	3.75
K ₂ O	1.29	1.23	0.98	0.95	0.99	1.10	1.03
H ₂ O ⁺	0.43	0.51	0.35	0.48	0.67	0.29	0.44
H ₂ O ⁻	0.16	0.35	0.20	0.45	0.07	0.22	0.46
P ₂ O ₅	0.31	0.32	0.21	0.21	0.22	0.40	0.41
TOTAL	99.21	100.72	98.87	100.09	99.84	100.58	100.57

<u>Trace Elements</u>	<u>Values in ppm.</u>						
BA	516	555	406	405	405	511	361
CO	24.00	54.00	61.00	80.00	24.00	48.00	41.00
CR	92.00	81.00	56.00	36.00	66.00	260	292
CU	35.00	48.00	43.00	51.00	63.00	73.00	42.00
LI	16.00	16.00	18.00	18.00	17.00	13.00	8.80
NI	74.00	78.00	50.00	64.00	51.00	164	142
RB	18.00	16.00	19.00	17.00	17.00	14.00	8.70
SR	994	1046	673	657	683	1147	1060
ZN	99.60	76.00	73.00	87.00	73.00	77.00	73.00
*FeO	6.08	6.39	5.93	5.85	5.85	7.22	7.24
D. I.	2.06	1.45	2.91	2.70	2.92	-1.11	-0.69
Na+K	5.29	5.31	5.03	5.11	5.14	4.79	4.78
RADIUS	10.50	10.50	3.00	3.00	3.00	7.75	14.50

Major Elements

	RC-12	BC-3	WI-14	BC-1	CP-4	DC-4	MC-1
BI02	53.11	54.38	59.63	54.04	59.83	52.65	53.02
TI02	0.95	0.94	0.76	0.89	0.75	1.13	0.85
AL203	16.54	17.86	18.13	16.80	17.10	17.81	18.65
FE203	3.51	3.24	2.22	5.30	1.91	2.25	4.22
FEO	3.88	3.73	3.70	2.46	3.73	6.14	3.96
MNO	0.12	0.12	0.11	0.14	0.10	0.15	0.14
MGO	8.23	6.01	3.04	6.36	3.25	6.22	6.05
CAO	7.97	8.27	6.31	8.03	5.86	8.38	8.52
NA2O	3.56	3.75	4.27	3.93	4.66	3.63	3.60
K2O	1.26	1.06	1.16	0.91	1.72	0.68	0.45
H2O+	0.24	0.16	0.33	0.04	0.54	0.39	0.28
H2O-	0.21	0.18	0.33	0.09	0.39	0.28	0.37
P2O5	0.33	0.27	0.22	0.29	0.17	0.32	0.18
TOTAL	99.91	99.97	100.21	99.28	100.01	100.03	100.29

Trace Elements

BA	455	428	425	329	517	156	153
CO	56.00	53.00	41.00	41.00	42.00	50.00	53.00
CR	406	185	45.00	294	63.00	181	197
CU	68.00	34.00	48.00	55.00	45.00	58.00	75.00
LI	12.00	11.00	17.00	12.00	11.00	12.00	11.00
NI	251	134	43.00	133	61.00	133	127
RB	13.00	12.00	21.00	19.00	34.00	9.40	4.10
SR	1024	1003	671	846	582	571	556
ZN	78.00	67.00	61.00	88.00	60.00	78.00	80.00
*FEO	7.04	6.65	5.70	7.23	5.45	8.16	7.76
D. I.	-1.34	-0.18	3.91	-0.40	4.60	-0.97	-1.10
NA+K	4.82	4.81	5.43	4.84	6.38	4.31	4.05
RADIUS	7.75	15.50	3.00	14.50	10.50	11.50	14.50

Major Elements

	DC-3	DC-5	MC-3	BC-2	65-1
S102	52.49	52.92	52.43	54.67	55.10
T102	0.97	1.06	0.84	0.87	0.91
AL2O3	17.72	17.74	18.37	18.08	17.91
FE2O3	7.74	3.89	8.10	3.59	4.33
FE0	0.44	4.66	0.04	3.50	2.75
MNG	0.16	0.15	0.14	0.12	0.12
MGO	6.41	6.22	6.03	5.94	5.77
CAO	7.70	8.22	7.86	7.97	7.90
NA2O	3.43	3.67	3.39	3.64	3.77
K2O	0.55	0.68	0.49	1.03	0.99
H2O+	0.45	0.35	0.46	0.28	0.26
H2O-	0.50	0.28	0.74	0.18	0.33
P2O5	0.44	0.30	0.18	0.30	0.29
TOTAL	99.00	100.14	99.07	100.17	100.43

Trace Elements

BA	273	300	315	427	391
CO	50.00	62.00	42.00	39.00	49.00
CR	240	182	161	166	170
CU	33.00	63.00	48.00	55.00	51.00
LI	9.30	11.00	8.30	9.70	12.00
NI	136	111	113	138	120
RB	11.00	11.00	6.40	12.00	12.00
SR	530	549	517	998	977
ZN	87.00	86.00	80.00	76.00	78.00
*FEO	7.40	8.16	7.33	6.73	6.65
D. I.	-0.73	-0.81	-0.68	0.10	0.28
NA+K	3.98	4.35	3.88	4.67	4.76
RADIUS	11.50	11.50	14.50	15.50	14.00

Williams Crater Complex

Major Elements

	FC-24	FC-25	FC-28	FC-29	FC-31	HF-2
SiO ₂	68.15	63.27	59.94	58.85	52.35	59.65
TiO ₂	0.60	0.78	0.72	0.82	1.20	0.73
Al ₂ O ₃	15.33	15.83	18.36	17.75	16.38	18.54
Fe ₂ O ₃	1.27	1.62	2.47	4.16	4.66	2.33
FeO	2.23	3.34	3.26	1.92	3.37	3.29
MnO	0.08	0.09	0.10	0.10	0.14	0.10
MgO	1.44	3.33	2.64	3.16	7.59	2.83
CaO	3.48	5.26	6.35	6.75	9.73	6.49
Na ₂ O	4.28	4.27	4.02	4.62	3.32	4.49
K ₂ O	2.32	1.86	1.18	1.89	0.95	1.34
H ₂ O ⁺	0.57	0.44	0.53	0.06	0.38	0.11
H ₂ O ⁻	0.20	0.31	0.41	0.12	0.35	0.14
F ₂ O ₅	0.13	0.28	0.31	0.44	0.55	0.29
TOTAL	100.08	100.68	100.29	100.64	100.97	100.33

Trace Elements

BA	651	596	542	787	161	526
CO	124	36.00	38.00	29.00	49.00	29.00
CR	23.00	108	35.00	45.00	300	31.00
CU	18.00	32.00	45.00	70.00	72.00	46.00
LI	30.00	24.00	18.00	17.00	10.00	16.00
NI	32.00	49.00	45.00	43.00	116	38.00
RR	52.00	40.00	23.00	26.00	9.20	22.00
SK	366	593	992	1839	947	978
ZN	46.00	57.00	68.00	76.00	73.00	65.00
#FeO	3.37	4.80	5.48	5.66	7.56	5.39
D. L.	9.19	5.64	4.19	4.01	-2.58	4.06
NA+K	6.60	6.13	5.20	6.51	4.27	5.83
RADIUS	6.50	6.50	6.50	6.50	6.50	nd

Major Elements

	FC-13	FC-16	FC-18	HF-3
SiO2	51.40	64.82	50.89	59.65
TiO2	1.13	0.73	1.16	0.62
Al 2O3	16.76	15.28	16.37	18.49
Fe2O3	5.84	1.27	2.87	2.22
FeO	2.40	3.16	5.24	3.39
MnO	0.14	0.09	0.14	0.10
MgO	7.61	3.04	7.40	2.87
CaO	9.49	4.57	9.43	6.53
Na2O	3.46	4.42	3.57	4.25
K2O	0.85	2.08	0.89	1.21
H2O+	0.45	0.52	0.45	0.59
H2O-	0.45	0.30	0.33	0.23
P2O5	0.40	0.18	0.42	0.27
TOTAL	100.38	100.46	99.16	100.42

Trace Elements

BA	387	608	386	511
CO	61.00	37.00	71.00	29.00
CR	242	109	235	33.00
CU	60.00	27.00	69.00	37.00
LI	12.00	24.00	11.00	19.00
NI	114	42.00	104	38.00
RB	15.00	39.00	15.00	23.00
SR	1015	482	1055	998
ZN	70.00	51.00	85.00	65.00
*FeO	7.65	4.30	7.82	5.39
D.I.	-2.66	6.73	-2.53	3.90
NA+K	4.31	6.60	4.46	5.46
RADIUS	6.50	6.50	6.50	nd

Timber Crater and Union Peak Cinder Cones

Major Elements

	TC-5	UP-3	UP-10	69-4	TC-2
SiO ₂	54.25	53.57	54.78	57.54	57.59
TiO ₂	1.08	0.91	0.88	0.82	0.86
Al ₂ O ₃	19.32	18.93	18.39	17.65	17.38
Fe ₂ O ₃	3.36	3.08	3.21	3.32	3.98
FeO	2.93	4.25	3.86	3.11	2.51
MnO	0.09	0.13	0.12	0.12	0.11
MgO	5.11	5.41	5.07	4.02	3.99
CaO	9.01	9.09	8.02	7.01	6.69
Na ₂ O	3.33	3.65	3.75	3.78	3.73
K ₂ O	0.90	0.60	0.79	1.40	1.13
H ₂ O ⁺	0.59	0.19	0.30	0.61	0.58
H ₂ O ⁻	0.55	0.24	0.32	0.43	0.54
P ₂ O ₅	0.43	0.17	0.22	0.29	0.32
TOTAL	100.95	100.22	99.71	100.13	99.41

Trace Elements

BA	152	137	159	540	521
CO	45.00	45.00	44.00	42.00	34.00
CR	88.00	106	109	117	122
CU	47.00	68.00	28.00	55.00	45.00
LI	12.00	9.50	12.00	16.00	17.00
NI	77.00	66.00	88.00	72.00	79.00
RB	13.00	7.60	11.00	20.00	21.00
SR	1687	769	783	719	757
ZN	58.00	65.00	66.00	68.00	161
#FeO	5.95	7.02	6.75	6.10	6.09
D. I.	-0.32	-0.91	0.40	2.69	2.72
NA+K	4.23	4.25	4.54	5.15	4.86
RADIUS	nd	nd	nd	nd	nd

Major Elements

	TC-6	UP-8	CPT-2	CPT-6	CPT-8
S102	57.78	52.55	53.00	54.51	50.08
T102	0.92	0.90	1.23	1.10	1.10
AL203	17.72	18.24	18.77	18.57	17.89
FE203	2.45	5.83	3.04	3.56	2.89
FE0	3.93	1.81	5.56	4.32	5.71
MNO	0.12	0.13	0.16	0.13	0.15
MGC	4.06	5.84	4.13	4.50	7.52
CAO	6.60	8.72	7.62	8.09	10.52
NA20	3.91	3.69	3.84	3.77	3.03
F20	1.23	0.54	1.25	0.84	0.40
H20+	0.26	0.11	0.49	0.46	0.46
H20-	0.50	0.21	0.26	0.31	0.31
P205	0.32	0.21	0.59	0.26	0.19
TOTAL	99.80	98.78	99.94	100.42	100.25

Trace Elements

BA	502	238	620	363	199
CO	29.00	42.00	34.00	34.00	44.00
CR	122	124	49.00	100.00	260
CU	53.00	76.00	68.00	46.00	77.00
LI	16.00	9.70	9.80	9.50	7.20
NI	67.00	94.00	40.00	63.00	145
RR	19.00	8.00	14.00	11.00	4.80
SR	721	752	795	723	547
ZN	97.00	71.00	135	84.00	71.00
#FE0	6.13	7.06	nd	nd	nd
D. L.	2.86	-1.12	1.36	0.70	-3.92
NA#	5.14	4.23	nd	nd	nd
RADIUS	nd	nd	nd	nd	nd

INAA Analyses

Values in ppm.

Element	Sample				
	BC-1	DC-4	CP-1	MC-1	RC-12
Abundance					
Error					
Cs	ND	0.402 <u>+0.053</u>	1.074 <u>+0.038</u>	ND	0.563 <u>+0.063</u>
Zr	ND	ND	ND	ND	ND
Sc	20.250 <u>+0.211</u>	21.061 <u>+0.221</u>	16.140 <u>+0.165</u>	21.734 <u>+0.227</u>	20.786 <u>+0.217</u>
Hf	2.498 <u>+0.092</u>	2.118 <u>+0.096</u>	3.190 <u>+0.065</u>	2.065 <u>+0.093</u>	2.886 <u>+0.095</u>
Ta	0.412 <u>+0.095</u>	ND	0.270 <u>+0.025</u>	ND	0.708 <u>+0.074</u>
Th	1.485 <u>+0.080</u>	ND	2.412 <u>+0.064</u>	0.738 <u>+0.077</u>	2.392 <u>+0.097</u>
U	ND	ND	0.851 <u>+0.074</u>	ND	
La	13.734*	8.976*	18.493 <u>+0.299</u>	8.505*	18.400*
Ce	27.425 <u>+0.450</u>	20.049 <u>+0.408</u>	39.800 <u>+0.500</u>	16.590 <u>+0.376</u>	39.715 <u>+0.560</u>
Sm	3.302*	2.496*	3.894 <u>+0.040</u>	2.400*	3.840*
Eu	3.064 <u>+0.032</u>	3.982 <u>+0.135</u>	1.311 <u>+0.043</u>	3.736 <u>+0.137</u>	2.658 <u>+0.200</u>

Tb	0.521 <u>+0.023</u>	3.982 <u>+0.025</u>	0.970 <u>+0.041</u>	0.530 <u>+0.024</u>	0.498 <u>+0.027</u>
Yb	1.869 <u>+0.139</u>	2.400 <u>+0.146</u>	1.650 <u>+0.061</u>	1.531 <u>+0.222</u>	1.590 <u>+0.132</u>
Lu	0.272*	0.256*	0.254 <u>+0.006</u>	0.198*	0.288*

	SC-3	WC-18	WI-1	WI-12	TC-6
Cs	ND	ND	1.287 <u>+0.108</u>	0.950 <u>+0.092</u>	0.499 <u>+0.052</u>
Zr	ND	262.344 <u>+31.703</u>	212.684 <u>+26.873</u>	ND	ND
Sc	19.217 <u>+0.402</u>	25.228 <u>+0.256</u>	15.340 <u>+0.156</u>	14.466 <u>+0.148</u>	16.285 <u>+0.176</u>
Hf	2.326 <u>+0.097</u>	2.820 <u>+0.074</u>	2.540 <u>+0.065</u>	2.300 <u>+0.054</u>	3.731 <u>+0.078</u>
Ta	0.803 <u>+0.056</u>	0.440 <u>+0.002</u>	0.270 <u>+0.002</u>	ND	0.527 <u>+0.043</u>
Th	2.059 <u>+0.103</u>	2.420 <u>+0.800</u>	1.512 <u>+0.057</u>	1.451 <u>+0.050</u>	1.807 <u>+0.069</u>
U	ND	ND	0.739 <u>+0.060</u>	0.651 <u>+0.066</u>	ND
La	14.400*	19.889 <u>+0.299</u>	11.190 <u>+0.184</u>	11.293 <u>+0.231</u>	18.000*
Ce	29.282 <u>+0.512</u>	41.000 <u>+0.500</u>	23.900 <u>+0.30</u>	23.600 <u>+0.304</u>	38.964 <u>+0.491</u>
Sm	3.456*	4.098*	2.957 <u>+0.030</u>	2.813 <u>+0.029</u>	3.744*
Eu	3.847 <u>+0.322</u>	1.310 <u>+0.053</u>	1.084 <u>+0.045</u>	1.058 <u>+0.037</u>	3.352 <u>+0.148</u>
Tb	0.434 <u>+0.027</u>	0.520 <u>+0.030</u>	0.477 <u>+0.130</u>	0.364 <u>+0.144</u>	0.566 <u>+0.039</u>
Yb	0.977 <u>+0.160</u>	1.784 <u>+0.159</u>	1.600 <u>+0.083</u>	1.456 <u>+0.062</u>	1.827 <u>+0.106</u>
Lu	0.288*	0.274 <u>+0.006</u>	0.275 <u>+0.005</u>	0.214 <u>+0.005</u>	0.304*

UP-3

Cs	ND
Zr	ND
Sc	23.867 +0.247
Hf	2.050 +0.062
Ta	0.454 +0.033
Th	0.794 +0.046
U	ND
La	9.135*
Ce	17.992 +0.289
Sm	2.592
Eu	3.469 +0.157
Tb	0.499 +0.109
Yb	1.294 +0.103
Lu	0.166

ND-not determined.

*-abundance estimated from graph.

REFERENCES

- Allegre, C. J., and Minster, J. F., 1978, Quantitative models of trace-element behavior in magmatic processes: *Earth and Planetary Science Letters*, v. 38, p. 1-25.
- Armstrong, R. L., 1978, Cenozoic igneous history of the U. S. Cordillera from latitude 42° to 49°N: *Geological Society of America Memoir* 152, p. 265-282.
- Bacon, C. R., 1983, Eruptive history of Mount Mazama and Crater Lake Caldera, Cascade Range, U. S. A.: *Journal of Volcanology and Geothermal Research*, v. 18, p. 57-115.
- Barnes, C. G., 1978, The geology of the Mount Bailey area, Oregon [M.S. thesis]: Eugene, Oregon, University of Oregon, 123 p.
- Barnes, C. G., and Ritchey, J. L., 1978, Tectonic implications of structural patterns in the Cascades of southern Oregon [abs.]: *Proceedings of the Oregon Academy of Sciences*, v. 14, p. 141-142.
- Blank, H. R., Jr., 1968, Aeromagnetic and gravity surveys of the Crater Lake Region, Oregon, in Hollis, D., ed., *Andesite Conference Guidebook: Oregon Department of Geology and Mineral Industries Bulletin* 62, p.42-52.
- Bloomfield, K., 1975, A late-Quaternary monogenetic volcanic field in central Mexico: *Geologische Rundschau*, v. 64, p. 476-497.
- Bottlinga, Y., Kudo, A., and Weill, D., 1966, Some observations on oscillatory zoning and crystallization of magmatic plagioclase: *The American Mineralogist*, v. 51, p. 792-807.
- Brikowski, T. H., 1983, Geology and petrology of Gearhart Mountain: A study of calc-alkaline volcanism east of the Cascades in Oregon [M.S. thesis]: Eugene, Oregon, University of Oregon, 157 p.

- Byrne, J. V., 1965, Bathymetry of Crater Lake, Oregon, in Peterson, N. V., and Groh, E. H., eds., Lunar Geologic Field Conference Guidebook: Oregon Department of Geology and Mineral Industries Bulletin 65, p. 46-51.
- Champion, D. E., 1983, Paleomagnetic "dating" of Holocene volcanic activity at Mount Mazama, Crater Lake, Oregon [abs.]: Geological Society of America Abstracts with Programs, v. 15, no. 5, p. 331.
- Clark, J. G., 1983, Geology and petrology of South Sister Volcano, High Cascade Range, Oregon [Ph.D. dissert.]: Eugene, Oregon, University of Oregon, 235 p.
- Cranson, K. R., 1980, Crater Lake- Gem of the Cascades, The Geological Story of Crater Lake National Park: Lansing, Michigan, K. R. Cranson Press, 121 p.
- Crowe, B., Halleck, P. M., and Nolf, B., 1978, Evolution of composite volcanoes [abs.]: The role of dike and sill emplacement within the volcanic edifice: Geological Society of America abstracts with programs, v. 10, no. 3, p. 101.
- Diller, J. S., and Patton, H. B., 1902, The geology and petrography of Crater Lake National Park: U. S. Geological Survey Professional Paper 3, 167p.
- Foshag, W. F., and Gonzalez, R., 1956, Birth and development of Paricutin Volcano, Mexico: U. S. Geological Survey Bulletin 965-D, p. 355-489.
- Gutmann, J. T., 1979, Structure and eruptive cycle of cinder cones in the Pinacate Volcanic Field and the controls of strombolian activity: Journal of Geology, v. 87, p. 448-454.
- Hanson, G. N., 1978, The application of trace elements to the petrogenesis of igneous rocks of granitic composition: Earth and Planetary Science Letters, v. 38, p. 26-43.
- Hering, C. W., 1981, Geology and petrology of the Yamsay Mountain Complex, south-central Oregon: A study of bimodal volcanism [Ph.D. dissert.]: Eugene, Oregon, University of Oregon, 194 p.

- Hughes, J. M., Stoiber, R. E., and Carr, M. J., 1980, Segmentation of the Cascade Volcanic Chain: *Geology*, v. 8, p. 15-17.
- Kuno, H., 1964, Differentiation of basalt magmas, in Hess, H. H., and Poldervaart, A., eds., *Basalts-The Poldervaart Treatise on Rocks of Basaltic Composition*: New York, Interscience Publishers, v. 2, p. 623-688.
- Lawrence, R. D., 1976, Strike-slip faulting terminates the Basin and Range Province in Oregon: *Geological Society of America Bulletin*, v. 87, p. 846-850.
- Luhr, J. F., and Carmichael, I. S. E., 1981, The Colima Volcanic Complex, Mexico: II. Late Quaternary cinder cones: *Contributions to Mineralogy and Petrology*, v. 76, p. 127-147.
- MacLeod, N. S., Sherrod, D. R., Chitwood, L. A., and McKee, E. H., 1981, Newberry Volcano, Oregon, in Johnston, D. A., and Donnelly-Nolan, J., eds., *Guides to some volcanic terranes in Washington, Idaho, Oregon, and Northern California*: U. S. Geological Survey Circular 838 p. 85-91.
- MacLeod, N. S., Walker, G. W., and McKee, E. H., 1977, Geothermal significance of eastward increase in age of Upper Cenozoic rhyolitic domes in southeastern Oregon, in *Proceedings: Second United Nations Symposium on the Development and Use of Geothermal Resources*: Washington, D. C., U. S. Government Printing Office, v.1, p. 465-474.
- Masuda, A., Nakamura, N., and Tanaka, T., 1973, Fine structures of mutually normalized rare-earth patterns of chondrites: *Geochimica et Cosmochimica Acta*, v. 37, p. 239-248.
- Maynard, L., 1974, The geology of Mount McLoughlin [M.S. thesis]: Eugene, Oregon, University of Oregon, 139 p.
- McBirney, A. R., 1968, Petrochemistry of Cascade Andesite Volcanoes, in Dole, H. M., ed., *Andesite Conference Guidebook*: Oregon Department of Geology and Mineral Industries Bulletin 62, p. 101-107.

- 1978, Volcanic evolution of the Cascade Range: Annual Reviews of Earth and Planetary Sciences, v. 6, p. 437-456.
- McGetchin, T. R., and Head, J. W., 1973, Lunar cinder cones: Science, v. 180, p. 68-71.
- McGetchin, T. R., Settle, M., and Chouet, B. A., 1974, Cinder cone growth modeled after Northeast Crater, Mount Etna, Sicily: Journal of Geophysical Research, v. 79, no. 23, p. 3257-3272.
- Mertzman, S. A., Jr., 1977, The petrology and geochemistry of the Medicine Lake Volcano, California: Contributions to Mineralogy and Petrology, v. 62, p. 221-247.
- 1980, The Scoria Cone pit crater and its uncollapsed relatives, Crater Lake National Park, Oregon [abs.]: Geological Society of America Abstracts with Programs, v.12, no.7, p. 482.
- Pike, R. J., 1978, Volcanoes on the inner planets: Some preliminary comparisons of gross topography: Proceedings of the 9th Lunar and Planetary Science Conference, p. 3239-3273.
- Pike, R. J., and Clow, G. D., 1981, Revised classification of Terrestrial volcanoes and catalog of topographic dimensions, with new results on edifice volume: U. S. Geological Survey Open File Report 81-1038 40 p.
- Porter, S. C., 1972, Distribution, morphology, and size frequency of cinder cones on Mauna Kea Volcano, Hawaii: Geological Society of America Gulletin, v. 83, p. 3607-3612.
- Ritchey, J. L., 1979, Origin of divergent magmas at Crater Lake, Oregon [Ph.D. dissert.]: Eugene, Oregon, University of Oregon, 209 p.
- Robyn, T. L., 1977, Geology and petrology of the Strawberry Volcanics, northeastern Oregon [Ph.D. dissert.]: Eugene, Oregon, University of Oregon, 197 p.
- Scott, D. H., and Trask, N. J., 1971, Geology of the Lunar Crater Volcanic Field, Nye County, Nevada: U. S., Geological Survey Professional Paper 599-I, 22 p.

- Settle, M., 1979, The structure and emplacement of cinder cone fields: *American Journal of Science*, v. 279, p. 1089-1107.
- White, C. M., and McBirney, A. R., 1978, Some quantitative aspects of orogenic volcanism in the Oregon Cascades: *Geological Society of America Memoir* 152, p. 369-388.
- Wilcox, R. E., 1948, Activity of Paricutin Volcano from April 1 to July 31, 1947: *Transactions American Geophysical Union*, v. 29, no. 1, p. 69-74.
- Williams, H., 1942, The geology of Crater Lake National Park: Washington, D. C., Carnegie Institution of Washington Publication 540, 162 p.
- _____ 1961, The floor of Crater Lake, Oregon: *American Journal of Science*, v. 259, p. 81-83.
- Williams, H., and McBirney, A. R., 1979, *Volcanology*: San Francisco, Freeman, Cooper, and Co., 397 p.
- Wood, C. A., 1979, Monogenetic volcanoes of the terrestrial planets: *Proceedings of the 10th Lunar and Planetary Science Conference*, p. 2815-2810.
- _____ 1980 a, Morphometric evolution of cinder cones: *Journal of Volcanology and Geothermal Research*, v. 7, p. 387-413.
- _____ 1980 b, Morphometric analysis of cinder cone degradation: *Journal of Volcanology and Geothermal Research*, v. 8, p. 137-160.